

Benefits of a Hydrogen Network in Europe

Fabian Neumann^a, Elisabeth Zeyen^a, Marta Victoria^{b,c}, Tom Brown^a

^a*Department of Digital Transformation in Energy Systems, Institute of Energy Technology, Technische Universität Berlin, Fakultät III, Einsteinufer 25 (TA 8), 10587 Berlin, Germany*

^b*Department of Mechanical and Production Engineering, Aarhus University, Inge Lehmanns Gade 10, 8000 Aarhus, Denmark*

^c*Novo Nordisk Foundation CO₂ Research Center, Aarhus University, Aarhus, Denmark*

Summary

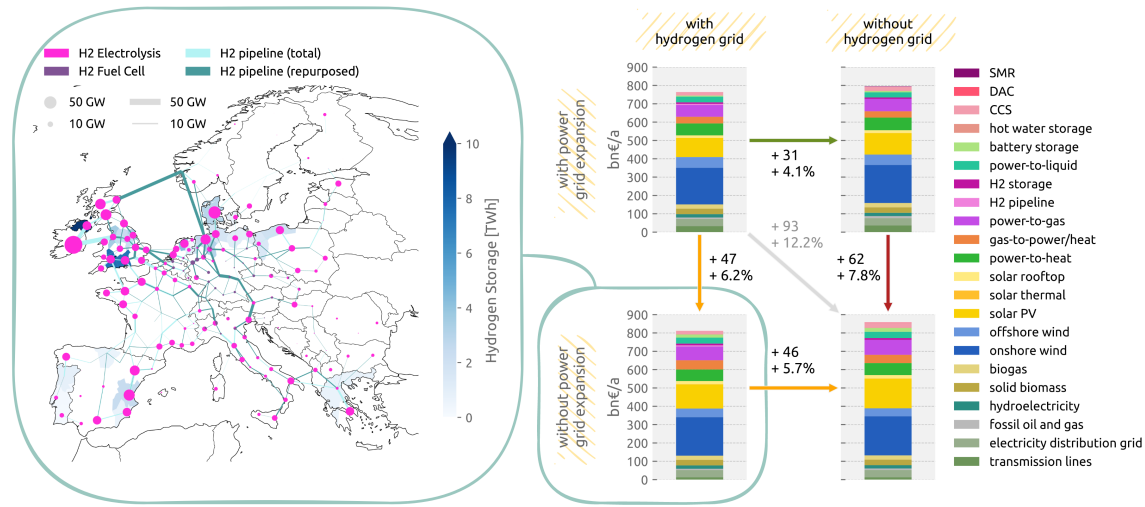
Electricity transmission expansion has suffered many delays in Europe in recent decades, despite its importance for integrating renewable electricity into the energy system. A hydrogen network which reuses the existing fossil gas network would not only help supply demand for low-emission fuels, but could also help to balance variations in wind and solar energy across the continent and thus avoid power grid expansion. We pursue this idea by varying the allowed expansion of electricity and hydrogen grids in net-zero CO₂ scenarios for a sector-coupled European energy system with high shares of renewables and self-sufficient supply. We cover the electricity, buildings, transport, agriculture, and industry sectors across 181 regions and model every third hour of a year. With this high spatio-temporal resolution, we can capture bottlenecks in transmission and the variability of demand and renewable supply. Our results show a consistent benefit of a pan-continental hydrogen backbone that connects high-yield regions with demand centers, synthetic fuel production and geological storage sites. Developing a hydrogen network reduces system costs by up to 6%, with highest benefits when electricity grid reinforcements cannot be realised. Between 58% and 66% of this backbone could be built from repurposed natural gas pipelines. However, we find that hydrogen networks can only partially substitute for power grid expansion, and that both can achieve strongest cost savings of 12% together.

Keywords: hydrogen backbone, sector-coupling, retrofitting, energy systems, transmission expansion, Europe, climate-neutral, renewables

Email address: f.neumann@tu-berlin.de (Fabian Neumann)

Graphical Abstract

Hydrogen infrastructure contributes to cost-effective climate-neutral European energy system designs.



Highlights

- examines benefit of a hydrogen network and gas pipeline retrofitting in net-zero CO₂ scenarios for Europe with high shares of renewables and no energy imports
- uses open energy system model PyPSA-Eur-Sec with 181 regions, 3-hourly resolution for a year and all energy sectors (electricity, buildings, transport, industry, agriculture) represented
- hydrogen network reduces system costs by up to 6%, with highest benefits when power grid expansion is restricted
- between 58-66% of hydrogen backbone uses retrofitted gas network pipelines
- cost benefit of electricity grid expansion is higher than of hydrogen network (8% versus 6%), but both together reduce costs by up to 12%

Context & Scale

Many different combinations of infrastructure would allow Europe to become climate-neutral by 2050. But not all solutions meet the same level of acceptance. For example, power transmission reinforcements have suffered many delays in recent decades, despite their importance for integrating renewable electricity. A hydrogen network which can reuse natural gas pipelines could offer a substitute for moving cheap but remote renewable energy across the continent to where demand is.

We study such trade-offs between building new electricity transmission lines and developing a new network of hydrogen pipelines in the European energy system with all sectors represented and net-zero CO₂ emissions. We find that a hydrogen backbone is consistently beneficial infrastructure and that a large part could repurpose unused gas pipelines. Energy transport as electrons and molecules offer complementary strengths, achieving highest cost savings together.

Words

5746 (excl. preamble, captions, [Experimental Procedures, Supplementary Information](#))

Introduction

There are many different combinations of infrastructure that would allow Europe to reach net-zero greenhouse gas emissions by 2050. However, not all technologies meet the same level of acceptance among the public. The last few decades have seen public resistance to new and existing nuclear power plants, projects with carbon capture and sequestration (CCS), onshore wind power plants, and overhead transmission lines. The lack of public acceptance can both delay the deployment of a technology and even stop its deployment altogether. This may make it harder to reach greenhouse gas reduction targets in time or cause rising costs through the substitution with other technologies. In particular, electricity transmission network expansion has suffered many delays in Europe in recent decades, despite its importance for integrating large amounts of renewable electricity such that all energy sectors can be decarbonised.

Hydrogen will likely become a pivotal energy carrier in such a climate-neutral energy system. Hydrogen is needed in the industry to produce ammonia for fertilisers and can be used for direct reduced iron for steelmaking. It is also a critical feedstock to produce synthetic methane and liquid hydrocarbons for use as aviation fuel and as a precursor to high-value chemicals. Hydrogen could also be used for heavy-duty land transport, shipping, and backup heat and power supply.

The limited social acceptance for electricity grid reinforcement and the advancing role of hydrogen raises the question of whether a new network of hydrogen pipelines could offer a replacement for balancing variable renewable electricity generation and moving energy across the continent. Such a vision for a *European Hydrogen Backbone (EHB)* has recently been expressed by Europe's gas industry in a series of reports.¹⁻⁴ It would offer an alternative route to connecting remote regions with abundant and cost-effective wind and solar potentials to densely-populated and industry-heavy regions with high demand but limited supply options.

Since Europe has a sizeable existing natural gas transmission network that is set to become increasingly redundant as the system transitions towards climate neutrality, the option to repurpose parts of the network to transport hydrogen instead, may make hydrogen networks even more attractive. This is because retrofitting gas pipelines would significantly lower the development costs compared to building new hydrogen pipelines. Moreover, repurposed and new pipelines may also meet higher levels of acceptance among the local populations than transmission lines. Unlike transmission towers, pipelines are less visible because they usually run below or near the ground. Particularly where gas pipelines already exist, the perceivable impact would be minimal.

However, few studies have evaluated the benefit of a hydrogen network in Europe so far. The EHB reports do not include an assessment based on the co-optimisation of energy system components.^{1–4} Other sector-coupling studies have not included hydrogen networks at all,^{5–8} or when they do, model Europe only at country-level resolution,^{9,10} have a country-specific focus with limited geographical scope or detail outside the focus area,¹¹ or neglect some energy sectors or non-energy demands that involve hydrogen.^{11–13} None of the studies have explored the interplay between hydrogen network expansion and electricity grid reinforcements. Neither have the potentials for lower development costs through pipeline retrofitting been taken into account so far.

This paper provides the first high-resolution examination of the trade-offs between electricity grid expansion and a new hydrogen network in scenarios for a European energy system with net-zero carbon dioxide emissions and high shares of renewable electricity production. We analyse four main scenarios to investigate if a hydrogen network can compensate for a potential lack of power grid expansion. The scenarios differ based on whether or not electricity and hydrogen grids can be expanded, including potentials for gas pipeline retrofitting. Evaluation criteria include the total system cost, the composition and spatial distribution of technologies and transmission infrastructure in the system. As a supplementary sensitivity analysis, we also evaluate the impact of restricted onshore wind potentials on these scenarios.

For our analysis, we use an open capacity expansion model of the European energy system, PyPSA-Eur-Sec, which, in contrast to many previous studies,^{5,14–20} combines a fully sector-coupled approach with a high spatio-temporal resolution and multi-carrier transmission infrastructure representation so that it can capture the various transport bottlenecks that constrain the cost-effective integration of variable renewable energy. The model co-optimises the investment and operation of generation, storage, conversion and transmission infrastructures for the least-cost outcome in a single linear optimisation problem, covering 181 regions and a 3-hourly time resolution for a full year. It incorporates spatially distributed demands of the electricity, industry, buildings, agriculture and transport sectors, including shipping and aviation as well as non-energy feedstock demands in the chemicals industry. Primary energy supply comes from wind, solar, biomass, hydro, and limited amounts of fossil oil and gas. The energy flows between the system's energy carriers are modelled by various technologies, including heat pumps, combined heat and power (CHP) plants, thermal storage, electric vehicles, batteries, power-to-X processes, fuel cells, and geological potentials of underground hydrogen storage. Data on electricity and gas transmission infrastructure is also included to determine grid expansion needs and retrofitting potentials. The model also features detailed management of carbon flows between capture, usage, sequestration and emissions

to the atmosphere to track carbon through the system. More details on the model are presented in the [Experimental Procedures](#) and [Supplementary Information](#). The model is open-source and based on open data such that results can be reproduced and assumptions may be modified by others (github.com/pypsa/pypsa-eur-sec).

All investigations are conducted with a constraint that carbon dioxide emissions into the atmosphere balance out to zero over the year, disregarding other greenhouse gas emissions. The model can sequester up to 200 MtCO₂ per year, allowing it to sequester industry process emissions that have a fossil origin, such as calcination in cement manufacture, but restricting the use of negative emission technologies compared to other works.¹⁸ In our scenarios, we also do not consider clean energy imports to Europe, thus assuming that Europe is self-sufficient in electricity and green fuels and feedstocks. Technology assumptions are taken widely from the Danish Energy Agency for the year 2030.²¹

Hydrogen network benefit is robust, strongest without power grid expansion

In [Figure 1](#), we first compare the total system costs and their composition between the four main scenarios, which vary in whether or not the power grid can be expanded beyond today's levels and if a new hydrogen backbone based on new and retrofitted pipelines can be built. Across all four scenarios, the total system costs are dominated by investments in generation from wind and solar and conversion from power to heat (primarily heat pumps) and to hydrogen and liquid hydrocarbons (for transport fuels and as a feedstock for the chemicals industry). System costs vary between 764 and 857 bn€/a, depending on available network expansion options.

Overall, we find that system costs are not overly affected by restrictions on the development of electricity or hydrogen transmission infrastructure. The realisable cost savings are small compared to total system costs, and systems without grid expansion present themselves as equally feasible alternatives. The combined net benefit of hydrogen and electricity grid expansion is 93 bn€/a; a system without either would be around 12% more expensive. This limited cost increase can be attributed to the high level of synthetic fuel production for industry, transport, and backup electricity and heating applications. The option for a flexible operation of conversion plants, cheap energy storage and low-cost energy transport as hydrocarbons between regions offer sufficient leeway to manage electricity and hydrogen transport restrictions effectively (see [Common features across four scenarios of European climate neutrality](#)).

The total net benefit of power grid expansion is between €46-62 billion per year compared to costs for transmission line reinforcements between €11-14 billion per year. System

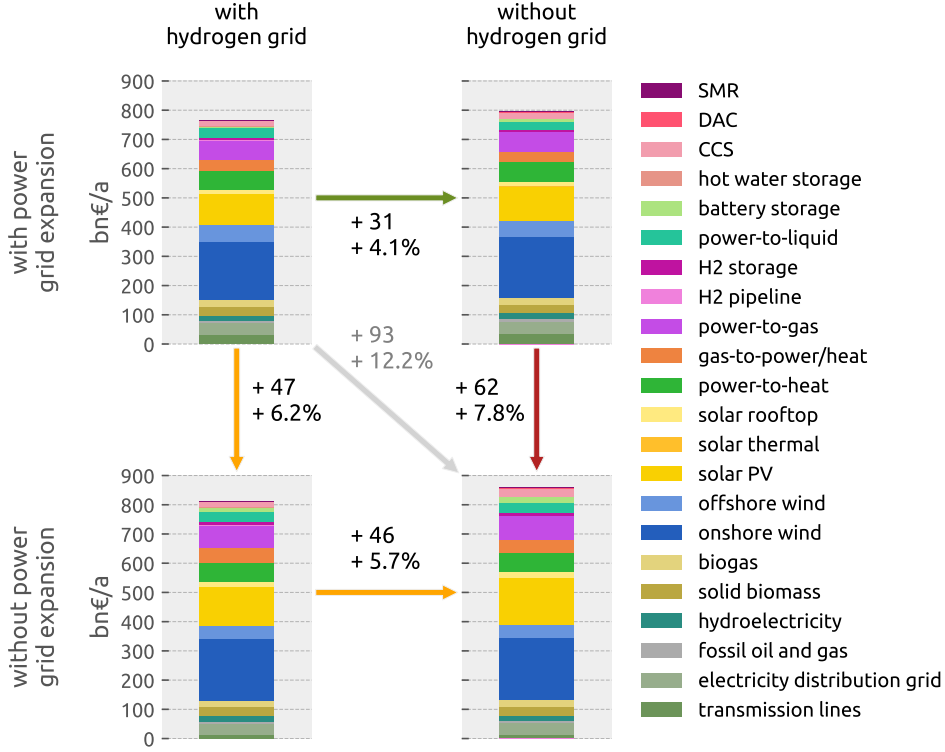


Figure 1: Benefits of electricity and hydrogen network infrastructure. The figure compares four scenarios with and without expansion of a hydrogen network (left to right) and the electricity grid (top to bottom). Each bar depicts the total system cost of one scenario alongside its cost composition. Arrows between the bars indicate absolute and relative cost increases as network infrastructures are successively restricted.

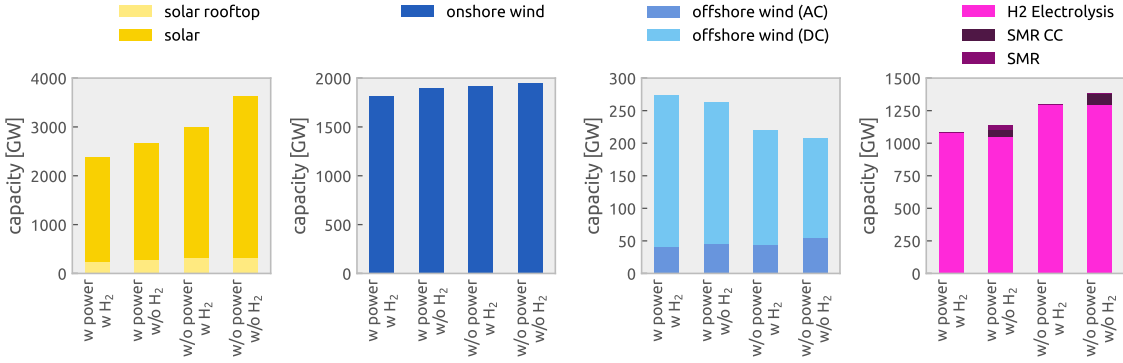


Figure 2: Installed capacities of solar (rooftop and utility-scale), onshore and offshore wind, and hydrogen production via electrolysis and conventional steam methane reforming (SMR) with and without carbon capture (CC) for the four electricity (w/wo power) and hydrogen (w/wo H₂) network expansion scenarios.

costs decrease despite the increasing investments in electricity transmission infrastructure. The benefit is strongest if no hydrogen network can compensate for the lack of electricity grid capacity to transport energy over long distances. [Section S13.1](#) presents additional intermediate results about the system cost sensitivity between a doubling of power grid capacity and no grid expansion. Electricity grid reinforcement enables renewable resources with better capacity factors to be integrated from further away, resulting in lower capacity needs for solar and wind. The grid also allows renewable variations to be smoothed in space and facilitates the integration of offshore wind, resulting in lower hydrogen demand for balancing power and heat and less hydrogen infrastructure. A restriction on the level of power grid expansion leads to more local production from solar photovoltaics and increased hydrogen production.

The presence of a new hydrogen backbone can reduce system costs by up to 6%. The net benefit between €31-46 billion per year (4-6%) largely exceeds the cost of the hydrogen network, which costs between €5-8 billion per year. Its benefit is strongest when the electricity grid is not expanded. However, even with high levels of power grid expansion, the hydrogen backbone is still beneficial infrastructure.

Although grid reinforcements provide slightly higher cost reductions, hydrogen and electricity transmission infrastructure are strongest together. Approximately half of the combined benefit of transmission infrastructure can be achieved by only building a new hydrogen backbone. In contrast, two-thirds of the benefit can be reached by exclusively reinforcing the electricity transmission system. Compared to the combined net benefit of 93 bn€/a, the individual benefits sum up to a value that is only 16% higher ($46+62 = 108$ bn€/a). Thus, offered cost reductions are mainly additive.

This also means that a hydrogen backbone cannot substitute perfectly for power grid reinforcements. It can only partially compensate for the lack of grid expansion, yielding roughly 75% of the electricity grid's benefit. Instead, energy transport as electrons and molecules seem to offer complementary strengths. From a system-level perspective, reductions of total costs achieved by network expansion are small. A system built exclusively around hydrogen network expansion is just around 2% more expensive than an alternative system that only allows electricity grid expansion.

Common features across four scenarios of European climate neutrality

Across all scenarios, we see 210 to 270 GW offshore wind, 1820 to 1950 GW onshore wind, and 2380 to 3630 GW solar photovoltaics ([Figure 2](#)). The wide range of solar capacities are due to an increased localisation of electricity generation when the expansion of transmission infrastructure is limited. Across all scenarios, the capacities of photovoltaics split

roughly into 10% rooftop PV and 90% utility-scale PV. The offshore share of wind generation capacities varies between 10% and 13% and is highest when transmission networks can be fully expanded.

The spatial distribution of investments per scenario is shown in [Figure 3](#). For instance, [Figure 3a](#) shows the least-cost solution with full electricity and hydrogen network expansion. While solar capacities are spread relatively evenly around the continent with a stronger presence in Southern Europe, both onshore and offshore wind are concentrated around the North Sea and the British Isles. When allowed, new electricity transmission capacity is built where they help the integration of wind and the transport to inland demand centres (see [Hydrogen network benefit is robust, strongest without power grid expansion](#)).

Furthermore, electrolyser capacities for power-to-hydrogen see a massive scale-up to between 1057 to 1297 GW depending on the permitted energy transport infrastructure ([Figure 2](#)). The capacities are lowest when the electricity grid can be expanded. In this case, their locations correlate strongly with wind capacities (Pearson correlation coefficient $R^2 = 0.85$ compared to $R^2 = 0.37$ for solar capacities, [Figure 3](#)). New hydrogen infrastructure accompanies the build-out of hydrogen production facilities. A system of hydrogen underground storage and pipelines in Europe helps to balance generation from renewables in time and space.

In space, a new pipeline network transports hydrogen from preferred production sites to the rest of Europe, where hydrogen is consumed by industry (for ammonia, high-value chemicals and steel production), heavy-duty transport, and fuel cells for power and heat backup. Varying in magnitude per scenario, we see major net flows of hydrogen from the British Isles and France to the Benelux Union and Germany, and from the North East of Spain to Southern France. Compared to net flows in the electricity network, which also balances renewable generation back and forth as weather systems pass the continent, the hydrogen network more distinctly targets energy transport over long distances (see also [Regional imbalance of supply and demand is reinforced by transmission](#) and [Figures S24 and S25](#)). The favoured network topology strongly depends on the potentials for cheap renewable electricity. If onshore wind potentials were restricted, e.g. due to limited social acceptance in Northern Europe, the network infrastructure would be tailored to deliver larger amounts of solar-based hydrogen from Southern Europe to Central Europe. We discuss this supplementary sensitivity analysis in [Sections S13.2](#) and [S13.3](#).

The development of a hydrogen backbone is driven by the fact that (i) industry demand for hydrogen is located in areas with less attractive renewable potentials, (ii) the best wind and solar potentials are located in the periphery of Europe, (iii) bottlenecks in the

electricity transmission network exist and give impetus to alternative energy transport options, and (iv) moving produced hydrogen to locations where the geological conditions allow for cheap underground storage is more cost-effective than local storage where there are no salt deposits and only steel tanks are available to the model. Another location factor for hydrogen network infrastructure is linked to the siting of synthetic liquid hydrocarbon production. Because we assume that waste heat from these processes can be recovered in district heating networks, urban areas with attractive renewable potentials nearby appear to be preferred sites for synthetic fuels production to which additional hydrogen would need to be transferred ([Figure S39](#)). Because of our assumption that oil and gas can be moved freely in the model, the spatial distribution of their demands is not a siting factor that is taken into account. Neither is the location of carbon dioxide sources.

The flexible operation of electrolyzers further supports the system integration of variable renewables in time. Hydrogen production leverages periods with exceptionally high wind speeds across Europe by running the electrolysis with average utilisation rates between 36% and 40% (see [Figures S33](#) and [S35](#)). The produced hydrogen is buffered in salt caverns which then allows again for a stable subsequent production of synthetic hydrocarbons. For Fischer-Tropsch plants, for instance, we see much higher average utilisation rates between 87% and 95% which aligns with such a plant's beneficial operating conditions and is caused by the high upfront investment costs we assume. Their operation is only interrupted in winter periods with low wind speeds and low ambient temperatures to give way to backup heat and power supply options (see [Figures S33](#) and [S35](#)). By exploiting periods of peak generation and curbing production in periods of scarcity, large amounts of variable renewable power generation that serves the systems' abundant synthetic fuel demands can be incorporated into the system cost-effectively. This ultimately leads to low levels of firm capacity. We observe OCGT and CHP plant capacities between 123 and 216 GW_{el} compared to peak electricity consumption of 2112 GW_{el}. The lowest values were attained when additional power transmission could be built.

Hydrogen storage is required to benefit from temporal balancing through flexible electrolyser operation. We find cost-optimal storage capacities between 62 to 66 TWh with a hydrogen network and 32 to 35 TWh without a hydrogen network while featuring similar filling level patterns throughout the year. Almost all hydrogen is stored in salt caverns, exploiting vast geological potentials across Europe mostly in Northern Ireland, England and Denmark. We observe no storage in steel tanks unless neither a hydrogen nor the electricity network can be expanded. In this case, we see up to 1.3 TWh of steel tank capacity, which represents only 4% of the respective total hydrogen storage capacity. If the hydrogen network development is restricted, less hydrogen storage is built since options

for cheap underground storage are limited to regions with salt deposits and become less accessible.

Together with the supporting infrastructure, the production of huge amounts of hydrogen (2437 TWh/a) offers versatile use cases. Most of the hydrogen is used to produce Fischer-Tropsch fuels for organic chemicals and transport fuels (1425 TWh/a), of which 356 TWh/a is useable as a by-product in the form of waste heat for district heating networks. A total of 778 TWh/a is used in shipping (two thirds) and land transport (one third). The industry sector consumes 196 TWh/a, excluding use of hydrogen for industry feedstock (e.g. high-value chemicals). Around 79 TWh/a of hydrogen is lost during synthetic fuel production. If the electricity grid expansion is restricted, but hydrogen can be transported, even more hydrogen is produced to be re-electrified in fuel cells during critical phases of system operation (100 TWh_{el} or 200 TWh_{H₂}). According to [Figure 3](#), these fuel cells would mostly be built inland in Germany. Only 30 TWh/a is used to produce methane, which is needed for process heat in some industrial applications and as a heating backup for power-to-heat units. This is because the model prefers to use the full potential for biogas (346 TWh/a) and limited amounts of fossil gas (371 TWh/a), which are offset by sequestering biogenic carbon dioxide, over synthetic production.

Only in scenarios where hydrogen network expansion was restricted, we observe notable synthetic methane production (H₂-to-CH₄, 329 to 563 TWh) and steam methane reforming with carbon capture (CH₄-to-H₂, 94 to 216 TWh). In these cases, the route via methane, which can still be transported freely through the gas network across Europe, is partially used to counteract hydrogen transmission constraints. Direct air capture (27 Mt_{CO₂}/a) was made use of only when both hydrogen and electricity network expansion were forbidden and levels of methanation were highest. In all other cases, sufficient carbon was available to the system from biogenic or fossil sources, while still being able to stay within set sequestration limits. For a comprehensive overview of energy and carbon flows in each scenario see [Figures S31 and S32](#).

Hydrogen backbone takes over role of bulk energy transport

[Figure 5](#) shows statistics on the total electricity and hydrogen transmission capacity built as well as how much energy is moved through the respective networks, while distinguishing between retrofitted and new capacities.

Depending on the level of power grid expansion, between 342 and 422 TWkm of hydrogen pipelines are built. The higher value is obtained when the hydrogen network partially offsets the lack of electricity grid reinforcement. On the other hand, restricting

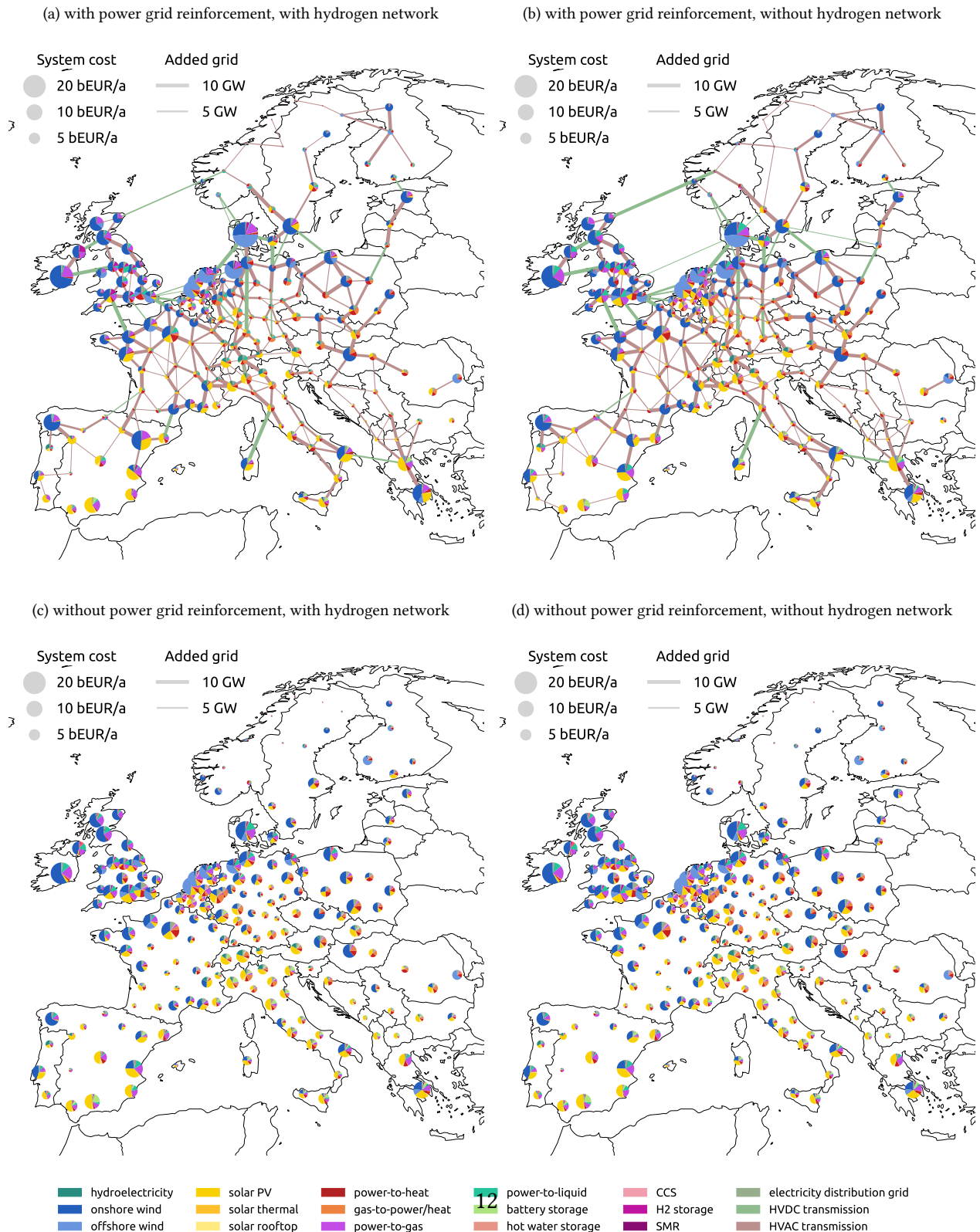


Figure 3: Regional distribution of system costs and electricity grid expansion for scenarios with and without electricity or hydrogen network expansion. The pie charts depict the annualised system cost alongside the shares of the various technologies for each region. The line widths depict the level of added grid capacity between two regions, which was capped at 10 GW.

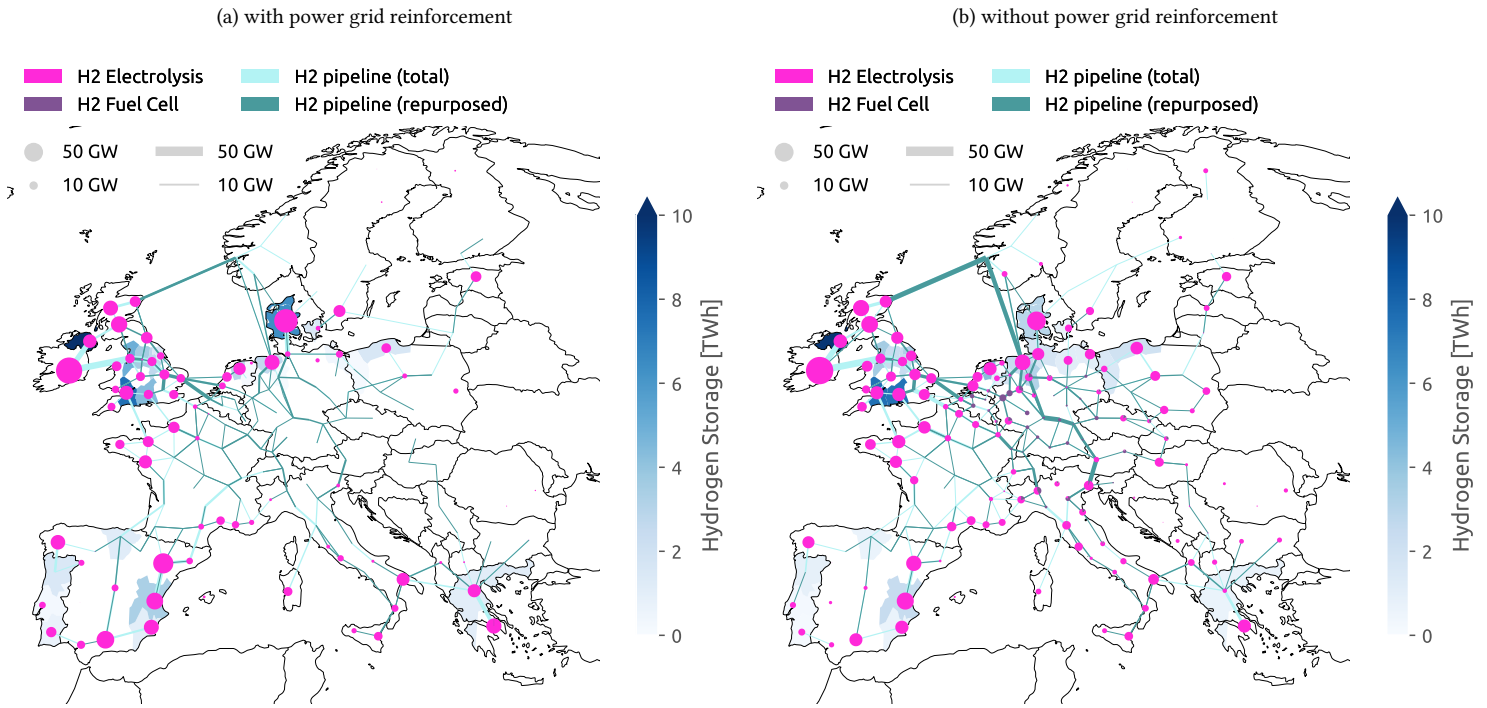


Figure 4: Optimised hydrogen network, storage, reconversion and production sites with and without electricity grid reinforcement. The size of the circles depicts the electrolysis and fuel cell capacities in the respective region. The line widths depict the optimised hydrogen pipeline capacities. The darker shade depicts the share of capacity built from retrofitted gas pipelines. The coloring of the regions indicates installed hydrogen storage capacities.

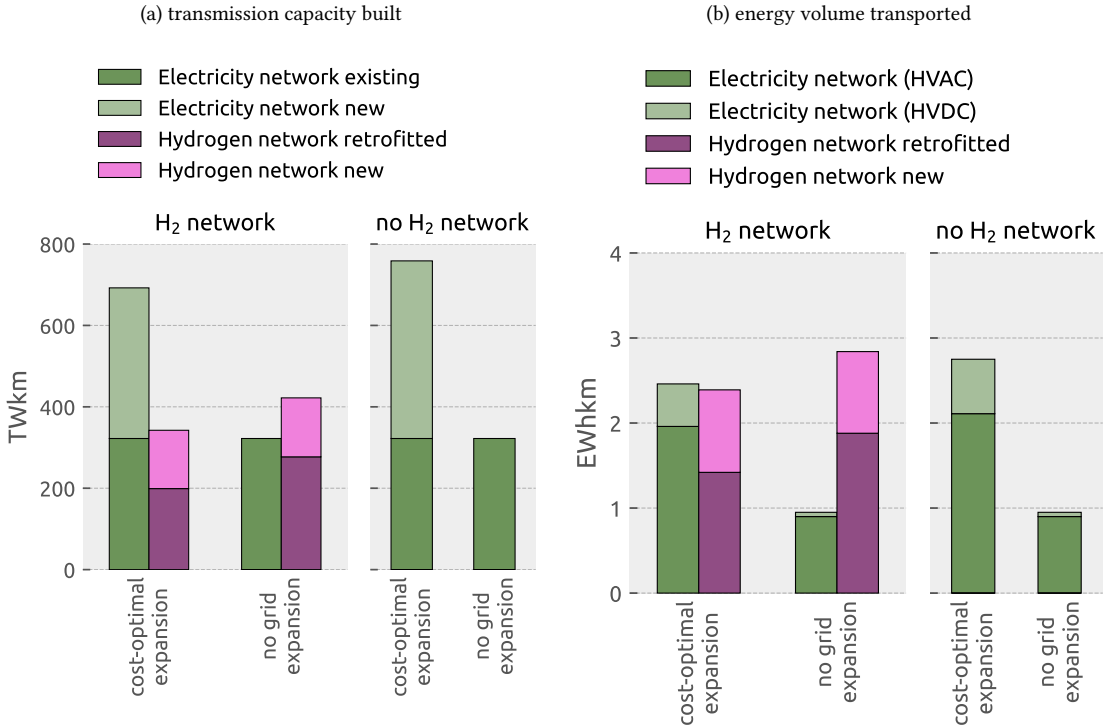


Figure 5: Transmission capacity built and energy volume transported for various network expansion scenarios. For the hydrogen network, a distinction between retrofitted and new pipelines is made. For the electricity network, a distinction is made between existing and added capacity or how much energy is moved via HVAC or HVDC power lines. Both measures weight capacity (TW) or energy (EWh) by the length (km) of the network connection.

hydrogen expansion only has a small effect on cost-optimal levels of power grid expansion. The length-weighted power grid capacity is a little more than doubled in the least-cost scenario; without a hydrogen network, the cost-optimal power grid capacity is 10% higher.

When both hydrogen and electricity grid expansion is allowed, both networks transport approximately the same amount of energy ([Figure 5b](#)). This is striking because the hydrogen network capacity is less than half that of the power grid and more comparable with today's power grid capacities ([Figure 5a](#)). In consequence, the utilisation rate of 59% of the hydrogen network is much higher than the 35% of the electricity grid ([Figure S41](#)). One plausible explanation for this observation is that the buffering of produced hydrogen in stores allows more coordinated bulk energy transport in hydrogen networks, whereas the power grid directly balances the variability of renewable electricity supply.

When electricity grid expansion is restricted, the hydrogen network plays a dominant role in transporting energy around Europe. In this case, around three times more energy is moved in the hydrogen network (2.8 EWhkm) than in the electricity network (1 EWhkm). However, expansion restrictions in the electricity network rather affect the division between hydrogen and electricity flows than the total volume of energy transported. The total energy moved as hydrogen or electricity is only reduced by 22% by imposing restrictions on both hydrogen and electricity transmission.

New hydrogen backbone can leverage repurposed natural gas pipelines

With our assumptions, developing electricity transmission lines is approximately 60% more expensive than building new hydrogen pipelines. We assume costs for a new hydrogen pipeline of 250 €/MW/km, whereas, for a new high-voltage transmission line, we assume 400 €/MW/km (see [Section S16](#)). Despite higher costs, we observe that grid reinforcements are preferred over hydrogen pipelines. Part of the reason may be that electricity is more versatile in our scenarios with high levels of direct electrification. If hydrogen has to be produced and then re-electrified, the efficiency losses mean additional generation capacity would be needed to compensate. However, pipelines are particularly attractive where the end-use is hydrogen-based.

The appeal of a hydrogen network is further spurred by existing natural gas infrastructure available to be retrofitted. Repurposing a natural gas pipeline to transport hydrogen instead cost just around half that of building a new hydrogen pipeline (117 versus 250 €/MW/km; see [Section S16](#)). For the capacity retrofit we include costs for required compressor substitutions and assume that for every unit of gas pipeline decommissioned,

60% of its capacity becomes available for hydrogen transport. In consequence, even detours of the hydrogen network topology may be cost-effective if, through rerouting, more repurposing potentials can be tapped.

As [Figure 4](#) illustrates, the optimised hydrogen network topology is highly concentrated in the North West of Europe. Individual pipeline connections between regions have optimised capacities up to 50 GW. Of the total hydrogen network volume, between 58% and 66% consists of repurposed gas pipelines. The share is highest when the electricity grid is not permitted to be reinforced. Up to a third of the existing natural gas network is retrofitted to transport hydrogen instead, leaving large capacities that are used neither for hydrogen nor methane transport, particularly in Germany, Poland, Italy and the North Sea. In our scenarios, a little more than 40% of retrofittable gas pipelines fully exhaust their conversion potential to hydrogen. The most notable corridors for gas pipeline retrofitting are located offshore across the North Sea and the English Channel and in England, Germany, Austria, and Northern Italy. The sizeable existing natural gas transmission capacities in Southern Italy and Eastern Europe are not repurposed for hydrogen transport in this self-sufficient scenario for Europe. However, this picture might change if clean energy import options were considered. Since most hydrogen is used to produce synthetic fuels and ammonia, if these were imported, much of the hydrogen demand would fall away, thereby also reducing the need for hydrogen transport infrastructure. Moreover, direct hydrogen imports into Europe may alter cost-effective network topologies as new import locations need to be connected rather than domestic production. For instance, the networks role might change from distributing energy from North Sea hydrogen hubs to integrating inbound pipelines from North-Africa with increased network capacities in Southern Europe.

Regional imbalance of supply and demand is reinforced by transmission

[Figure 6](#) shows the net energy surpluses and deficits of each region alongside so-called Lorenz curves that depict regional inequities between supply and demand for each carrier and how they vary among the four network expansion scenarios.

In line with previously shown capacity expansion plans, energy surplus is found largely in the wind-rich coastal and solar-rich Southern regions that supply the inland regions of Europe, which have high demands but less attractive renewable potentials. The net energy surplus of individual regions amounts to up to 200 TWh. Examples are Danish offshore wind power exports and large wind-based production sites for synthetic fuels in Ireland. For Ireland, this surplus is roughly three times as high as its final energy demand, resulting in the situation that three quarters of its energy production is exported. Net

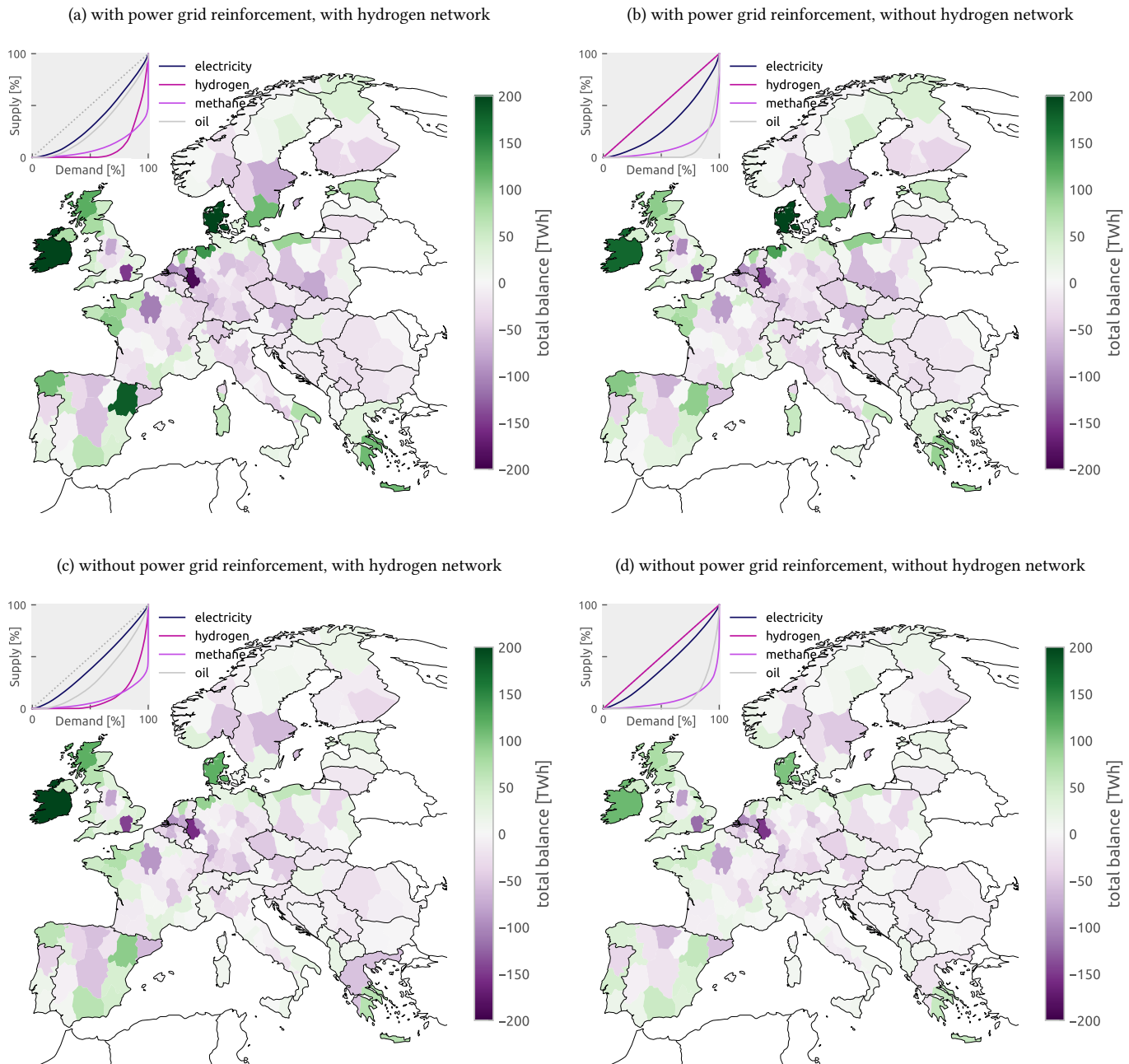


Figure 6: Regional total energy balances for scenarios with and without electricity or hydrogen network expansion, revealing regions with net energy surpluses and deficits. The Lorenz curves on the upper left of each map depict the regional inequity of electricity, hydrogen, methane and oil supply relative to demand. If the annual sums of supply and demand are equal in each region, the Lorenz curve resides on the identity line. But the more unequal the regional supply is relative to demand, the further the curve dents into the bottom right corner of the graph.

deficits of single regions have similarly high values, close to 200 TWh. Examples are, in particular, the metropolitan areas around London and Paris, as well as the industrial cluster between Rotterdam and the Ruhr valley.

Energy transport infrastructure fuels the uneven regional distribution of supply relative to demand. This is illustrated by the Lorenz curves presented in [Figure 6](#) for different energy carriers and network expansion scenarios. The Lorenz curves plot the carrier's cumulative share of supply versus the cumulative share of demand, sorted by the ratio of supply and demand in ascending order. If the annual sums of supply and demand are equal in each region, the Lorenz curve resides on the identity line. However, the more unequal the regional supply is relative to demand, the further the curve dents into the bottom right corner of the graph.

For the least-cost scenario, [Figure 6a](#) highlights that hydrogen supply is more regionally imbalanced relative to demand than electricity supply. Roughly 60% of the hydrogen demand is consumed in regions that produce less than 1% of the total hydrogen supply. Conversely, 40% of the hydrogen supply is produced in regions that consume less than 5% of total hydrogen demand. Naturally, reduced electricity grid expansion causes more evenly distributed electricity supply ([Figures 6c](#) and [6d](#)). If hydrogen transport is restricted ([Figures 6b](#) and [6d](#)), the production of liquid hydrocarbons is increased in renewable-rich regions because they can be transported at low cost. In this case, 70% of the demand for oil-based products is consumed in regions that produce less than 1% of the total supply. With full network expansion, 70% of demand is consumed in regions that produce 16% of the total supply.

Discussion

To put our results into a broader perspective, for the discussion we compare them to related literature and proposals presented in the gas industry's European Hydrogen Backbone reports. This is followed by an appraisal of the limitations of our study.

Comparison to Related Literature

Compared to the net-zero scenarios from the European Commission^{[19](#)}, we see much larger renewable electricity generation, reaching beyond 8750 TWh/a compared to 2500 TWh/a.^{[19](#)} In terms of total electricity produced, our results show almost a tripling of today's generation. By 2050, it rises to 270% compared to 150% in the Commission's report.^{[19](#)} Roughly one third goes to regular electricity demand, one third goes to newly electrified sectors in heating, transport and industry, and another third goes to hydrogen production (dominated by demand for Fischer-Tropsch fuels). The major difference to the Commission's

scenarios¹⁹ is caused by their lower electrification rates in other sectors, higher biomass potentials, and a strong reliance on imports of fossil oil for non-energy uses such as plastics that were not counted towards net emissions as we do in this study.

In Brown et al.⁵, an optimal grid expansion brought a benefit of 64 bn€/a compared to the case with no transmission between European countries, which is higher than the 47 bn€/a benefit found here. There are at least four causes for this difference: the model here has higher resolution (181 compared to 30 regions) which allows better placement of wind at good sites; here we start from today's grid; in Brown et al.⁵ there was no hydrogen pipeline network and no underground hydrogen storage; and finally we have higher demand for hydrogen from industry and synthetic fuels, which provides a large flexible load that helps to integrate wind and solar in time.

Caglayan et al.¹² also consider European decarbonisation scenarios with both electricity transmission and new hydrogen pipelines, but at a lower spatial resolution (96 regions). A similar pattern of hydrogen pipeline expansion towards the British Isles and North Sea is seen, but lower overall hydrogen capacities (258 GW compared to our 1057 to 1297 GW) because industry, shipping, aviation, agriculture and non-electrified heating are not included. Caglayan et al.¹² also find cost-optimal hydrogen underground storage of 130 TWh, whereas our scenarios involve less cavern storage between 32 and 66 TWh because the larger demand for hydrogen means there is both more wind and solar generation as well as more flexible demand. Therefore, less storage is needed for weekly and monthly balancing.

A large number of feasible and cost-effective designs for a climate-neutral European energy system was also recently presented by Pickering et al.⁶. Their 98-region model with 2-hourly resolution likewise includes all energy sectors including non-energy feedstocks and also optimises for fully self-sufficient energy supply chains within Europe. However, they do not focus on hydrogen infrastructure. Hydrogen transport is not considered so that hydrogen must be produced locally, whereby power grid expansion gains importance. Moreover, their scenarios disregard geological potentials for low-cost storage in salt aquifers and the option to retrofit gas pipelines. Owing to high storage cost in steel tanks and fewer assumed end-uses of hydrogen (e.g. in shipping and heavy-duty transport), their scenarios involve less hydrogen storage (0 to 6 TWh versus 32 to 66 TWh) and lower electrolyser capacities (290 to 855 GW versus 1057 to 1297 GW) compared to our results. Furthermore, whereas our model allows limited use of fossil fuels and with options for carbon capture and sequestration, Pickering et al.⁶ are more restrictive by eliminating the use of fossil energy sources and only considering direct air capture as carbon source for synthetic hydrocarbons. Overall, total system costs lie in a similar range between 730 and 866 bn€/a compared to costs between 746 and 839 bn€/a in our study (both exclud-

Table 1: Comparison of new and retrofitted hydrogen network built between our scenarios and the European Hydrogen Backbone (April 2021)³. Spatial coverage uses ISO 3166-1 alpha-2 country codes.

Scenario	Repurposed [TWkm]	New [TWkm]	Spatial Coverage
European Hydrogen Backbone ³	208	101	EU27+UK+CH -PT-LT-LV-HR-BG-RO-MT-CY
PyPSA-Eur-Sec (with grid expansion)	199	143	EU27+UK+CH+NO+Balkan-MT-CY
PyPSA-Eur-Sec (no grid expansion)	277	145	EU27+UK+CH+NO+Balkan-MT-CY

ing existing hydroelectric facilities). However, the composition differs. Pickering et al.⁶ have higher spendings on power-to-liquids owing to cost assumptions about conversion plants, higher costs for power-to-heat technologies due to higher heat demands, lower expenditures for generation due to lower PV cost assumptions, and neglected costs for electricity distribution grids.

Comparison to the European Hydrogen Backbone

Our results align well with the proposals for a European Hydrogen Backbone (EHB) from the gas industry.¹⁻⁴ Whereas the reports are presented as visions rather than proposals based on detailed network planning, here, we present supporting modelling results based on temporally resolved spatial co-planning of energy infrastructures. We see cost-optimal hydrogen network investments between 5-8 bn€/a, while the EHB report from April 2021³ finds similar costs between 4-10 bn€/a across 21 countries¹. The extension to 28 countries from April 2022⁴ reports costs between 7-14 bn€/a.

Table 1 compares the hydrogen network volume of the EHB from April 2021 with 21 European countries to our analysis.³² The volume is measured as the length-weighted sum of pipeline capacities (TWkm) and distinguishes between repurposed and new pipeline capacities. Both analyses build a similarly sized hydrogen network. With electricity grid expansion, our results show a hydrogen network that is 11% larger; without grid expansion this difference rises to 37%. Furthermore, the share of retrofitted gas pipelines in the hydrogen backbone is comparable. The 69% volume share of repurposed natural gas pipelines³ agrees with our findings where between 58% and 66% of hydrogen pipelines are retrofitted gas pipelines.

¹To calculate the annuity of the overnight hydrogen network costs listed in the EHB reports, a lifetime of 50 years and a discount rate of 7% are assumed like for this paper's modelling.

²The newer EHB report from April 2022⁴ lacks sufficient data to calculate length-weighted network capacities.

Selected limitations of the study and scope for future investigations

In the presented scenarios, Europe is largely energy self-sufficient. While limited amounts of fossil gas and oil imports are allowed, no imports of renewable electricity, chemical energy carriers or commodities from outside of Europe are considered. However, with imports system needs for electricity and hydrogen transmission infrastructure may change substantially. New hydrogen import hubs would require different bulk transmission routes. The import of large amounts of carbon-based fuels and ammonia would furthermore diminish the demand for hydrogen overall, and hence also the need to transport it. This effect of imports on infrastructure needs should be explored in future work.^{22–24}

Additionally, the very uneven distribution of energy supply in our results may interfere with the level of social acceptance for new infrastructure to an extent that may block a swift energy transition.^{25,26} Hence, future investigations should weigh the cost surcharge of increased regionally self-sufficient energy supply against the potential benefit of higher public acceptance and increased resilience.

Moreover, previous research has shown that there are many directions in the feasible space where the system composition can be changed with only a small change in system costs. This breadth of options makes robust statements about specific infrastructure needs more vague. While we present selected design trade-offs regarding transmission networks, a more comprehensive exploration of near-optimal solutions in sector-coupled systems using techniques like Modelling-to-Generate-Alternatives (MGA),^{6,27–29} would reveal an even broader range of alternative system layouts.

Besides, there are many more limitations. For instance, high-quality data on demands and infrastructure is not always publicly available; projections for future technology costs and assumptions are uncertain and we neglect the dynamics of technological learning by doing; we also do not consider new nuclear power plants; heat demands and the availability of renewables vary considerably year by year such that our stricture to a single year may limit the solutions' robustness to interannual weather variability; and for the transport and industry sectors we make some exogenous assumptions about process switching, drive trains, alternative fuels for industry heat and recycling rates which may have turned out differently if they were endogenously optimised. For computational reasons, we also need to limit the model's spatial resolution to 181 regions and we ignore the nonlinearity of electricity and gaseous flow physics. Nevertheless, we believe our results can demonstrate the conditions under which a hydrogen backbone in Europe would be beneficial.

Conclusion

In this work, we have demonstrated the benefit of a hydrogen network in net-zero CO₂ scenarios for Europe with high shares of renewables. Analysis was performed using the open sector-coupled energy system model PyPSA-Eur-Sec featuring high spatio-temporal coverage of all energy sectors (electricity, buildings, transport, agriculture and industry across 181 regions and 3-hourly resolution for a year). With this level of spatial, temporal, technological and sectoral resolution, it is possible to represent grid bottlenecks as well as the variability and regional distribution of demand and renewable supply. Thereby, the system's infrastructure needs regarding generation, storage, transmission and conversion can be assessed. This includes in particular trade-offs between electricity grid reinforcement, which has limited public support, and developing a hydrogen network, for which increasingly unused gas pipelines can be repurposed.

One of the biggest changes seen in the energy system besides renewables expansion is the build-out of hydrogen infrastructure. Huge new electrolyser capacities enter the system and operate flexibly to aid renewables integration. Furthermore, underground storage in salt caverns is developed for seasonal balancing and a new continent-spanning hydrogen pipeline network is built to connect cheap supply and storage potentials with demand centres. This new hydrogen backbone is found to be supported by considerable amounts of gas pipeline retrofitting: between 58% and 66% of the network uses repurposed pipelines.

Our analysis reveals that a hydrogen network can reduce system costs by up to 6%. Its benefit is shown to be highest when the expansion of the power grid is restricted. However, hydrogen networks can only partially substitute for grid expansion. We found that in fact both ways of transporting energy and balancing renewable generation complement each other and achieve the highest cost savings of up to 12% together. At the same time, these findings also support the interpretation that neither electricity nor hydrogen network expansion are essential for achieving a cost-effective system design if such a cost premium can be accepted to achieve alternative goals.

In conclusion, there appear to be many infrastructure trade-offs regarding how energy is transported across Europe with limited impacts on total system cost such that policymakers could choose from a wide range of near-optimal compromise energy system designs with equally low cost but possibly higher acceptance.

Experimental Procedures

In this section the core characteristics and assumptions of the model PyPSA-Eur-Sec are presented. More detailed descriptions of specific sectors, energy carriers, renewable po-

tentials, transmission infrastructure modelling, and mathematical problem formulation are covered in the supplementary material under [Sections S1 to S12](#).

The European sector-coupled energy system model PyPSA-Eur-Sec uses linear **optimisation** to minimise total annual operational and investment costs subject to technical and physical constraints, assuming perfect competition and perfect foresight over one uninterrupted year of 3-hourly operation (see [Section S12](#) for mathematical formulation). In this study, we used the historical year 2013 for weather-dependent inputs. Apart from existing electricity and gas transmission infrastructure and hydroelectric facilities, no other existing assets are assumed (*greenfield optimisation* or *overnight scenario*), so that the model assumes a long-term equilibrium in a market with perfect competition and foresight, and disregards pathway dependencies. Cost assumptions are taken, where possible, from predictions for the year 2030 by the Danish Energy Agency (see [Section S16](#)).²¹ The model is implemented in the free and open software framework Python for Power System Analysis (PyPSA).³⁰

PyPSA-Eur-Sec builds upon the model from Brown et al.,⁵ which covered electricity, heating in buildings and ground transport in Europe with one node per country. PyPSA-Eur-Sec adds biomass on the supply side, industry, agriculture, aviation and shipping on the demand side, and higher spatial resolution to suitably assess infrastructure requirements. In this study, the European continent is divided into 181 regions. Unavoidable process emissions, feedstock demands in the chemicals industry and the need for dense fuels for aviation, also required the addition of a detailed representation of the carbon cycles, including carbon capture from industry processes, biomass combustion and directly from the air (DAC).

[Figure S1](#) gives an **overview** of the supply, transmission, storage and demand sectors implemented in the model. To render interactions in the sector-coupled energy system, we model the energy carriers electricity, heat, methane, hydrogen, carbon dioxide and liquid hydrocarbons (oil, naphtha) across the different energy sectors. Generator capacities (for onshore wind, offshore wind, utility-scale and rooftop solar photovoltaic (PV), biomass, hydroelectricity, oil and natural gas), heating capacities (for heat pumps, resistive heaters, gas boilers, combined heat and power (CHP) plants and solar thermal collector units), synthetic fuel production (electrolysers, methanation, Fischer-Tropsch, steam methane reforming, fuel cells), storage capacities (stationary and electric vehicle batteries, hydrogen storage in caverns and steel tanks, pit thermal energy storage, pumped-hydro and reservoirs, and carbon-based fuels like methane and oil), carbon capture (from industry process emissions, steam methane reforming, CHP plants and directly from the air), and transport capacities of electricity transmission lines, new hydrogen and repurposed nat-

ural gas pipelines are all subject to optimisation, as well as the operational dispatch of each unit in each represented hour.

Exogenous assumptions in the model include a constant demand for the different materials and energy carriers in each sector, the extent of land transport electrification, the use of liquified hydrogen as shipping fuel and kerosene in aviation, the ratio of district heating to decentralised heating in densely populated regions, efficiency gains due to building retrofitting, hydroelectricity capacities (for reservoir and run-of-river generators and pumped hydro storage).

The time series and potentials of variable renewable **energy supply** (wind, solar, hydro, ambient heat) are computed from historical weather data (ERA5³¹ and SARAH-2³²). Potentials for wind and solar generation take various land eligibility constraints into account, e.g. suitable land types and exclusion zones around populated and protected areas. As long as emissions can be offset by negative emission technologies and sequestration potentials are not exhausted, limited amounts of fossil oil and gas can still be used as primary energy supply. While no assumption about the origin of fossil energy is made, imports of renewables-based products into Europe are not considered.

The full **transmission** network for European electricity transport is taken from the electricity-only model version, PyPSA-Eur,³³ and is clustered down to 181 representative regions based on the methodology used in Hörsch and Brown³⁴ and Frysztacki et al.³⁵. This level of aggregation reflects, at the upper end, the computational limit to solve a temporally resolved sector-coupled energy system optimisation problem and, at the lower end, the requirements to preserve the most important transmission corridors that cause bottlenecks and limit the system integration of renewables. Power flows are modelled using a cycle-based load flow linearization from Hörsch et al.³⁶ that significantly improves computational performance. Hydrogen pipeline flows assume a simple transport model. This means that while incoming and outbound flows must balance for each region and pipes can transport hydrogen only within their capacity limits, no further physical gaseous flow constraints are applied. The potential for gas pipeline retrofitting is estimated based on consolidated network data from the SciGRID-gas project³⁷ such that for every unit of gas pipeline decommissioned, 60% of its capacity becomes available for hydrogen transport.¹

For **industry**, we assume that the demand for materials (such as steel, cement, and high-value chemicals) remain constant. The assumed industry transformation is characterised by electrification, process switching to low-emission alternatives (e.g. switching to hydrogen for direct reduction of iron ore³⁸), more recycling of steel, plastics and aluminium³⁹, fuel switching for high- and mid-temperature process heat to biomass and

methane, use synthetic fuels for ammonia and organic chemicals, and allow carbon capture. It is assumed that no plastic or other non-energy product is sequestered in landfill, but that all carbon in plastics eventually makes its way back to the atmosphere, either through combustion or decay; this approach is stricter than other models.¹⁹

The **transport** sector comprises light and heavy road, rail, shipping and aviation transport. For road and rail, electrification and fuel cell vehicles are available. For shipping, liquid hydrogen is considered. Aviation consumes kerosene whose origin (fossil or synthetic) is endogenously determined. Half of the battery electric vehicle fleet for passenger transport is assumed to engage in demand response schemes as well as vehicle-to-grid operation.

The **buildings** sector includes decentral heat supply in individual housing as well as centralised district heating for urban areas. Heating demand can be met through air- and ground-sourced heat pumps, gas boilers, CHPs, resistive heaters as well as waste heat from synthetic fuel production in district heating networks. For district heating networks, seasonal heat storage options are also available. Efficiency gains from building retrofitting are exogenous to the model based on Zeyen et al.⁴⁰

For **biomass**, only waste and residues from agriculture and forestry are permitted, using the medium potential estimates from the JRC ENSPRESO database.⁴¹ This results in 347 TWh per year of biogas that can be upgraded and 1186 TWh per year of solid biomass residues and waste for the whole of Europe. Biomass can be used in combined electricity and heat generation with and without CCS, as well as to provide low- to medium-temperature process heat in industry.

Carbon capture is needed in the model both to capture and sequester process emissions with a fossil origin, such as those from calcination of fossil limestone in the cement industry, as well as to use carbon for the production of hydrocarbons for dense transport fuels and as a chemical feedstock, for example to produce plastic. CO₂ can be captured from exhaust gases (industry process emissions, steam methane reforming, CHP plants) or by direct air capture. Captured CO₂ can be used to produce synthetic hydrocarbons via the Sabatier or Fischer-Tropsch process. Up to 200 MtCO₂ /a may be sequestered underground, which is sufficient to capture process emissions but limits the system's reliance on negative emission technologies.

Acknowledgements

We are grateful for helpful comments by Johannes Hampp.

License

Creative Commons Attribution 4.0 International License (CC-BY-4.0)

Author Contributions

F.N.: Conceptualization – Data curation – Formal Analysis – Investigation – Methodology – Software – Supervision – Validation – Visualization – Writing - original draft – Writing - review & editing E.Z.: Data curation – Formal Analysis – Investigation – Software – Validation – Writing - review & editing M.V.: Formal Analysis – Investigation – Methodology – Software – Writing - review & editing T.B.: Conceptualization – Data curation – Formal Analysis – Funding acquisition – Investigation – Methodology – Project administration – Resources – Software – Supervision – Writing - original draft – Writing - review & editing

Data and Code Availability

A dataset of the model results is available on *zenodo* at [doi:10.5281/zenodo.6821258](https://doi.org/10.5281/zenodo.6821258). The code to reproduce the experiments is available on *Github* at github.com/fneum/spatial-sector. We also refer to the documentation of PyPSA (pypsa.readthedocs.io), PyPSA-Eur (pypsa-eur.readthedocs.io), and PyPSA-Eur-Sec (pypsa-eur-sec.readthedocs.io). Technology data was taken from github.com/pypsa/technology-data (v0.3.0). An interactive scenario explorer is under development at share.streamlit.io/fneum/spatial-sector-dashboard.

References

- [1] Gas for Climate, [European Hydrogen Backbone - How a dedicated hydrogen infrastructure can be created](#), Tech. rep. (Jun. 2020).
URL https://gasforclimate2050.eu/wp-content/uploads/2020/07/2020_European-Hydrogen-Backbone_Report.pdf
- [2] Gas for Climate, [European Hydrogen Backbone - Analysing future demand, supply, and transport of hydrogen](#), Tech. rep. (Jun. 2021).
URL https://gasforclimate2050.eu/wp-content/uploads/2021/06/EHB_Analysing-the-future-demand-supply-and-transport-of-hydrogen_June-2021.pdf
- [3] Gas for Climate, [Extending the European Hydrogen Backbone - A European Hydrogen Infrastructure Vision Covering 21 Countries](#), Tech. rep. (Apr. 2021).
URL https://gasforclimate2050.eu/wp-content/uploads/2021/06/European-Hydrogen-Backbone_April-2021_V3.pdf

- [4] Gas for Climate, European Hydrogen Backbone - A European Hydrogen Infrastructure Vision Covering 28 Countries, Tech. rep. (Apr. 2022).
 URL <https://gasforclimate2050.eu/wp-content/uploads/2022/04/EHB-A-European-hydrogen-infrastructure-vision-covering-28-countries.pdf>
- [5] T. Brown, D. Schlachtberger, A. Kies, S. Schramm, M. Greiner, Synergies of sector coupling and transmission extension in a cost-optimised, highly renewable European energy system, Energy (2018). [arXiv:1801.05290](#), [doi:10.1016/j.energy.2018.06.222](#).
- [6] B. Pickering, F. Lombardi, S. Pfenninger, Diversity of options to eliminate fossil fuels and reach carbon neutrality across the entire European energy system, Joule 6 (6) (2022) 1253–1276. [doi:10.1016/j.joule.2022.05.009](#).
- [7] M. Child, C. Kemfert, D. Bogdanov, C. Breyer, Flexible electricity generation, grid exchange and storage for the transition to a 100% renewable energy system in Europe, Renewable Energy 139 (2019) 80–101. [doi:10.1016/j.renene.2019.02.077](#).
- [8] M. Kendziorski, L. Göke, C. von Hirschhausen, C. Kemfert, E. Zozmann, Centralized and decentral approaches to succeed the 100% energiewende in Germany in the European context: A model-based analysis of generation, network, and storage investments (May 2022). [arXiv:2205.09066](#).
 URL <http://arxiv.org/abs/2205.09066>
- [9] European Commission. Directorate General for Energy., METIS Study on Costs and Benefits of a Pan-European Hydrogen Infrastructure: In Assistance to the Impact Assessment for Designing a Regulatory Framework for Hydrogen : METIS 3, Study S3., Publications Office, LU, 2021.
 URL <https://data.europa.eu/doi/10.2833/736971>
- [10] M. Victoria, E. Zeyen, T. Brown, Speed of technological transformations required in Europe to achieve different climate goals, Joule 6 (5) (2022) 1066–1086. [doi:10.1016/j.joule.2022.04.016](#).
- [11] H. C. Gils, H. Gardian, J. Schmugge, Interaction of hydrogen infrastructures with other sector coupling options towards a zero-emission energy system in Germany, Renewable Energy 180 (2021) 140–156. [doi:10/gmsxn7](#).
- [12] D. G. Caglayan, H. U. Heinrichs, D. Stolten, M. Robinius, The impact of temporal complexity reduction on a 100% renewable european energy system with hydrogen infrastructure (2019).
 URL <https://www.preprints.org/manuscript/201910.0150/v1>

- [13] D. G. Caglayan, H. U. Heinrichs, M. Robinius, D. Stolten, Robust design of a future 100% renewable european energy supply system with hydrogen infrastructure, International Journal of Hydrogen Energy 46 (57) (2021) 29376–29390. doi: [10.1016/j.ijhydene.2020.12.197](https://doi.org/10.1016/j.ijhydene.2020.12.197).
- [14] H.-M. Henning, A. Palzer, A comprehensive model for the German electricity and heat sector in a future energy system with a dominant contribution from renewable energy technologies—Part I: Methodology, Renewable and Sustainable Energy Reviews 30 (2014) 1003–1018. doi:[10.1016/j.rser.2013.09.012](https://doi.org/10.1016/j.rser.2013.09.012).
- [15] B. Mathiesen, H. Lund, D. Connolly, H. Wenzel, P. Østergaard, B. Möller, S. Nielsen, I. Ridjan, P. Karnøe, K. Sperling, F. Hvelplund, Smart Energy Systems for coherent 100% renewable energy and transport solutions, Applied Energy 145 (2015) 139–154. doi:[10.1016/j.apenergy.2015.01.075](https://doi.org/10.1016/j.apenergy.2015.01.075).
- [16] D. Connolly, H. Lund, B. Mathiesen, Smart Energy Europe: The technical and economic impact of one potential 100% renewable energy scenario for the European Union, Renewable and Sustainable Energy Reviews 60 (2016) 1634–1653. doi: [10.1016/j.rser.2016.02.025](https://doi.org/10.1016/j.rser.2016.02.025).
- [17] K. Löffler, K. Hainsch, T. Burandt, P.-Y. Oei, C. Kemfert, C. von Hirschhausen, Designing a Model for the Global Energy System—GENeSYS-MOD: An Application of the Open-Source Energy Modeling System (OSeMOSYS), Energies 10 (10) (2017) 1468. doi:[10.3390/en10101468](https://doi.org/10.3390/en10101468).
- [18] H. Blanco, W. Nijs, J. Ruf, A. Faaij, Potential for hydrogen and Power-to-Liquid in a low-carbon EU energy system using cost optimization, Applied Energy 232 (2018) 617–639. doi:[10.1016/j.apenergy.2018.09.216](https://doi.org/10.1016/j.apenergy.2018.09.216).
- [19] European Commission, In-depth analysis in support of the Comission Communication COM(2018) 773 A Clean Planet for all. A European long-term strategic vision for a prosperous, modern, competitive and climate neutral economy, Tech. rep. (2018).
URL https://ec.europa.eu/clima/system/files/2018-11/com_2018_733_analysis_in_support_en.pdf
- [20] M. Victoria, K. Zhu, T. Brown, G. Andresen, M. Greiner, Early decarbonisation of the European energy system pays off, Nature Communications 11 (1) (2020) 6223. doi:[10.1038/s41467-020-20015-4](https://doi.org/10.1038/s41467-020-20015-4).

- [21] Danish Energy Agency, [Technology data](#) (2020).
URL <https://ens.dk/en/our-services/projections-and-models/technology-data>
- [22] M. Fasihi, O. Efimova, C. Breyer, Techno-economic assessment of CO₂ direct air capture plants, *Journal of Cleaner Production* 224 (2019) 957–980. doi:[10.1016/j.jclepro.2019.03.086](https://doi.org/10.1016/j.jclepro.2019.03.086).
- [23] P.-M. Heuser, D. S. Ryberg, T. Grube, M. Robinius, D. Stolten, Techno-economic analysis of a potential energy trading link between Patagonia and Japan based on CO₂ free hydrogen, *International Journal of Hydrogen Energy* 44 (25) (2019) 12733–12747. doi:[10/ggd8rh](https://doi.org/10/ggd8rh).
- [24] J. Hampp, M. Düren, T. Brown, [Import options for chemical energy carriers from renewable sources to Germany](#), arXiv:2107.01092 [physics] (Jul. 2021). arXiv:2107.01092.
URL <http://arxiv.org/abs/2107.01092>
- [25] J.-P. Sasse, E. Trutnevyte, Distributional trade-offs between regionally equitable and cost-efficient allocation of renewable electricity generation, *Applied Energy* 254 (2019) 113724. doi:[10/gf69s8](https://doi.org/10/gf69s8).
- [26] J.-P. Sasse, E. Trutnevyte, Regional impacts of electricity system transition in Central Europe until 2035, *Nature Communications* 11 (1) (2020) 4972. doi:[10/ghdwjs](https://doi.org/10/ghdwjs).
- [27] F. Neumann, T. Brown, The near-optimal feasible space of a renewable power system model, *Electric Power Systems Research* 190 (2021) 106690. doi:[10.1016/j.epsr.2020.106690](https://doi.org/10.1016/j.epsr.2020.106690).
- [28] F. Lombardi, B. Pickering, E. Colombo, S. Pfenninger, Policy Decision Support for Renewables Deployment through Spatially Explicit Practically Optimal Alternatives, *Joule* (2020) S2542435120303482 doi:[10/gg8z6v](https://doi.org/10/gg8z6v).
- [29] T. T. Pedersen, M. Victoria, M. G. Rasmussen, G. B. Andresen, Modeling all alternative solutions for highly renewable energy systems, *Energy* 234 (2021) 121294. doi:[10.1016/j.energy.2021.121294](https://doi.org/10.1016/j.energy.2021.121294).
- [30] T. Brown, J. Hörsch, D. Schlachtberger, PyPSA: Python for Power System Analysis, *Journal of Open Research Software* 6 (2018) 4. doi:[10.5334/jors.188](https://doi.org/10.5334/jors.188).
- [31] H. Hersbach, B. Bell, P. Berrisford, S. Hirahara, A. Horányi, J. Muñoz-Sabater, J. Nicolas, C. Peubey, R. Radu, D. Schepers, A. Simmons, C. Soci, S. Abdalla, X. Abellan, G. Balsamo, P. Bechtold, G. Biavati, J. Bidlot, M. Bonavita, G. De Chiara,

- P. Dahlgren, D. Dee, M. Diamantakis, R. Dragani, J. Flemming, R. Forbes, M. Fuentes, A. Geer, L. Haimberger, S. Healy, R. J. Hogan, E. Hólm, M. Janisková, S. Keeley, P. Laloyaux, P. Lopez, C. Lupu, G. Radnoti, P. de Rosnay, I. Rozum, F. Vamborg, S. Villaume, J.-N. Thépaut, The ERA5 global reanalysis, *Quarterly Journal of the Royal Meteorological Society* 146 (730) (2020) 1999–2049. [doi:10/gg9wx7](https://doi.org/10/gg9wx7).
- [32] U. Pfeifroth, S. Kothe, R. Müller, J. Trentmann, R. Hollmann, P. Fuchs, M. Werscheck, Surface radiation data set - heliosat (SARAH) - edition 2 (2017). [doi:10/f77h](https://doi.org/10/f77h).
 - [33] J. Hörsch, F. Hofmann, D. Schlachtberger, T. Brown, PyPSA-Eur: An open optimisation model of the European transmission system, *Energy Strategy Reviews* 22 (2018) 207–215. [arXiv:1806.01613](https://arxiv.org/abs/1806.01613), [doi:10.1016/j.esr.2018.08.012](https://doi.org/10.1016/j.esr.2018.08.012).
 - [34] J. Hörsch, T. Brown, The role of spatial scale in joint optimisations of generation and transmission for European highly renewable scenarios, in: Proceedings of 14th International Conference on the European Energy Market (EEM 2017), Dresden, 2017. [doi:10.1109/eem.2017.7982024](https://doi.org/10.1109/eem.2017.7982024).
 - [35] M. M. Frysztacki, J. Hörsch, V. Hagenmeyer, T. Brown, The strong effect of network resolution on electricity system models with high shares of wind and solar, *Applied Energy* 291 (2021) 116726. [arXiv:2101.10859](https://arxiv.org/abs/2101.10859), [doi:10/gmdkqc](https://doi.org/10/gmdkqc).
 - [36] J. Hörsch, H. Ronellenfitsch, D. Witthaut, T. Brown, Linear optimal power flow using cycle flows, *Electric Power Systems Research* 158 (2018) 126–135. [arXiv:1704.01881](https://arxiv.org/abs/1704.01881), [doi:10/gdb8kx](https://doi.org/10/gdb8kx).
 - [37] A. Pluta, W. Medjroubi, J. C. Dietrich, J. Dasenbrock, H.-P. Tetens, J. E. Sandoval, O. Lunsdorf, SciGRID_gas - Data Model of the European Gas Transport Network, in: 2022 Open Source Modelling and Simulation of Energy Systems (OSMSES), IEEE, Aachen, Germany, 2022, pp. 1–7. [doi:10.1109/OSMSES54027.2022.9769122](https://doi.org/10.1109/OSMSES54027.2022.9769122).
 - [38] V. Vogl, M. Åhman, L. J. Nilsson, Assessment of hydrogen direct reduction for fossil-free steelmaking, *Journal of Cleaner Production* 203 (2018) 736–745. [doi:10.1016/j.jclepro.2018.08.279](https://doi.org/10.1016/j.jclepro.2018.08.279).
 - [39] Material Economics, **The circular economy – A powerful force for climate mitigation**, Tech. rep.
URL <https://www.sitra.fi/app/uploads/2018/06/the-circular-economy-a-powerful-force-for-climate-mitigation.pdf>

- [40] E. Zeyen, V. Hagenmeyer, T. Brown, Mitigating heat demand peaks in buildings in a highly renewable European energy system, Energy 231 (2021) 120784. [arXiv: 2012.01831](https://arxiv.org/abs/2012.01831), [doi:10.1016/j.energy.2021.120784](https://doi.org/10.1016/j.energy.2021.120784).
- [41] P. Ruiz, W. Nijs, D. Tarvydas, A. Sgobbi, A. Zucker, R. Pilli, R. Jonsson, A. Camia, C. Thiel, C. Hoyer-Klick, F. Dalla Longa, T. Kober, J. Badger, P. Volker, B. Elbersen, A. Brosowski, D. Thrän, ENSPRESO - an open, EU-28 wide, transparent and coherent database of wind, solar and biomass energy potentials, Energy Strategy Reviews 26 (2019) 100379. [doi:10/ggbgnk](https://doi.org/10/ggbgnk).

Supplementary Information

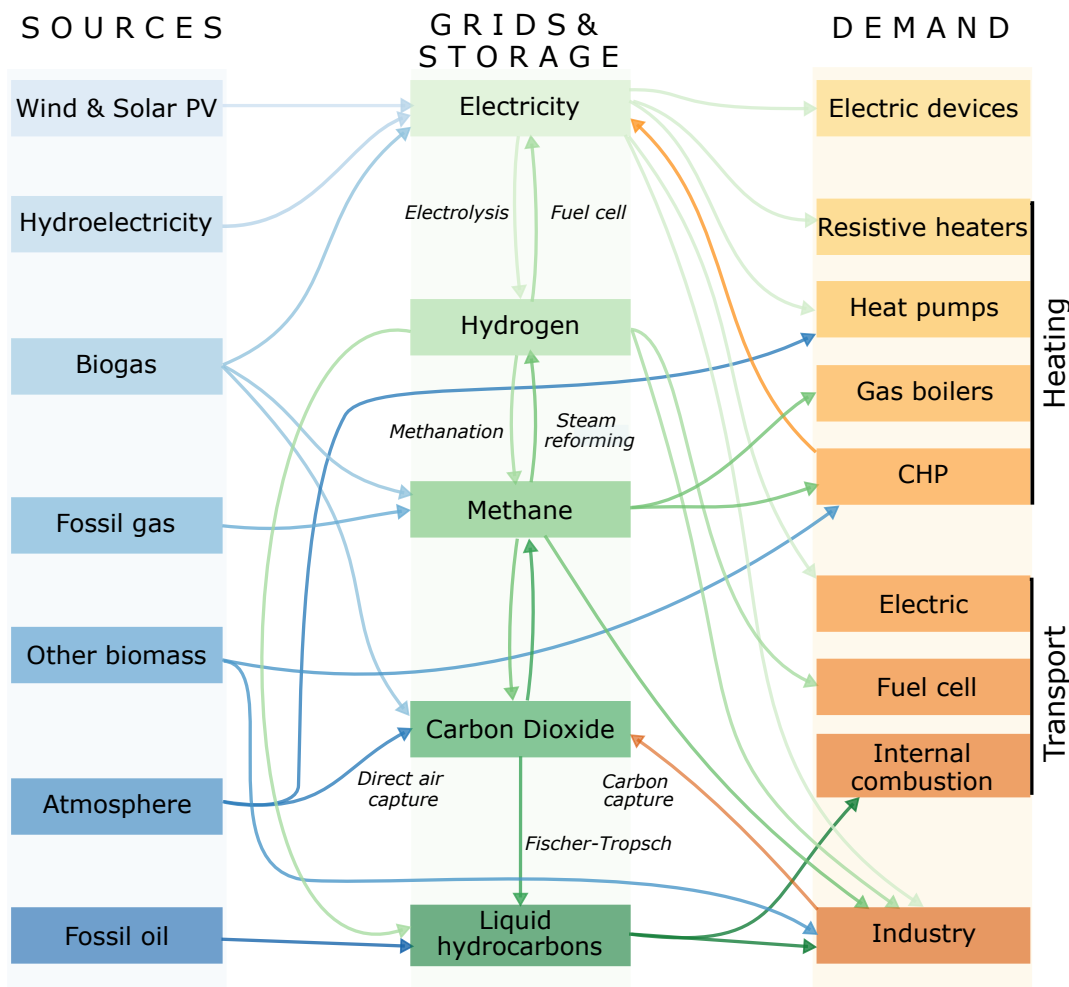


Figure S1: Overview of the circulation of energy and carbon in PyPSA-Eur-Sec.

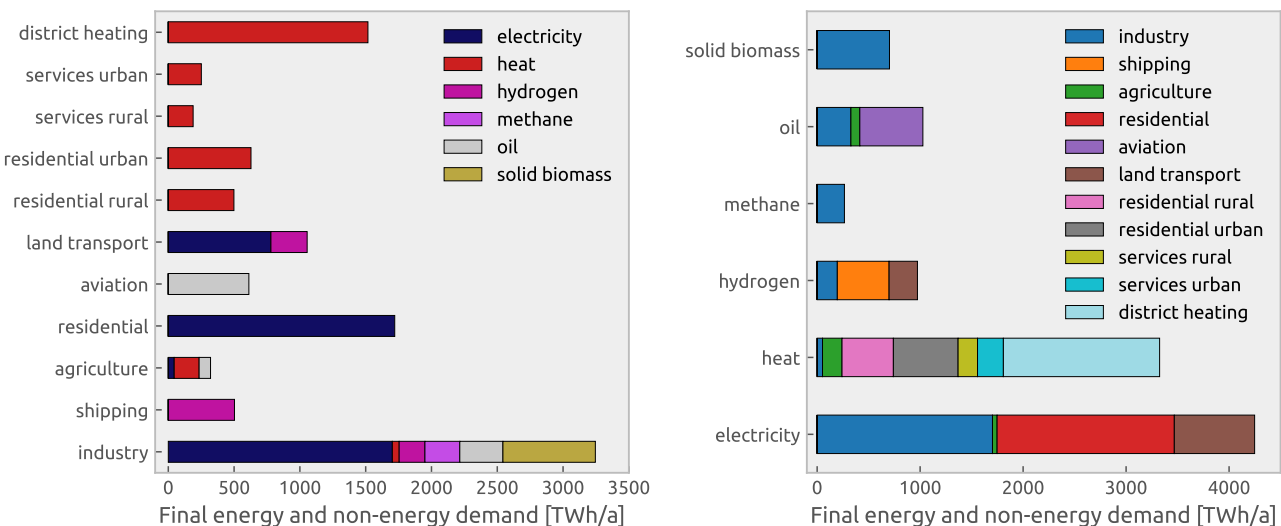


Figure S2: Annual final energy and non-energy demand by carrier and sector.

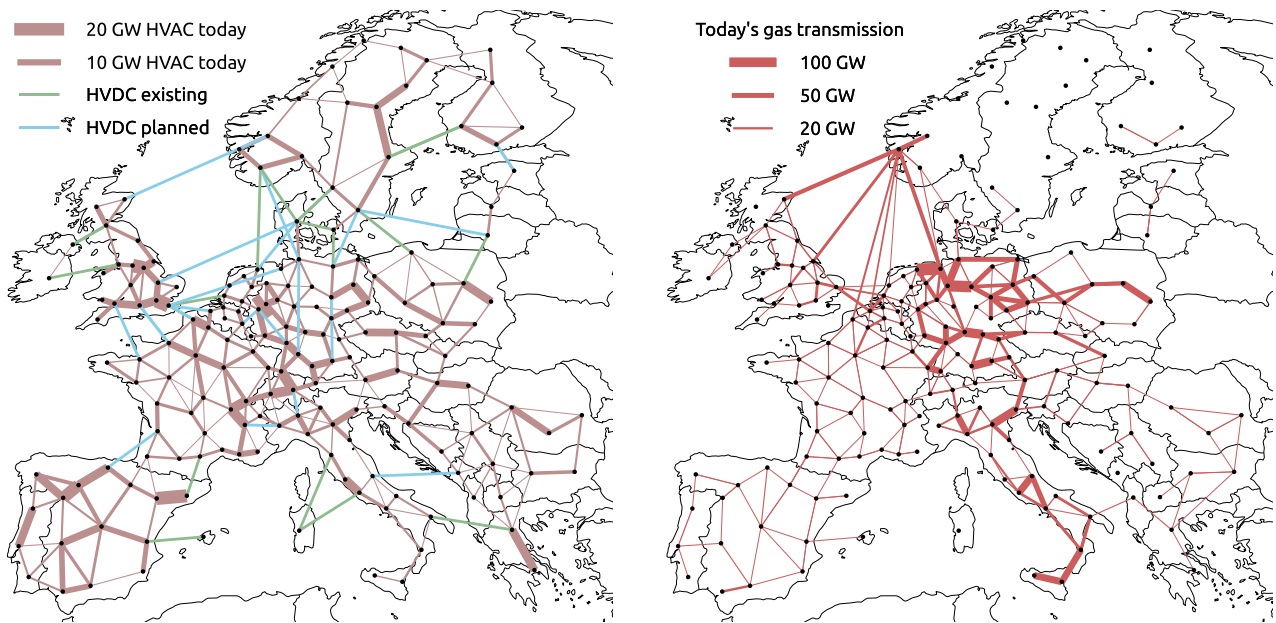


Figure S3: Clustered electricity and gas transmission networks before capacity expansion.

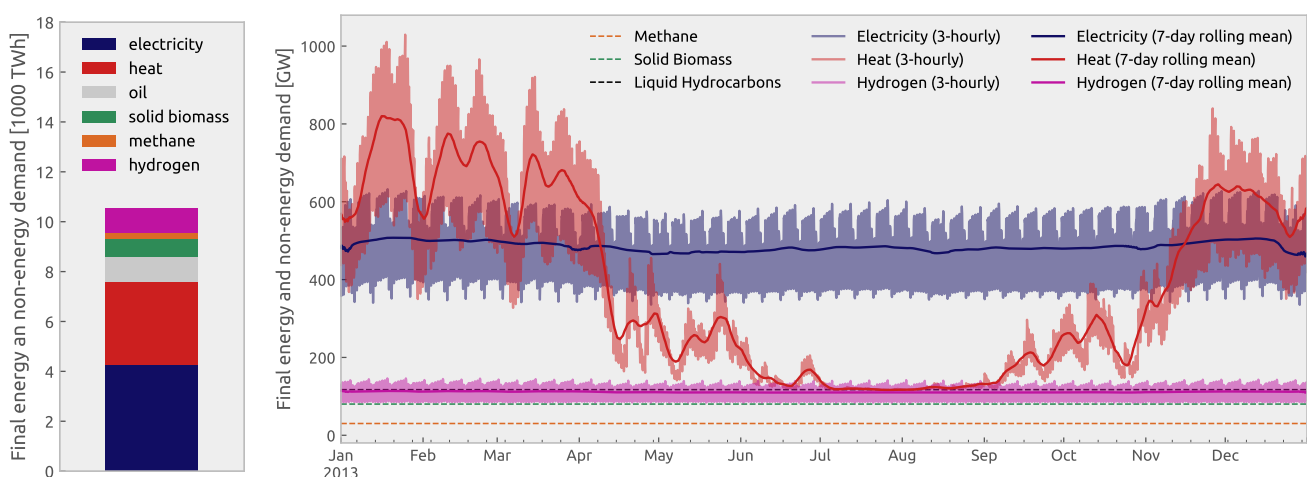


Figure S4: Annual final energy and non-energy demand (left) and system-level time series of demand by carrier (right).

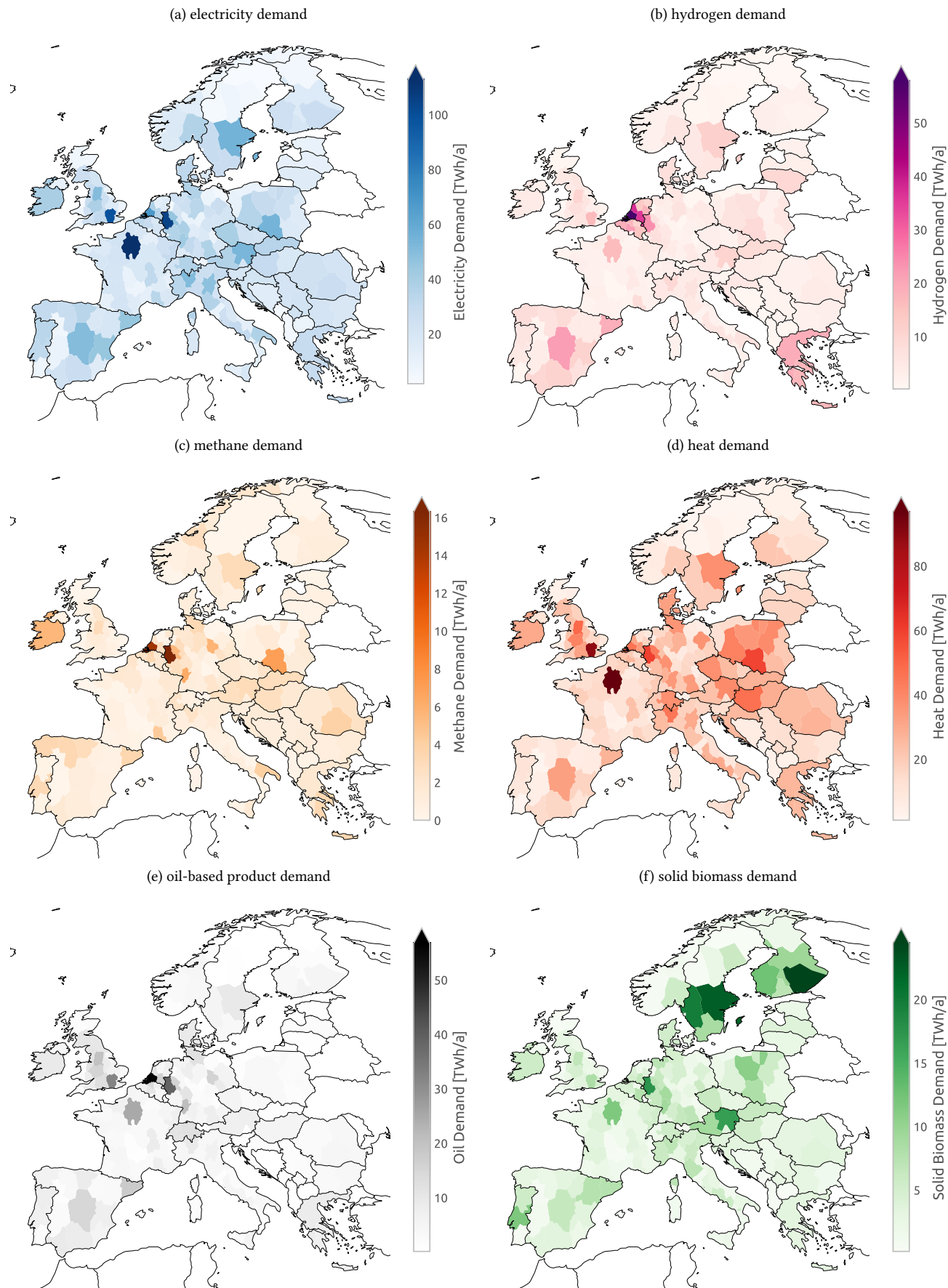


Figure S5: Spatial diversity of final energy and non-energy demand.

S1. Model Overview

PyPSA-Eur-Sec is an open model dataset of the European energy system at the transmission network level that covers the electricity, heating, transport and industry sectors. PyPSA-Eur-Sec builds a linear optimisation problem to plan energy system infrastructure from various open data sources using the workflow management tool Snakemake,^{S1} which is then solved with the commercial solver Gurobi.^{S2} The overall circulation of energy and carbon is shown in [Figure S1](#). The modelling approaches for the items listed there are described in detail in the following sections [Sections S2 to S11](#). A mathematical formulation of the model is provided in [Section S12](#). The clustered model resolution is shown in [Figure S3](#) together with the existing electricity and gas grid capacities. The carriers electricity, hydrogen, heat and biomass are nodally resolved, whereas other carriers like gas, oil and carbon dioxide are copperplated in the current version to reduce the problem's computational burden.

S2. Electricity Sector

Modelling of electricity supply and demand in Europe largely follows the open electricity generation and transmission model PyPSA-Eur^{S33}. PyPSA-Eur processes publicly available data on the topology of the power transmission network, historical time series of weather observations and electricity consumption, conventional power plants, and renewable potentials.

S2.1. Electricity Demand

Hourly electricity demand at country-level for the reference year 2013 published by ENTSO-E is retrieved via the interface of the Open Power System Data (OPSD) initiative.^{S4} Existing electrified heating is subtracted from this demand, so that power-to-heat options can be optimised separately. Furthermore, current industry electricity demand is subtracted and handled separately considering further electrification in the industry sector (see [Section S4](#)).

For the distribution of electricity demand for industry we leverage geographical data from the industrial database developed within the Hotmaps project.^{S5} The remaining electricity demand for households and services is heuristically distributed inside each country to 40% proportional to population density and to 60% proportional to gross domestic product based on a regression performed by Hörsch et al.^{S33}. The total spatial distribution of electricity demands is shown in [Figure S5a](#).

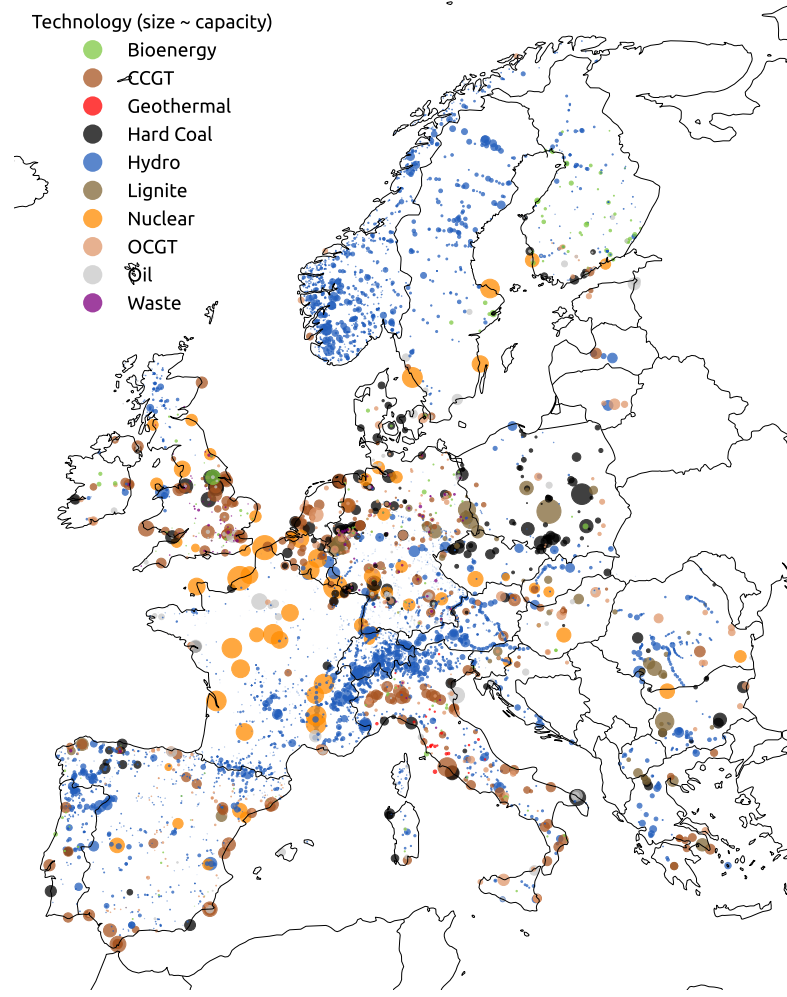


Figure S6: Existing conventional power plant capacities in Europe by technology. Marker size is proportional to nominal capacity.

S2.2. Electricity Supply

For conventional electricity generators, PyPSA-Eur-Sec uses the open *powerplantmatching* tool, which merges datasets from a variety of sources.^{S6} As shown in [Figure S6](#), it provides data on the power plants about their location, technology and fuel type, age, and capacity, including hard coal, lignite, oil, open and combined cycle gas turbines (OCGT and CCGT), and nuclear generators. Furthermore, existing run-of-river, pumped-hydro storage plants, and hydro-electric dams, are also part of the dataset, for which inflow is modelled based on runoff data from reanalysis weather data and scaled hydropower generation statistics (see [Section S6.2](#)). In general, we suppose these to be non-extendable due to assumed geographical constraints.

Expandable renewable generators include onshore and offshore wind, utility-scale and rooftop solar photovoltaics, biomass from multiple feedstocks. The model decides to build new capacities based on available land and on the weather resource (see [Section S6.1](#) and [Section S6.2](#)). Because the continent-wide availability of data on the locations of wind and solar installations is fragmentary, we disregard already existing wind and solar capacities. Moreover, new OCGT and CCGT as well as gas or biomass-fueled combined heat and power (CHP) generators may be built. For CHP generators we assume back-pressure operation with heat production proportional to electricity output. Specific techno-economic assumptions, like costs, lifetimes and efficiencies are included in [Section S16](#).

S2.3. Electricity Storage

Electric energy can be stored in batteries (home, utility-scale, electric vehicles), existing pumped-hydro storage (PHS), hydrogen storage and other synthetically produced energy carriers (like methane and oil). For stationary batteries we distinguish costs for inverters and for storage at home or utility-scale. With these assumptions, home battery storage is about 40% more expensive than utility-scale battery storage (see [Section S16](#)). The batteries' energy and power capacities can be independently sized.

To store electricity, hydrogen may be produced by water electrolysis (see [Section S7.2](#)), stored in overground steel tanks or underground salt caverns (see [Section S7.4](#)), and re-electrified in a utility-scale fuel cell. Synthetic methane can be re-electrified through an open cycle gas turbine (OCGT) or a combined heat and power (CHP) plant.

S2.4. Electricity Transport

The topology of the European electricity transmission network is represented at substation level based on maps released in the interactive ENTSO-E map^{S7} using a modified version of the GridKit tool.^{S8} As displayed in [Figure S7](#), the dataset includes HVAC lines at and above 220 kV across the multiple synchronous zones of the ENTSO-E area, but

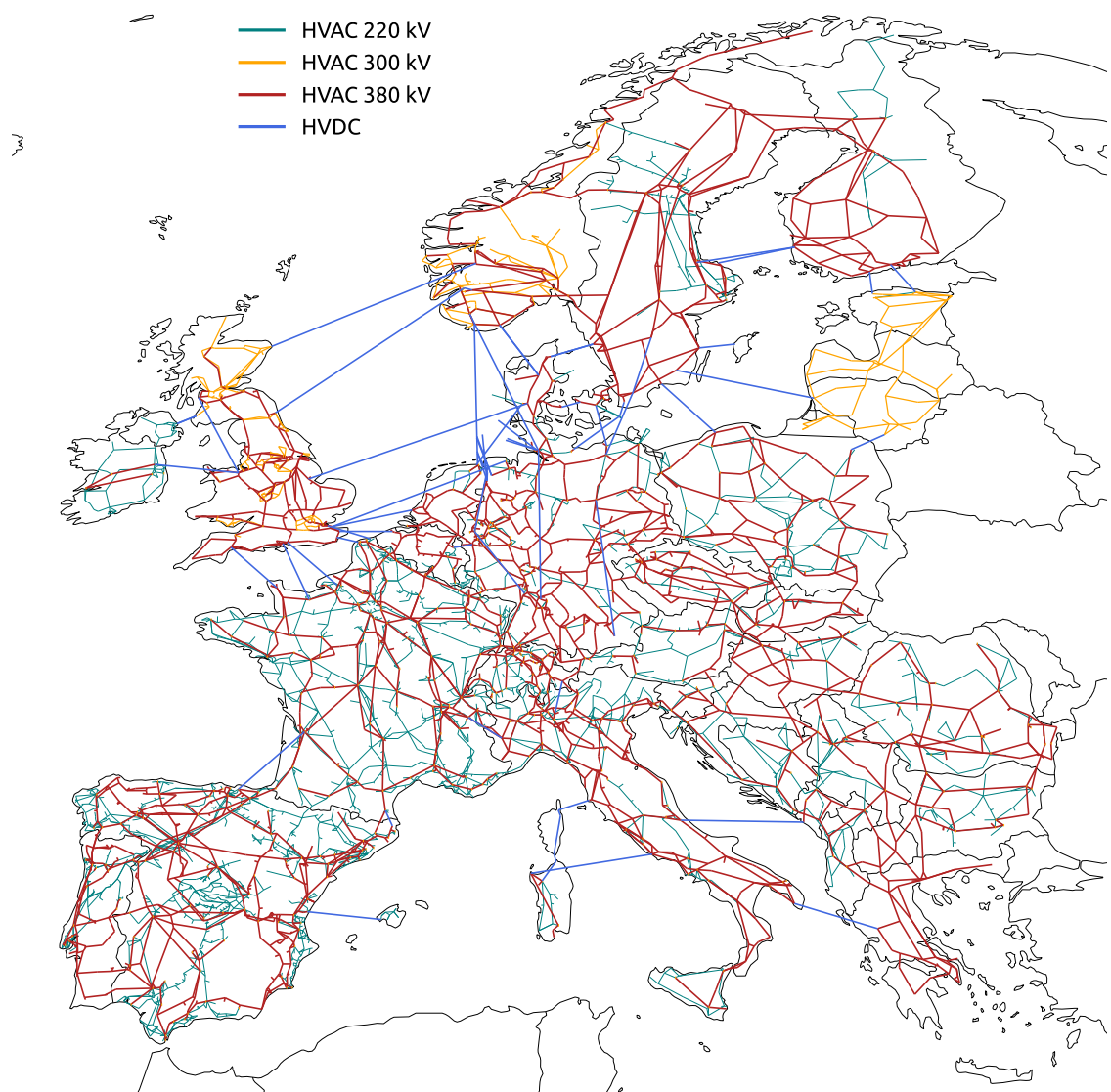


Figure S7: Unclustered European electricity transmission network by voltage level including planned TYNDP projects. Network data was retrieved from entsoe.eu/data/map and tyndp.entsoe.eu.

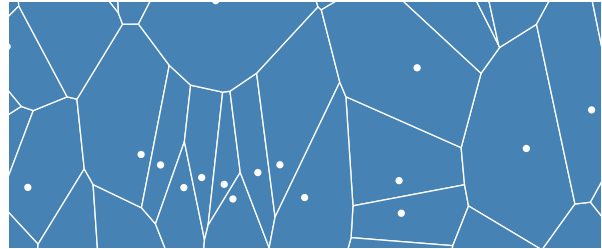


Figure S8: Exemplary Voronoi cells of the transmission network's substations.

excludes Turkey and North-African countries which are also synchronised to the continental European grid, interconnections to Russia, Belarus and Ukraine as well as small island networks with less than four nodes at transmission level, such as Cyprus, Crete and Malta. In total, the network encompasses around 3000 substations, 6600 HVAC lines and around 70 HVDC links, some of which are planned projects from the Ten Year Network Development Plant (TYNDP) that are not yet in operation.^{S9}

The transmission network topology determines the basic regions of the PyPSA-Eur-Sec model. Each substation has an associated Voronoi cell that describes the region that is closer to the substation than to any other substation except for country borders, which are kept to retain the integrity of country totals. Exemplary Voronoi cells are illustrated in Figure S8. We use these as geographical catchment area for demands, renewable resource potentials, and power plants, assuming that supply and demand always connect to the closest substation. The Voronoi cells are also computed for offshore regions based on the countries' Exclusive Economic Zones (EEZs) and the adjacent onshore substations.

Capacities and electrical characteristics of transmission lines and substations, such as impedances and thermal ratings, are inferred from standard types for each voltage level from Oeding and Oswald.^{S10} For each HVAC line, we further restrict line loading to 70% of the nominal rating to approximate $N - 1$ security, which protects the system against overloading if any one transmission line fails. This conservative security margin is commonly applied in the industry.^{S11} Dynamic line rating is not considered. Power flow is modelled through lossless linearised power flow equations using an efficient cycle-based formulation of Kirchhoff's voltage law.^{S36}

Solving the capacity expansion optimisation for the whole European energy system at full network resolution is too large to be solved in reasonable time. Therefore, we simplify the network topology by lowering the spatial resolution. We initially remove the network's radial paths, i.e. nodes with only one connection, by linking remote resources to adjacent nodes and transforming the network to a uniform voltage level of 380 kV. We also aggregate generators of the same kind that connect to the same substation. Based on

these initial simplification, the network resolution is further reduced to a variable number of nodes, in this case to 181 regions, by using a *k-means* clustering algorithm, which uses regional electricity consumption as weights.^{S34,S35} Only substations within the same country can be aggregated. The equivalent lines connecting the clustered regions are determined by the aggregated electro-technical characteristics of original transmission lines. Their weighted cost takes into consideration the underwater fraction of the lines and adds 25% to the crow-fly distance to approximate routing constraints. The clustered electricity network resolution and associated model regions, as shown in Figure S3, are applied uniformly to the other nodally resolved energy carriers as well.

Contrary to the transmission level, the grid topology at the distribution level (at and below 110 kV) is not included. Only the total power exchange capacity between transmission and distribution level is co-optimised. Costs of 500 €/kW are assumed as well as lossless distribution. Rooftop PV, heat pumps, resistive heaters, home batteries, electric vehicles and electricity demands are connected to the low-voltage level. All other remaining technologies connect directly to the transmission grid. In this way, distribution grid capacity is developed if it is beneficial to balance the local mismatch between supply and demand.

S3. Transport Sector

Transport and mobility comprises light and heavy road, rail, shipping and aviation transport. Annual energy demands for this sector are derived from the JRC-IDEES database.^{S15}

S3.1. Land Transport

The diffusion of battery electric vehicles (BEV) and fuel cell electric vehicles (FCEV) in land transport is exogenously defined. For 2050, we assume that 85% of land transport is electrified and 15% uses hydrogen fuel cells. No more internal combustion engines exist.

The energy savings gained by electrifying road transport, are computed through country-specific factors that compare the current final energy consumption of cars per distance travelled (average for Europe 0.7 kWh/km^{S15}) to the 0.18 kWh/km assumed for the battery-to-wheel efficiency of electric vehicles.

Weekly profiles of distances travelled published by the German Federal Highway Research Institute (BASt)^{S16} are used to generate hourly time series for each European country taking into account their local time. Furthermore, a temperature dependence is included in the time series to account for heating/cooling demand in transport. For tem-

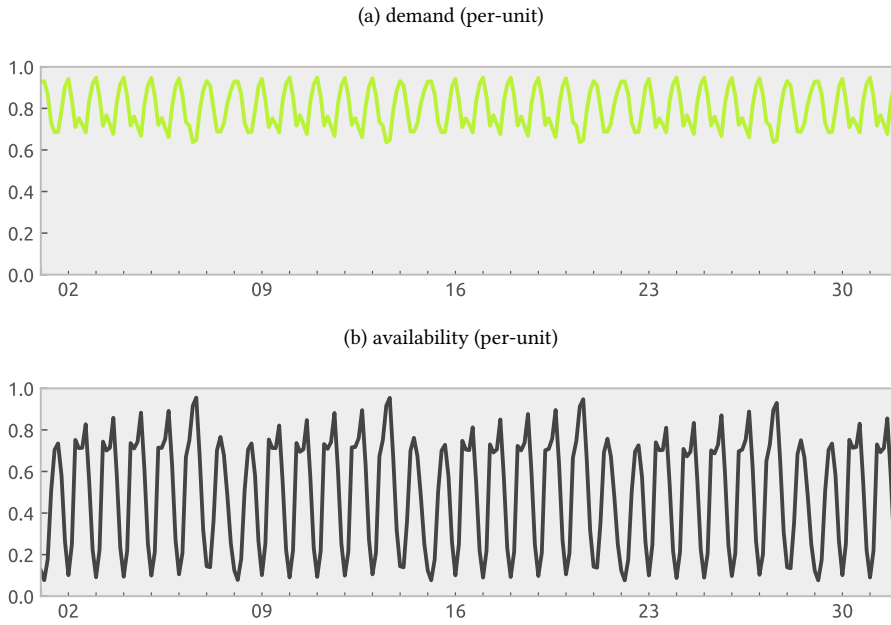


Figure S9: Normalised time series of battery electric vehicle demand and availability in December.

peratures below 15 °C and above 20 °C temperature coefficients of 0.98 %/°C and 0.63 %/°C are assumed. ^{S17}

For battery electric vehicles, we assume a storage capacity of 50 kWh, a charging capacity of 11 kW and a 90% charging efficiency. We assume that half of the BEV fleet can shift their charging time and participate in vehicle-to-grid (V2G) services to facilitate system operation. The BEV state of charge is forced to be higher than 75% at 7am every day to ensure that the batteries are sufficiently charged for the peak usage in the morning. This also restricts BEV demand to be shifted within a day and prevent EV batteries from becoming seasonal storage. The percentage of BEV connected to the grid at any time is inversely proportional to the transport demand profile, which translates into an average/minimum availability of 80%/62% of the time. These values are conservative compared to most of the literature, where average parking times of the European vehicle fleet is estimated at 92%. The battery cost of BEV is not included in the model since it is assumed that BEV owners buy them to primarily satisfy their mobility needs.

S3.2. Aviation

The aviation sector consumes kerosene that is synthetically produced or of fossil origin (see [Section S9.2](#)).

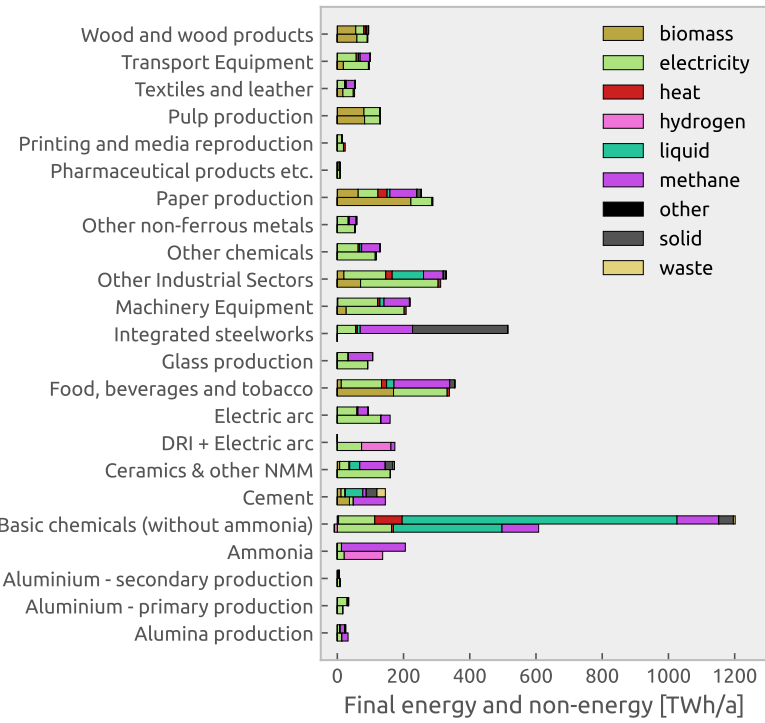


Figure S10: Final consumption of energy and non-energy feedstocks in industry today (top bar) and our future scenario in 2050 (bottom bar)

S3.3. Shipping

The shipping sector consumes liquid hydrogen. The liquefaction costs for hydrogen are taken into account. Other fuel options, like methanol or ammonia, are currently not considered.

S4. Industry Sector

Industry demand is split into a dozen different sectors with specific energy demands, process emissions of carbon dioxide, as well as existing and prospective mitigation strategies. [Section S4.1](#) provides a general description of the modelling approach for the industry sector in PyPSA-Eur-Sec. The following subsections describe the current energy demands, available mitigation strategies, and whether mitigation is exogenously fixed or co-optimised with the other components of the model for each industry subsector in more detail. In 2015, those subsectors with the largest final energy consumption in Europe were iron and steel, chemicals industry, non-metallic mineral products, pulp, paper and printing, food, beverages and tobacco, and non-ferrous metals. [S15](#)

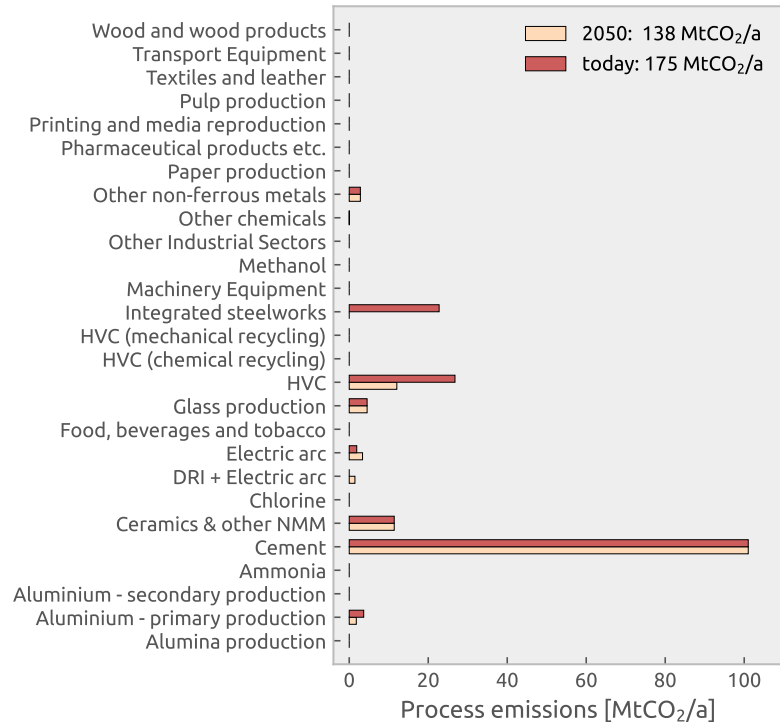


Figure S11: Process emissions in industry today (top bar) and in 2050 without carbon capture (bottom bar)

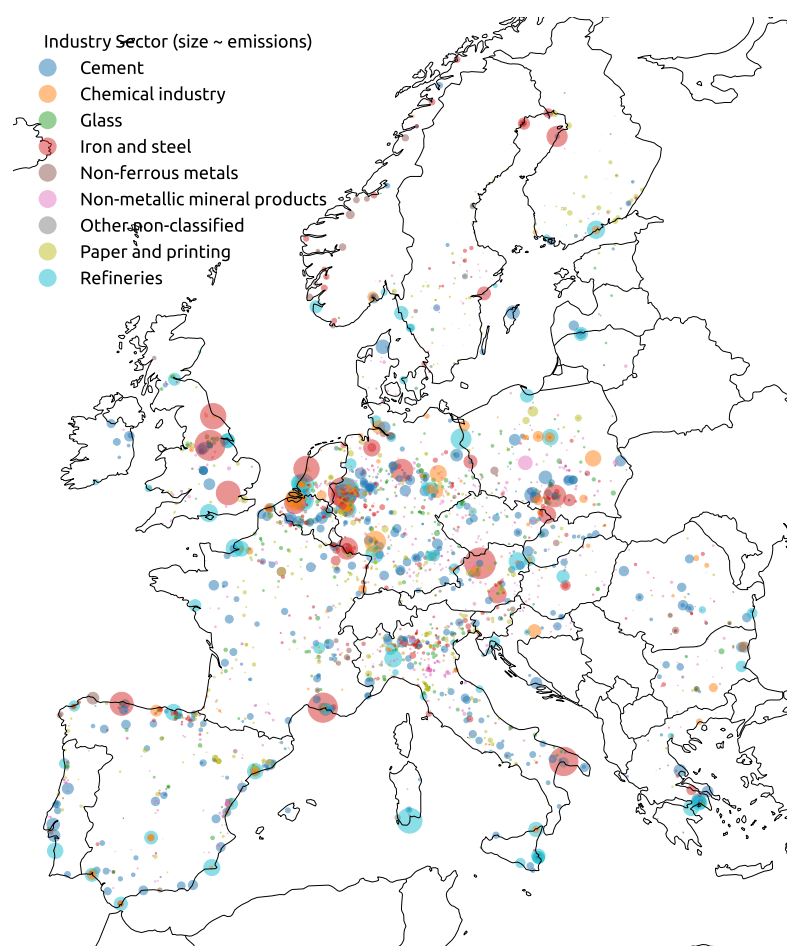


Figure S12: Distribution of industries according to emissions data from the Hotmaps industrial sites database. Marker size is proportional to the industrial site's reported emission levels.

S4.1. Overview

Greenhouse gas emissions associated with industry can be classified into energy-related and process-related emissions. Today, fossil fuels are used for process heat energy in the chemicals industry, but also as a non-energy feedstock for chemicals like ammonia (NH_3), ethylene (C_2H_4) and methanol (CH_3OH). Energy-related emissions can be curbed by using low-emission energy sources. The only option to reduce process-related emissions is by using an alternative manufacturing process or by assuming a certain rate of recycling so that a lower amount of virgin material is needed.

The overarching modelling procedure can be described as follows. First, the energy demands and process emissions for every unit of material output are estimated based on data from the JRC-IDEES database^{S15} and the fuel and process switching described in the subsequent sections. Second, the 2050 energy demands and process emissions are calculated using the per-unit-of-material ratios based on the industry transformations and the country-level material production in 2015, ^{S15} assuming constant material demand. Missing or too coarsely aggregated data in the JRC-IDEES database^{S15} is supplemented with additional datasets: Eurostat energy balances,^{S18} USGS for ammonia production,^{S19} DECHEMA for methanol and chlorine,^{S20} and national statistics from Switzerland.^{S21}

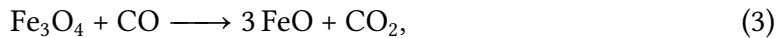
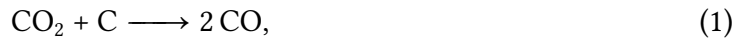
Where there are fossil and electrified alternatives for the same process (e.g. in glass manufacture or drying) we assume that the process is completely electrified. Current electricity demands (lighting, air compressors, motor drives, fans, pumps) will remain electric. Where process heat is required our approach depends on the temperature required.^{S22,S23} Processes that require temperatures below 500 °C are supplied with solid biomass, since we assume that residues and wastes are not suitable for high-temperature applications (Section S5.2). We see solid biomass use primarily in the pulp and paper industry, where it is already widespread, and in food, beverages and tobacco, where it replaces natural gas. Industries which require high temperatures (above 500 °C), such as metals, chemicals and non-metallic minerals are either electrified where suitable processes already exist, or the heat is provided with synthetic methane. Hydrogen for high-temperature process heat was not considered in our scenarios.^{S24} For Europe, Rehfeldt et al.^{S23} estimated that, from 2015 industrial heat demand, 45% is above 500 °C, 30% within 100 to 500 °C, 25% below 100 °C. Similarly, Naegler et al.^{S22} estimate that 48% is above 400 °C, 27% within 100 to 400 °C, 25% below 100 °C. Due to the high share of high-temperature process heat demand, we disregard geothermal and solar thermal energy as source for process heat. The final consumption of energy and non-energy feedstocks in industry today in comparison to our future scenario in 2050 are presented in Figure S10.

Inside each country the industrial demand is then distributed using the Hotmaps Industrial Database, which is illustrated in Figure S12.^{S5} This open database includes georeferenced industrial sites of energy-intensive industry sectors in EU28, including cement, basic chemicals, glass, iron and steel, non-ferrous metals, non-metallic minerals, paper, refineries subsectors. The use of this spatial dataset enables the calculation of regional and process specific energy demands. This approach assumes that there will be no significant migration of energy-intensive industries like, for instance, studied by Toktarova et al.^{S25} for the steel industry.

S4.2. Iron and Steel

Two alternative routes are used today to manufacture steel in Europe. The primary route (integrated steelworks) represents 60% of steel production, while the secondary route (electric arc furnaces), represents the other 40%.^{S26}

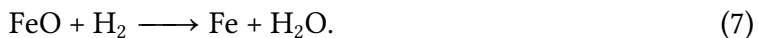
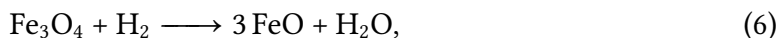
The primary route uses blast furnaces in which coke is used to reduce iron ore into molten iron.



which is then converted to steel. The primary route of steelmaking implies large process emissions of 0.22 t_{CO₂}/t of steel, amounting to 7% of global greenhouse gas emissions.^{S27}

In the secondary route, electric arc furnaces (EAF) are used to melt scrap metal. This limits the CO₂ emissions to the burning of graphite electrodes,^{S28} and reduces process emissions to 0.03 t_{CO₂}/t of steel.

Integrated steelworks can be replaced by direct reduced iron (DRI) and subsequent processing in an electric arc furnace (EAF)



This circumvents the process emissions associated with the use of coke. For hydrogen-based DRI we assume energy requirements of 1.7 MWh_{H₂}/t steel^{S38} and 0.322 MWh_{el}/t steel^{S30}.

The shares of steel produced via each of the three routes by 2050 is exogenously set in the model. We assume that hydrogen-based DRI plus EAF replaces integrated steelworks for primary production completely, representing 30% of total steel production (down from 60%). The remaining 70% (up from 40%) are manufactured through the secondary route using scrap metal in EAF. According to a Material Economics report,^{S39} circular economy practices even have the potential to expand the share of the secondary route to 85% by increasing the amount and quality of scrap metal collected. Bioenergy as alternative to coke in blast furnaces has not been considered.^{S32,S33}

For the remaining subprocesses in this sector, the following transformations are assumed. Methane is used as energy source for the smelting process. Activities associated with furnaces, refining and rolling, product finishing are electrified assuming the current efficiency values for these cases. These transformations result in changes in process emissions as outlined in [Figure S11](#).

S4.3. Chemicals Industry

The chemicals industry includes a wide range of diverse industries ranging from the production of basic organic compounds (olefins, alcohols, aromatics), basic inorganic compounds (ammonia, chlorine), polymers (plastics), end-user products (cosmetics, pharmaceuticals).

The chemicals industry consumes large amounts of fossil-fuel based feedstocks,^{S34} which can also be produced from renewables as outlined for hydrogen in [Section S7.2](#), for methane in [Section S8.2](#), and for oil-based products in [Section S9.2](#). The ratio between synthetic and fossil-based fuels used in the industry is an endogenous result of the optimisation.

The basic chemicals consumption data from the JRC IDEES^{S15} database comprises high-value chemicals (ethylene, propylene and BTX), chlorine, methanol and ammonia. However, it is necessary to separate out these chemicals because their current and future production routes are different.

Statistics for the production of ammonia, which is commonly used as a fertiliser, are taken from the United States Geological Survey (USGS) for every country.^{S19} Ammonia can be made from hydrogen and nitrogen using the Haber-Bosch process.^{S34}



The Haber-Bosch process is not explicitly represented in the model, such that demand for ammonia enters the model as a demand for hydrogen ($6.5 \text{ MWh}_{\text{H}_2}/\text{t}_{\text{NH}_3}$) and electricity ($1.17 \text{ MWh}_{\text{el}}/\text{t}_{\text{NH}_3}$).^{S35} Today, natural gas dominates in Europe as the source for the

hydrogen used in the Haber-Bosch process, but the model can choose among the various hydrogen supply options described in [Section S7.2](#)

The total production and specific energy consumption of chlorine and methanol is taken from a DECHEMA report.^{S20} According to this source, the production of chlorine amounts to 9.58 Mt_{Cl}/a, which is assumed to require electricity at 3.6 MWh_{el}/t of chlorine and yield hydrogen at 0.937 MWh_{H₂}/t of chlorine in the chloralkali process. The production of methanol adds up to 1.5 Mt_{MeOH}/a, requiring electricity at 0.167 MWh_{el}/t of methanol and methane at 10.25 MWh_{CH₄}/t of methanol.

The production of ammonia, methanol, and chlorine production is deducted from the JRC IDEES basic chemicals, leaving the production totals of high-value chemicals. For this, we assume that the liquid hydrocarbon feedstock comes from synthetic or fossil-origin naphtha (14 MWh_{naphtha}/t of HVC, similar to Lechtenböhmer et al.^{S26}), ignoring the methanol-to-olefin route. Furthermore, we assume the following transformations of the energy-consuming processes in the production of plastics: the final energy consumption in steam processing is converted to methane since requires temperature above 500 °C (4.1 MWh_{CH₄}/t of HVC);^{S23} and the remaining processes are electrified using the current efficiency of microwave for high-enthalpy heat processing, electric furnaces, electric process cooling and electric generic processes (2.85 MWh_{el}/t of HVC).

The process emissions from feedstock in the chemical industry are as high as 0.369 t_{CO₂}/t of ethylene equivalent. We consider process emissions for all the material output, which is a conservative approach since it assumes that all plastic-embedded CO₂ will eventually be released into the atmosphere. However, plastic disposal in landfilling will avoid, or at least delay, associated CO₂ emissions.

Circular economy practices drastically reduce the amount of primary feedstock needed for the production of plastics in the model^{S36–S39} and, consequently, also the energy demands and level of process emissions^{S40} (see [Figure S11](#)). We assume that 30% of plastics are mechanically recycled requiring 0.547 MWh_{el}/t of HVC,^{S38} 15% of plastics are chemically recycled requiring 6.9 MWh_{el}/t of HVC based on pyrolysis and electric steam cracking,^{S41} and 10% of plastics are reused (equivalent to reduction in demand). The remaining 45% need to be produced from primary feedstock. In comparison, Material Economics^{S39} presents a scenario with circular economy scenario with 27% primary production, 18% mechanical recycling, 28% chemical recycling, and 27% reuse. Another new-processes scenario has 33% primary production, 14% mechanical recycling, 40% chemical recycling, and 13% reuse.

S4.4. Non-metallic Mineral Products

This subsector includes the manufacturing of cement, ceramics, and glass.

Cement

Cement is used in construction to make concrete. The production of cement involves high energy consumption and large process emissions. The calcination of limestone to chemically reactive calcium oxide, also known as lime, involves process emissions of 0.54 t_{CO₂}/t cement.^{S42}



Additionally, CO₂ is emitted from the combustion of fossil fuels to provide process heat. Thereby, cement constitutes the biggest source of industry process emissions in Europe (Figure S11).

Cement process emissions can be captured assuming a capture rate of 90%.^{S21} Whether emissions are captured is decided by the model taking into account the capital costs of carbon capture modules. The electricity and heat demand of process emission carbon capture is currently ignored. For net-zero emission scenarios, the remaining process emissions need to be compensated by negative emissions.

With the exception of electricity demand and biomass demand for low-temperature heat (0.06 MWh/t and 0.2 MWh/t), the final energy consumption of this subsector is assumed to be supplied by methane (0.52 MWh/t), which is capable of delivering the required high-temperature heat. This implies a switch from burning solid fuels to burning gas which will require adjustments of the kilns.^{S44}

Other mitigation strategies to reduce energy consumption or process emissions (using new raw materials, recovering unused cement from concrete at end of life, oxyfuel cement production to facilitate carbon sequestration, electric kilns for heat provision) are at a early development stage and have therefore not been considered.^{S45}

Ceramics

The ceramics sector is assumed to be fully electrified based on the current efficiency of already electrified processes which include microwave drying and sintering of raw materials, electric kilns for primary production processes, electric furnaces for the product finishing.^{S15} In total, the final electricity consumption is 0.44 MWh/t of ceramic. The manufacturing of ceramics includes process emissions of 0.03 t_{CO₂}/t of ceramic. For a detailed overview of the ceramics industry sector see Furszyfer Del Rio et al.^{S46}

Glass

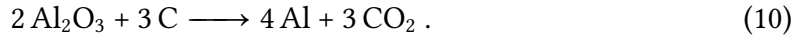
The production of glass is assumed to be fully electrified based on the current efficiency of electric melting tanks and electric annealing which adds up to an electricity demand of 2.07 MWh_{el}/t of glass^{S26}. The manufacturing of glass incurs process emissions of 0.1 t_{CO₂}/t of glass. Potential efficiency improvements, which according to Lechtenböhmer et al.^{S26} could reduce energy demands to 0.85 MWh_{el}/t of glass, have not been considered. For a detailed overview of the glass industry sector see Furszyfer Del Rio et al.^{S47}

S4.5. Non-ferrous Metals

The non-ferrous metal subsector includes the manufacturing of base metals (aluminium, copper, lead, zinc), precious metals (gold, silver), and technology metals (molybdenum, cobalt, silicon).

The manufacturing of aluminium accounts for more than half of the final energy consumption of this subsector. Two alternative processing routes are used today to manufacture aluminium in Europe. The primary route represents 40% of the aluminium production, while the secondary route represents the remaining 60%.

The primary route involves two energy-intensive processes: the production of alumina from bauxite (aluminium ore) and the electrolysis to transform alumina into aluminium via the Hall-Héroult process



The primary route requires high-enthalpy heat (2.3 MWh/t) to produce alumina which is supplied by methane and causes process emissions of 1.5 t_{CO₂}/t aluminium. According to Friedrichsen et al.,^{S28} inert anodes might become commercially available by 2030 that would eliminate the process emissions. However, they have not been considered in this study. Assuming all subprocesses are electrified, the primary route requires 15.4 MWh_{el}/t of aluminium.

In the secondary route, scrap aluminium is remelted. The energy demand for this process is only 10% of the primary route and there are no associated process emissions. Assuming all subprocesses are electrified, the secondary route requires 1.7 MWh/t of aluminium. Following Friedrichsen et al.,^{S28} we assume a share of recycled aluminium of 80% by 2050.

For the other non-ferrous metals, we assume the electrification of the entire manufacturing process with an average electricity demand of 3.2 MWh_{el}/t lead equivalent.

S4.6. Other Industry Subsectors

The remaining industry subsectors include (a) pulp, paper, printing, (b) food, beverages, tobacco, (c) textiles and leather, (d) machinery equipment, (e) transport equipment, (f) wood and wood products, (g) others. Low- and mid-temperature process heat in these industries is assumed to be supplied by biomass,^{S48} while the remaining processes are electrified. None of the subsectors involve process emissions.

Energy demands for the agriculture, forestry and fishing sector per country are taken from the JRC IDEES database.^{S15} Missing countries are filled with eurostat data.^{S18} Agricultural energy demands are split into electricity (lighting, ventilation, specific electricity uses, electric pumping devices), heat (specific heat uses, low enthalpy heat) machinery oil (motor drives, farming machine drives, diesel-fueled pumping devices). Heat demand is for this sector is classified as services rural heat. Time series for demands are assumed to be constant and distributed inside countries in proportion to population.

S5. Heating Sector

S5.1. Heat Demand

Building heating considering space and water heating in the residential and services sectors is resolved for each region, both for individual buildings and district heating systems, which include different supply options.

Annual heat demands per country are retrieved from JRC-IDEES^{S15} for the year 2011 and split into space and water heating. The space heating demand is reduced by retrofitting measures that improve the buildings' thermal envelopes. This reduction is exogenously fixed at 29%.^{S40} For space heating, the annual demands are converted to daily values based on the population-weighted Heating Degree Day (HDD) using the *atlite* tool,^{S50} where space heat demand is proportional to the difference between the daily average ambient temperature (read from ERA5^{S31}) and a threshold temperature above which space heat demand is zero. A threshold temperature of 15 °C is assumed. The daily space heat demand is distributed to the hours of the day following heat demand profiles from BDEW.^{S52} These differ for weekdays and weekends/holidays and between residential and services demand. Hot water demand is assumed to be constant throughout the year.

For every country, heat demand is split between low and high population density areas. These country-level totals are then distributed to each region in proportion to their rural and urban populations respectively. Urban areas with dense heat demand can be supplied with large-scale district heating systems. We assume that by 2050, 60% of urban heat demand is supplied by district heating networks. Lump-sum losses of 15% are assumed

in district heating systems. Cooling demand is supplied by electricity and included in the electricity demand. Cooling demand is assumed to remain at current levels.

The regional distribution of the total heat demand is depicted in [Figure S5d](#). As [Figure S4](#) reveals, the total heat demand is similar to the total electricity demand but features much more pronounced seasonal variations. The total building heating demand adds up to 3084 TWh/a of which 78% occurs in urban areas.

S5.2. Heat Supply

Different supply options are available depending on whether demand is met centrally through district heating systems or decentrally through appliances in individual buildings. Supply options in individual buildings include gas and oil boilers, air- and ground-sourced heat pumps, resistive heaters, and solar thermal collectors. For large-scale district heating systems more options are available: combined heat and power (CHP) plants consuming gas or biomass from waste and residues with and without carbon capture (CC), large-scale air-sourced heat pumps, gas and oil boilers, resistive heaters and fuel cell CHPs. Additionally, waste heat from the Fischer-Tropsch and Sabatier processes for the production of synthetic hydrocarbons can supply district heating systems. Ground-source heat pumps are only allowed in rural areas because of space constraints. Thus, only air-source heat pumps are allowed in urban areas. This is a conservative assumption, since there are many possible sources of low-temperature heat that could be tapped in cities (e.g. waste water, ground water, or natural bodies of water). Costs, lifetimes and efficiencies for these technologies are listed in [Section S16](#).

CHPs are based on back pressure plants operating with a fixed ratio of electricity to heat output. The efficiencies of each are given on the back pressure line, where the back pressure coefficient c_b is the electricity output divided by the heat output. For biomass CHP, we assume $c_b = 0.46$, whereas for gas CHP, we assume $c_b = 1$.

The coefficient of performance (COP) of air- and ground-sourced heat pumps depends on the ambient or soil temperature respectively. Hence, the COP is a time-varying parameter. Generally, the COP will be lower during winter when temperatures are low. Because the ambient temperature is more volatile than the soil temperature, the COP of ground-sourced heat pumps is less variable. Moreover, the COP depends on the difference between the source and sink temperatures

$$\Delta T = T_{sink} - T_{source}. \quad (11)$$

For the sink water temperature T_{sink} we assume 55 °C. For the time- and location-dependent source temperatures T_{source} , we rely on the ERA5 reanalysis weather data.^{[S31](#)} The temperature differences are converted into COP time series using results from a regression

Table S1: Land types considered suitable for every technology from Corine Land Cover database. Land type codes are referenced in brackets.

Solar PV	artificial surfaces (1-11), agriculture land except for those areas already occupied by agriculture with significant natural vegetation and agro-forestry areas (12-20), natural grasslands (26), bare rocks (31), sparsely vegetated areas (32)
Onshore wind	agriculture areas (12-22), forests (23-25), scrubs and herbaceous vegetation associations (26-29), bare rocks (31), sparsely vegetated areas (32)
Offshore wind	sea and ocean (44)

analysis performed in.^{S53} For air-sourced heat pumps (ASHP), we use the function

$$COP(\Delta T) = 6.81 + 0.121\Delta T + 0.000630\Delta T^2; \quad (12)$$

for ground-sourced heat pumps (GSHP), we use the function

$$COP(\Delta T) = 8.77 + 0.150\Delta T + 0.000734\Delta T^2. \quad (13)$$

The resulting time series are displayed in Figure S16. The spatial diversity of heat pump coefficients is shown in Figure S17.

S5.3. Heat Storage

Thermal energy storage (TES) is available in large water pits associated with district heating networks and small water tanks for individual, decentral applications. A thermal energy density $46.8 \text{ kWh}_{\text{th}}/\text{m}^3$ is assumed, corresponding to temperature difference of 40 K. The decay of thermal energy $1 - \exp(-1/24\tau)$ is assumed to have a time constant of $\tau = 180$ days for central TES and $\tau = 3$ days for individual TES. The charging and discharging efficiencies are 90% due to pipe losses.

S6. Renewables

S6.1. Potentials

Eligible areas for developing renewable infrastructure are calculated per technology and substation's Voronoi cell using the *atlite*^{S50} tool and shown in Figure S13.

The land available for wind and utility-scale solar PV capacities in a particular region is constrained by eligible codes of the CORINE^{S54} land use database (100m resolution) and is further restricted by distance criteria and the natural protection areas specified in the

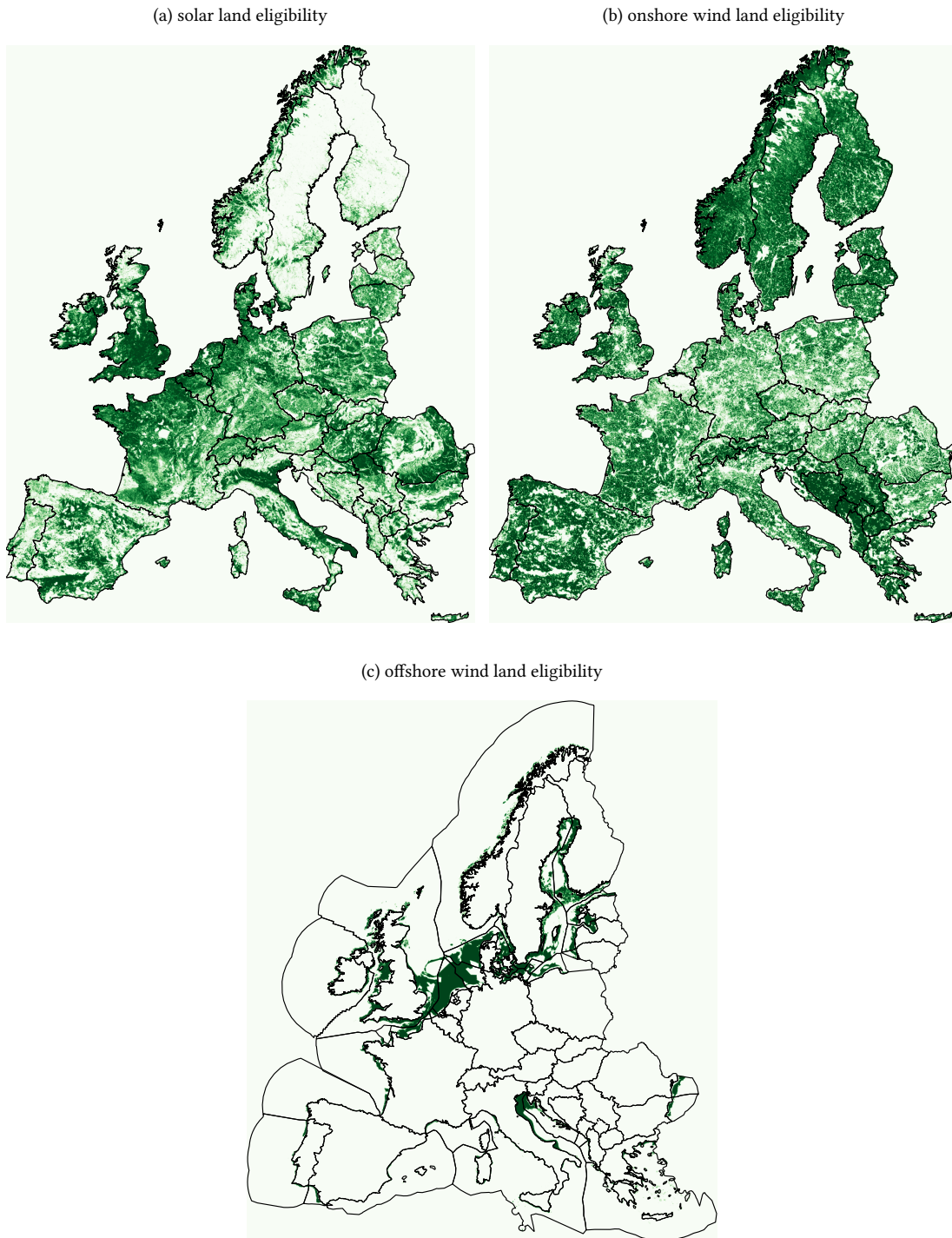


Figure S13: Land eligibility for the development of renewable generation capacities. Green color indicates areas eligible to build wind or utility-scale solar parks based on suitable land types, natural protection areas, and water depths.

Natura 2000^{S55} dataset. These criteria are summarised in [Table S1](#). The installable potentials for rooftop PV are included with an assumption of 1 kWp per person (0.1 kW/m^2 and $10 \text{ m}^2/\text{person}$). A more sophisticated potential estimate can be found in Bódis et al.^{S56}. Moreover, offshore wind farms may not be built at sea depths exceeding 50 m, as indicated by the GEBCO^{S57} bathymetry dataset. This currently disregards the possibility of floating wind turbines.^{S58–S62} For near-shore locations (less than 30 km off the shore) AC connections are considered, whereas for far-shore locations, DC connections including AC-DC converter costs are assumed. Reservoir hydropower and run-of-river capacities are exogenously fixed at current values and not expandable.

To express the potential in terms of installable capacities, the available areas are multiplied with allowed deployment densities, which we consider to be a fraction of the technology's technical deployment density to preempt public acceptance issues. These densities are 3 MW/m^2 for onshore wind, 2 MW/m^2 for offshore wind, 5.1 MW/m^2 for utility-scale solar. For a review of alternative potential wind potential assessments, see McKenna et al.^{S63} and Ryberg et al.^{S64}.

S6.2. Time Series

The location-dependent renewables availability time series are generated based on two gridded historical weather datasets ([Figure S14](#)). We retrieve wind speeds at 100 m, surface roughness, soil and air temperatures, and surface run-off from rainfall or melting snow from the global ERA5 reanalysis dataset provided by the ECMWF^{S31}. It provides hourly values for each of these parameters since 1950 on a $0.25^\circ \times 0.25^\circ$ grid. In Germany, such a weather cell expands approximately 20 km from east to west and 31 km from north to south. For the direct and diffuse solar irradiance, we use the satellite-aided SARAH-2 dataset^{S32}, which assesses cloud cover in more detail than the ERA5 dataset. It features values from 1983 to 2015 at an even higher resolution with a $0.05^\circ \times 0.05^\circ$ grid and 30-minute intervals^{S32}. In general, the reference weather year can be freely chosen for the optimisation, but in this contribution all analyses are based on the year 2013, which is regarded as characteristic year for both wind and solar resources (e.g.^{S66}).

Models for wind turbines, solar panels, heat pumps and the inflow into hydro basins convert the weather data to hourly time series for capacity factors and performance coefficients. Using power curves of selected wind turbines types (Vestas V112 for onshore, NREL 5MW for offshore), wind speeds scaled to the according hub height are mapped to power outputs. For offshore wind, we additionally take into account wake effects by applying a uniform correction factor of 88.55% to the capacity factors^{S67}. The solar photovoltaic panels' output is calculated based on the incidence angle of solar irradiation, the panel's tilt angle, and conversion efficiency. Similarly, solar thermal generation is de-

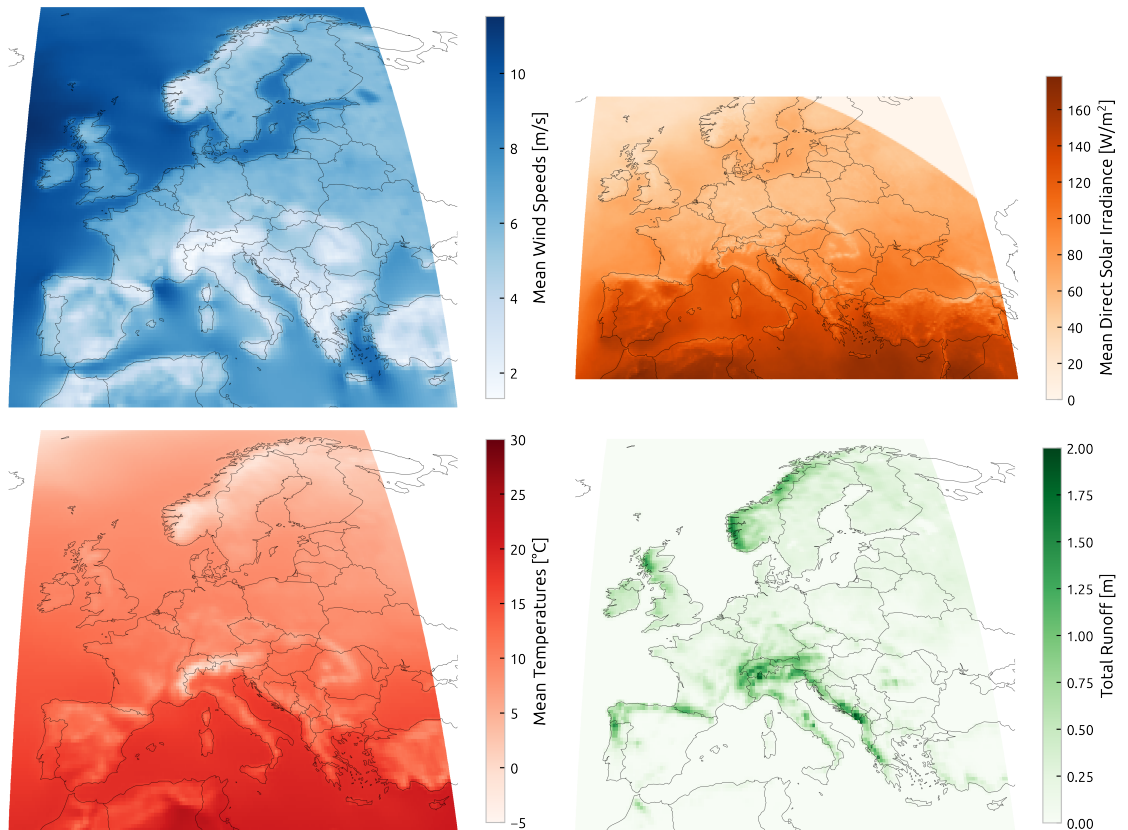


Figure S14: weather data

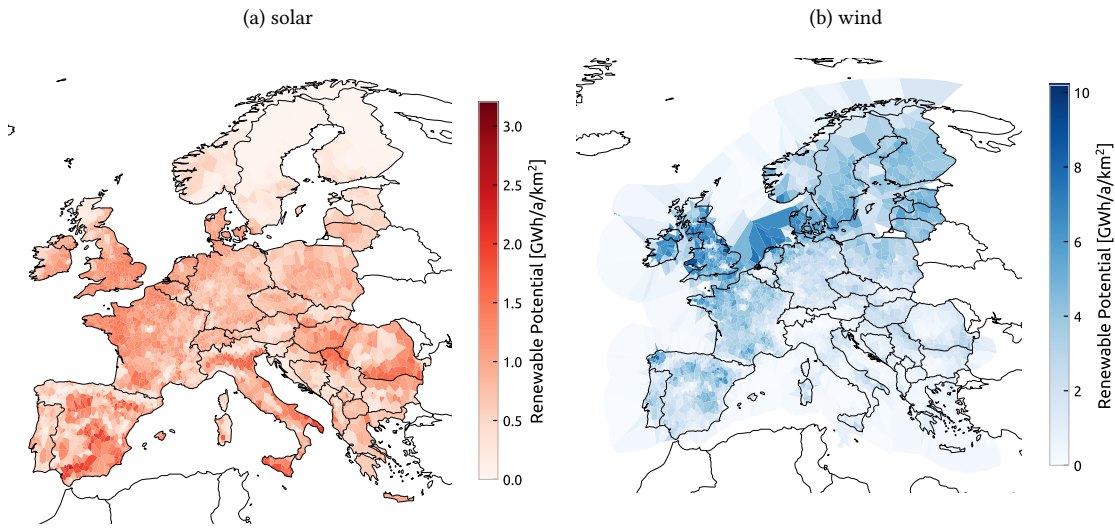


Figure S15: Available energy density for wind and utility-scale solar PV power generation.

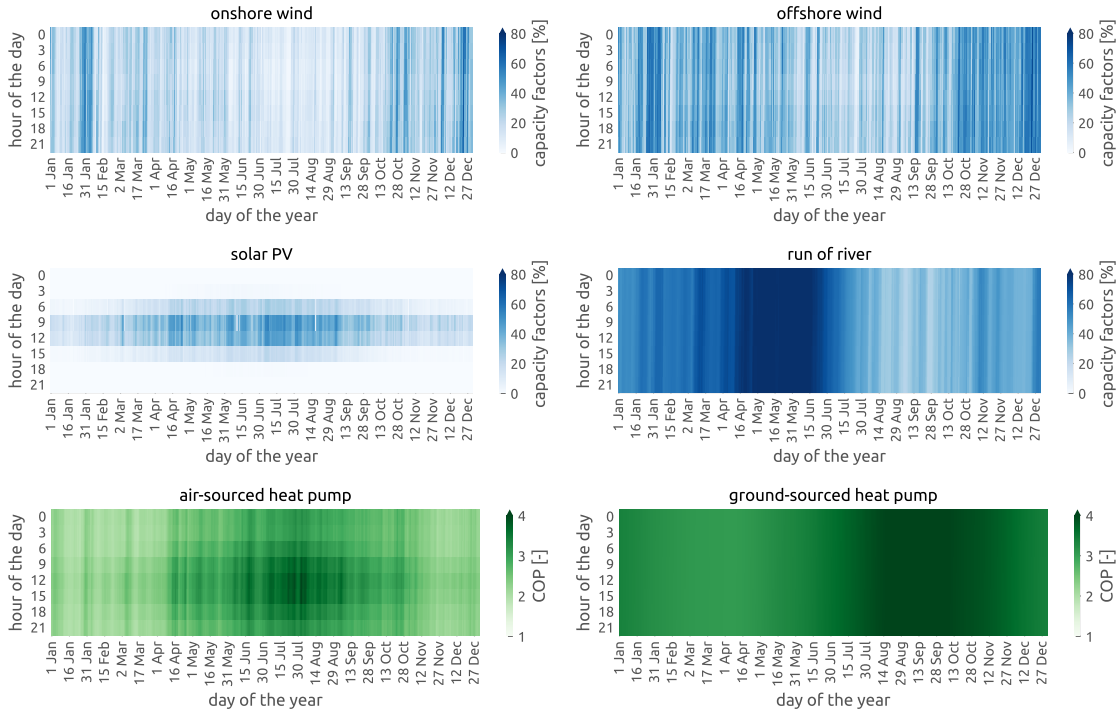


Figure S16: Spatially aggregated capacity factor time series of renewable energy sources.

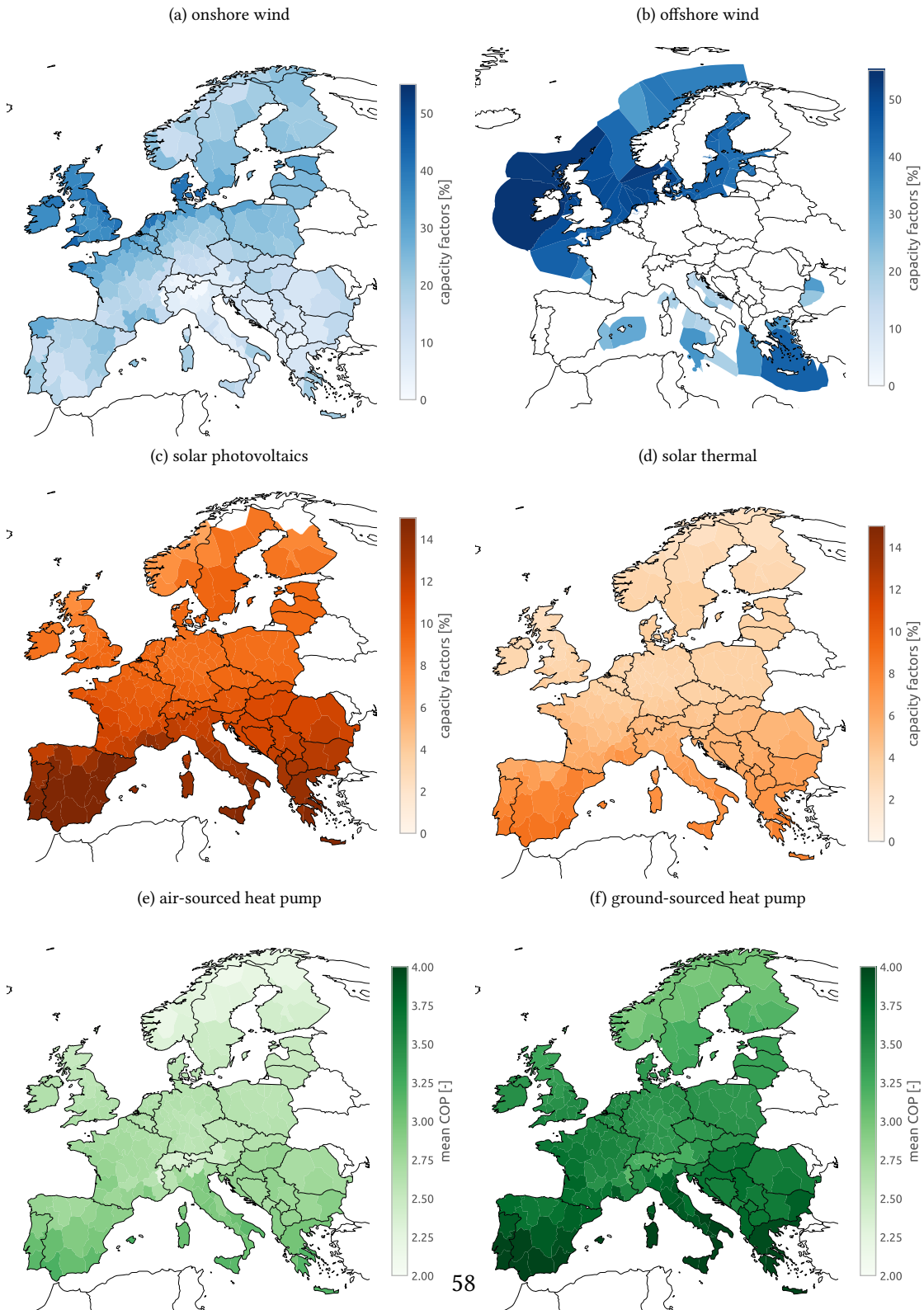


Figure S17: Regional distribution of average capacity factors of renewable energy sources.

terminated based on collector orientation and a clear-sky model based on ^{S68}. The creation of heat pump time series follows regression analyses that map soil or air temperatures to the coefficient of performance (COP)^{S53,S69}. Hydroelectric inflow time series are derived from run-off data from ERA5 and scaled using EIA annual hydropower generation statistics ^{S70}. The open-source library *atlite*^{S50} provides functionality to perform all these calculations efficiently. Finally, the obtained time series are aggregated to each region heuristically in proportion to each grid cell's mean capacity factor. This assumes a capacity layout proportional to mean capacity factors. The resulting spatial and temporal variability of capacity factors are shown in [Figures S16](#) and [S17](#).

In combination with the capacity potentials derived from the assumed land use restrictions, the time-averaged capacity factors are used to display in [Figure S15](#) the energy that could be produced from wind and solar energy in the different regions of Europe.

S7. Hydrogen

S7.1. Hydrogen Demand

Hydrogen is consumed in the industry sector to produce ammonia and direct reduced iron (DRI) (see [Section S4.2](#)). Hydrogen is also consumed to produce synthetic methane and liquid hydrocarbons (see [Section S8.2](#) and [Section S9.2](#)) which have multiple uses in industry and other sectors. For transport applications, the consumption of hydrogen is exogenously fixed. It is used in heavy-duty land transport (see [Section S3.1](#)) and as liquified hydrogen in the navigation sector (see [Section S3.3](#)). Furthermore, stationary fuel cells may re-electrify hydrogen (with waste heat as a byproduct) to balance renewable fluctuations. The regional distribution of hydrogen demands is shown in [Figure S5b](#).

S7.2. Hydrogen Supply

Today, most hydrogen is produced from natural gas by steam methane reforming (SMR)



combined with a water-gas shift reaction



We consider this route of production with and without carbon capture (CC), assuming a capture rate of 90%. These routes are also referred to as blue and grey hydrogen. The methane input can be of fossil or synthetic origin.

Furthermore, we consider water electrolysis (green hydrogen) which uses electric energy to split water into hydrogen and oxygen



For the electrolysis, we assume alkaline electrolyzers since they have lower cost^{S21} and higher cumulative installed capacity^{S71} than polymer electrolyte membrane (PEM) electrolyzers. Waste heat from electrolysis is not leveraged in the model.

The split between these three different technology options and their installed capacities are a result of the optimisation depending on the techno-economic assumptions listed in [Section S16](#).

S7.3. Hydrogen Transport

Hydrogen can be transported in pipelines. These can be retrofitted natural gas pipelines or completely new pipelines. The cost of retrofitting a gas pipeline is about half that of building a new hydrogen pipeline. These costs include the cost for new compressors but neglect the energy demand for compression.

The endogenous retrofitting of gas pipelines to hydrogen pipelines is implemented in a way, such that for every unit of gas pipeline decommissioned, 60% of its nominal capacity are available for hydrogen transport on the respective route, following assumptions from the European Hydrogen Backbone report.^{S1} When the gas network is not resolved, this value denotes the potential for repurposed hydrogen pipelines.

New pipelines can be built additionally on all routes where there currently is a gas or electricity network connection. These new pipelines will be built where no sufficient retrofitting options are available. The capacities of new and repurposed pipelines are a result of the optimisation.

S7.4. Hydrogen Storage

Hydrogen can be stored in overground steel tanks or underground salt caverns. The annuitised cost for cavern storage is around 30 times lower than for storage in steel tanks including compression. For underground storage potentials for hydrogen in European salt caverns we take data from Caglayan et al.^{S73} and map it to each of the 181 model regions ([Figure S18](#)). We include only those caverns that are located on land and within 50 km of the shore (nearshore). We impose this restriction to circumvent environmental problems associated with brine water disposal.^{S73} The storage potential is abundant and the constraining factor is more where they exist and less how large the energy storage potentials are.

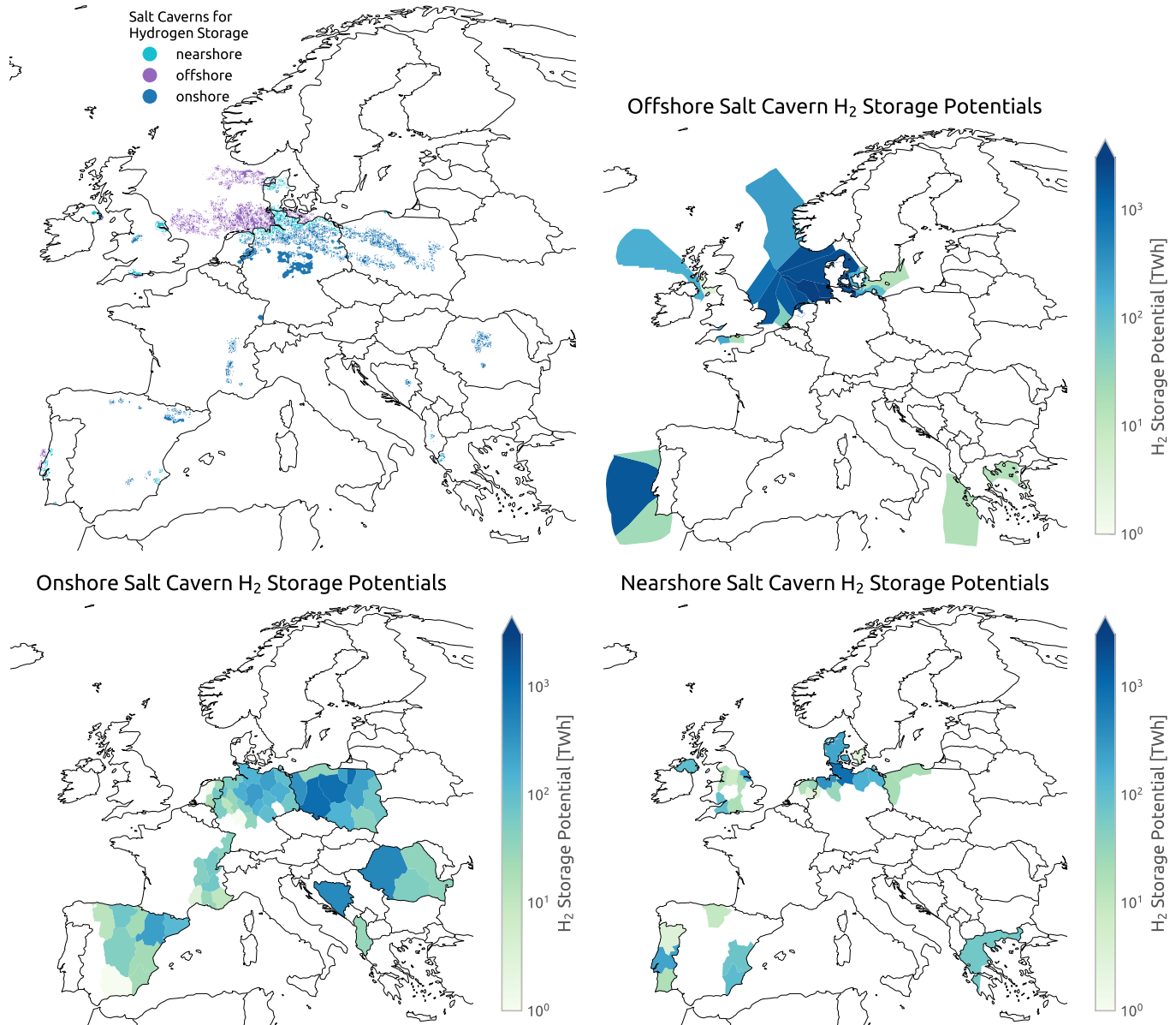


Figure S18: Potentials for hydrogen underground storage in salt caverns. Potentials are separated into offshore, onshore and near-shore (within 50km of the coast) potentials.

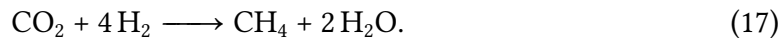
S8. Methane

S8.1. Methane Demand

Methane is used in individual and large-scale gas boilers, in CHP plants with and without carbon capture, in OCGT and CCGT power plants, and in some industry subsectors for the provision of high temperature heat (see [Section S4](#)) Methane is not used in the transport sector because of engine slippage. The regional distribution of methane demands is shown in [Figure S5b](#). However, the results shown in the main body of the paper relax all methane transmission costs and constraints.

S8.2. Methane Supply

Besides methane from fossil origins, the model also considers biogenic and synthetic sources. If gas infrastructure is regionally resolved (see [Section S8.3](#)), fossil gas can enter the system only at existing and planned LNG terminals, pipeline entry-points, and intra-European gas extraction sites (see [Section S8.3](#)), which are retrieved from the SciGRID Gas IGGIELGN dataset^{[S37](#)} and the GEM Wiki.^{[S75](#)} Biogas can be upgraded to methane (see [Section S10.1](#)). Synthetic methane can be produced by processing hydrogen and captures CO₂ in the Sabatier reaction



Direct power-to-methane conversion with efficient heat integration developed in the HELMETH project is also an option.^{[S76](#)} The share of synthetic, biogenic and fossil methane is an optimisation result depending on the techno-economic assumptions listed in [Section S16](#).

S8.3. Methane Transport

The existing European gas transmission network is represented based on the SciGRID Gas IGGIELGN dataset,^{[S37](#)} as shown in [Section S8.3](#). This dataset is based on compiled and merged data from the ENTSOG maps^{[S77](#)} and other publicly available data sources. It includes data on the capacity, diameter, pressure, length, and directionality of pipelines. Missing capacity data is conservatively inferred from the pipe diameter following conversion factors derived from an EHB report^{[S2](#)}. The gas network is clustered to the model's 181 regions (see [Figure S3](#)). Gas pipelines can be endogenously expanded or repurposed for hydrogen transport (see [Section S7.3](#)). Gas flows are represented by a lossless transport model.

The results presented in the main body of the article regard the gas transmission network only to determine the retrofitting potentials for hydrogen pipelines. These assume

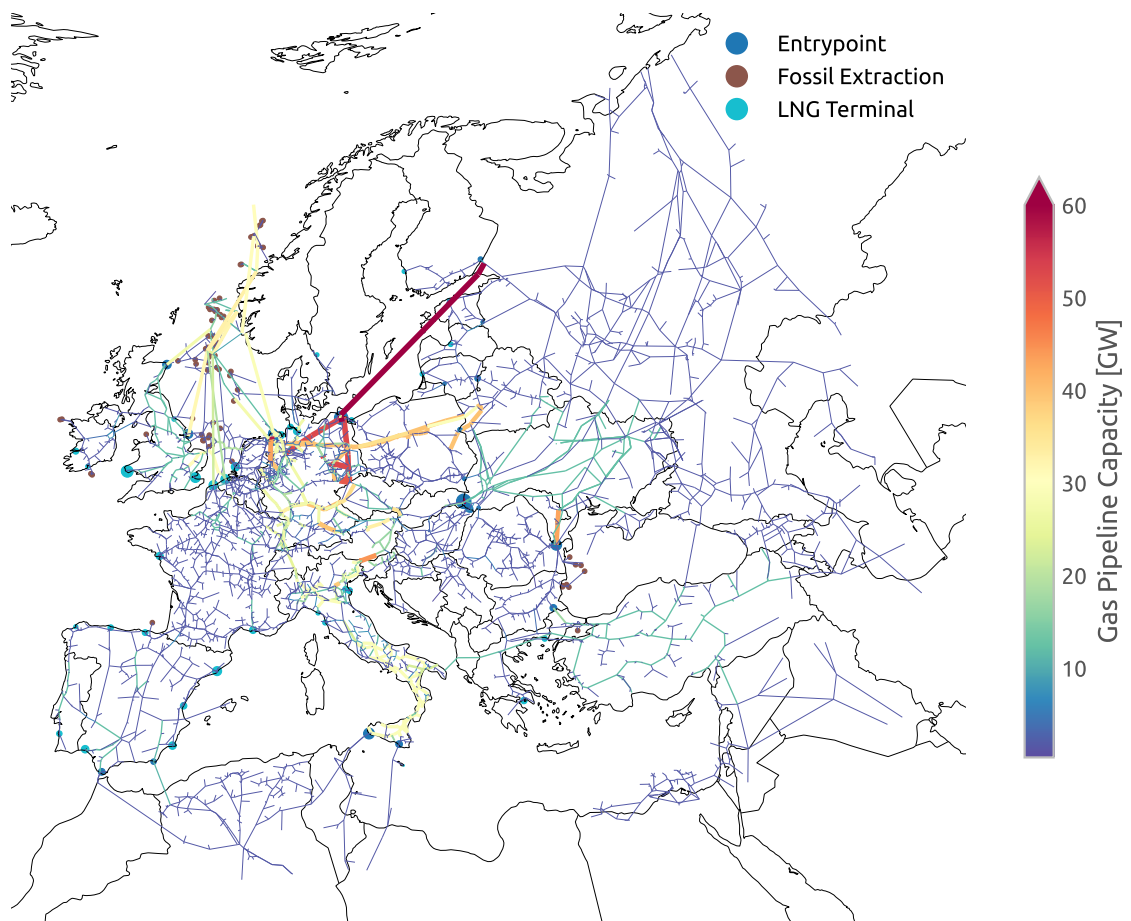


Figure S19: Unclustered European gas transmission network based on the SciGRID Gas IGGIELGN dataset. The pipelines are color-coded by estimated capacities. Markers indicate entry-points, sites of fossil resource extraction, and LNG terminals.

methane to be transported without cost or capacity constraints, since future demand is predicted to be low compared to available transport capacities even if a certain share is repurposed for hydrogen transport such that no bottlenecks are expected. Selected runs with gas network infrastructure included are presented in [Section S15](#).

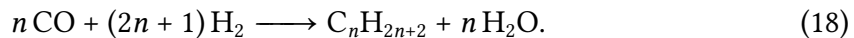
S9. Oil-based Products

S9.1. Oil-based Product Demand

Naphtha is used as a feedstock in the chemicals industry (see [Section S4.3](#)). Furthermore, kerosene is used as transport fuel in the aviation sector (see [Section S3.2](#)). Non-electrified agriculture machinery also consumes gasoline. The regional distribution of the demand for oil-based products is shown in [Figure S5e](#). However, this carrier is copperplated in the model, which means that transport costs and constraints are neglected.

S9.2. Oil-based Product Supply

In addition to fossil origins, oil-based products can be synthetically produced by processing hydrogen and captured CO₂ in Fischer-Tropsch plants



with costs as included in [Section S16](#). The waste heat from the Fischer-Tropsch process is supplied to district heating networks.

S9.3. Oil-based Product Transport

Liquid hydrocarbons are assumed to be transported freely among the model region since future demand is predicted to be low, transport costs for liquids are low and no bottlenecks are expected.

S10. Biomass

S10.1. Biomass Supply and Potentials

Regional biomass supply potentials are taken from the JRC ENSPRESO database ^{S41}. This dataset includes various biomass feedstocks at NUTS2 resolution for low, medium and high availability scenarios. We use the medium availability scenario for 2030, assuming no biomass import from outside Europe. The data for NUTS2 regions is mapped to PyPSA-Eur-Sec model regions in proportion to the area overlap.

Only residues from agriculture, forestry, and biodegradable municipal waste are considered as energy feedstocks. Fuel crops are avoided because they compete with scarce

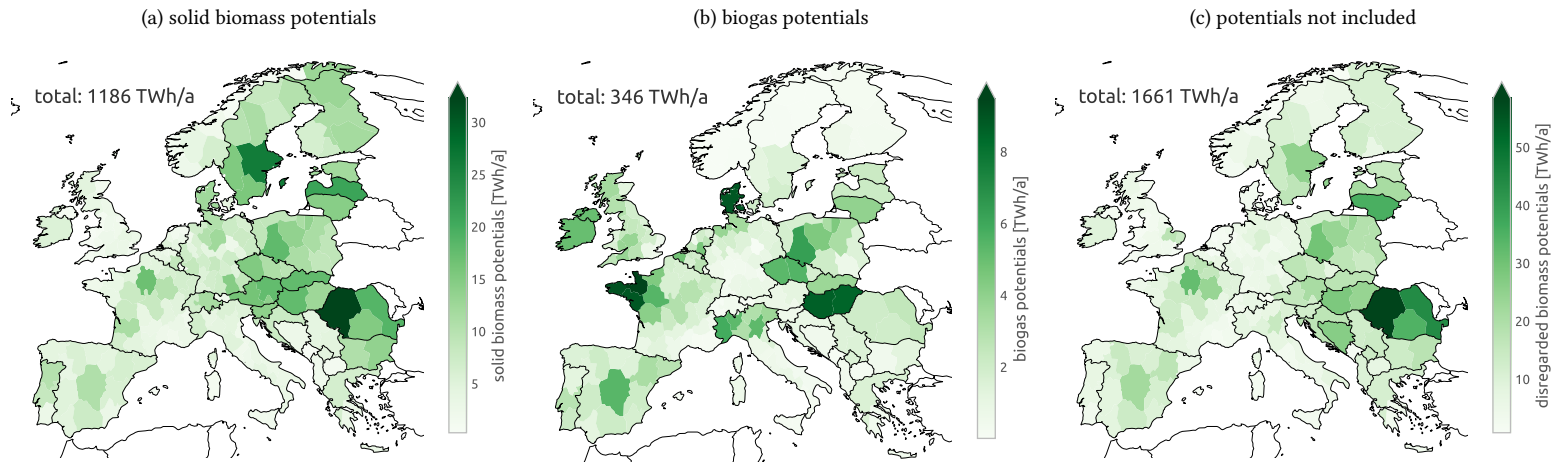


Figure S20: Regional distribution of biomass potentials separated by solid biomass, biogas and potentials not included. Only residual biomass feedstocks are included. Potentials are based on the medium availability scenario for 2030 from the JRC ENSPRESO database.

land for food production, while primary wood as well as wood chips and pellets are avoided because of concerns about sustainability.^{S80} Manure and sludge waste are available to the model as biogas, whereas other wastes and residues are classified as solid biomass. Solid biomass resources are available for combustion in combined-heat-and-power (CHP) plants and for medium temperature heat (below 500 °C) applications in industry. The technical characteristics for the solid biomass CHP are taken from the Danish Energy Agency Technology Database^{S21} assumptions for a medium-sized back pressure CHP with wood pellet feedstock; this has very similar costs and efficiencies to CHPs with feedstocks of straw and wood chips.

A summary of which feedstocks are used in the model is shown in [Table S2](#); the respective regional distribution of potentials is included in [Figure S20](#). In 2015, the EU28 biomass energy consumption consisted of 180 TWh of biogas, 1063 TWh of solid biofuels, 109 TWh renewable municipal waste and 159 TWh of liquid biofuels.^{S41} In comparison, PyPSA-Eur-Sec implies a doubling of biogas consumption and similar amounts of solid biofuels, but a shift from energy crops and primary wood to residues and wastes. Zappa et al.^{S81} additionally allowed the use of roundwood chips and pellets, and grassy, willow and poplar energy crops.

S10.2. Biomass Demand

Solid biomass provides process heat up to 500 °C in industry and can also feed CHP plants in district heating networks. As noted in [Section S4](#), solid biomass is used as heat supply

Application	Source	Potential [TWh/a]
solid biomass	primary agricultural residues; forest energy residue; secondary forestry residues: woodchips, sawdust; forestry residues from landscape care; biodegradable municipal waste	1186
biogas	wet and dry manure; biodegradable sludge	346
not used	energy crops: sugar beet bioethanol, rape seed and other oil crops, starchy crops, grassy, willow, poplar; roundwood fuelwood; roundwood chips and pellets	1661

Table S2: Use of biomass potentials according to classifications from the JRC ENSPRESO database in the medium availability scenario for 2030.

in the paper and pulp and food, beverages and tobacco industries, where required temperatures are lower. [S22, S23](#) The regional distribution of solid biomass demand is shown in [Figure S5f](#).

S10.3. Biomass Transport

Solid biomass is assumed to be transported freely among the modelled regions. Biogas can be upgraded and then transported via the methane network. While the methane network is neglected, biogas can also be moved without cost or constraints.

S11. Carbon dioxide capture, usage and sequestration (CCU/S)

Carbon management becomes important in net-zero scenarios. [S82](#) PyPSA-Eur-Sec includes carbon capture from air, electricity generators and industrial facilities, carbon dioxide storage and transport, the usage of carbon dioxide in synthetic hydrocarbons, as well as the ultimate sequestration of carbon dioxide underground.

S11.1. Carbon Capture

Carbon dioxide can be captured from industry process emissions, steam methane reforming, methane or biomass used for process heat in the industry, combined heat and power plants (CHP using biomass or methane), and directly from the air using direct air capture (DAC). The capacities of each carbon capture technology are co-optimised.

As shown in [Figure S11](#), the model includes industrial process emissions with fossil-origin totalling 127 Mt_{CO₂}/a based on the JRC-IDEES database. [S15](#) Process emissions originate, for instance, from limestone in cement production. These emissions need to be captured and sequestered or offset to achieve net-zero emissions. Industry process emissions are

captured assuming a capture rate of 90% and assuming costs of CO₂ capturing like in the cement industry.^{S21} The electricity and heat demand of process emission carbon capture is currently ignored.

For steam methane reforming (SMR), CHP units, and biomass and methane demand in industry the model can decide between two options (with and without carbon capture) with different costs. Here, we also apply a capture rate of 90%.

DAC includes the energy requirements of the adsorption phase with inputs electricity and heat to assist adsorption process and regenerate adsorbent, as well as the compression of CO₂ prior to storage which consumes electricity and rejects heat. We assume a net energy consumption of 1.8 MWh/t_{CO₂} heat and 0.47 MWh/t_{CO₂} electricity based on DEA data.^{S21} These values are a bit higher compared to Breyer et al.,^{S83} who assume requirements of 1.2 MWh/t_{CO₂} heat at 100 °C and 0.2 MWh_{el}/t_{CO₂} electricity.

S11.2. Carbon Usage

Captured CO₂ can be used to produce synthetic methane and liquid hydrocarbons (e.g. naphtha). See [Section S8.2](#) and [Section S9.2](#). If carbon captured from biomass is used, the CO₂ emissions of the synthetic fuels are net-neutral.

S11.3. Carbon Transport and Sequestration

Captured CO₂ can also be stored underground up to an annual sequestration limit of 200 Mt_{CO₂}/a. Compared to other studies, this is a conservative assumption but sufficient to capture and sequester process emissions. The sequestration of captured CO₂ from bioenergy results in net negative emissions. As stored carbon dioxide is modelled as a single node for Europe, transport constraints are neglected. For CO₂ transport and sequestration we assume a cost of 20 €/t_{CO₂} based on IEA data.^{S84}

S12. Mathematical Model Formulation

The objective is to minimise the total annual system costs of the energy system that comprises both investment costs and operational expenditures of generation, storage, transmission and conversion infrastructure. To express both as annual costs, we use the annuity factor $(1 - (1 + \tau)^{-n})/\tau$ that, like a mortgage, converts the upfront investment of an asset to annual payments considering its lifetime n and cost of capital τ . Thus, the objective includes on one hand the annualised capital costs c_* for investments at bus i in generator capacity $G_{i,r} \in \mathbb{R}^+$ of technology r , storage energy capacity $E_{i,s} \in \mathbb{R}^+$ of technology s , electricity transmission line capacities $P_\ell \in \mathbb{R}^+$, and energy conversion and

transport capacities $F_k \in \mathbb{R}^+$ (links), as well as the variable operating costs o_* for generator dispatch $g_{i,r,t} \in \mathbb{R}^+$ and link dispatch $f_{k,t} \in \mathbb{R}^+$ on the other:

$$\min_{G,E,P,F,g} \left[\sum_{i,r} c_{i,r} \cdot G_{i,r} + \sum_{i,s} c_{i,s} \cdot E_{i,s} + \sum_{\ell} c_{\ell} \cdot P_{\ell} + \sum_k c_k \cdot F_k + \right. \quad (19)$$

$$\left. \sum_t w_t \cdot \left(\sum_{i,r} o_{i,r} \cdot g_{i,r,t} + \sum_k o_k \cdot f_{k,t} \right) \right]. \quad (20)$$

Thereby, the representative time snapshots t are weighted by the time span w_t such that their total duration adds up to one year; $\sum_{t \in \mathcal{T}} w_t = 365 \cdot 24h = 8760h$. A bus i represents both a regional scope and an energy carrier. Represented carriers include electricity, heat (various subdivisions), hydrogen, methane, oil and carbon dioxide.

In addition to the cost-minimising objective function, we further impose a set of linear constraints that define limits on (i) the capacities of generation, storage, conversion and transmission infrastructure from geographical and technical potentials, (ii) the availability of variable renewable energy sources for each location and point in time (iii) the limit for CO₂ emissions or transmission expansion, (iv) storage consistency equations, and (v) a multi-period linearised optimal power flow (LOPF) formulation. Overall, this results in a large linear problem (LP).

The capacities of generation, storage, conversion and transmission infrastructure are constrained from above by their installable potentials and from below by any existing components:

$$\underline{G}_{i,r} \leq G_{i,r} \leq \bar{G}_{i,r} \quad \forall i, r \quad (21)$$

$$\underline{E}_{i,s} \leq E_{i,s} \leq \bar{E}_{i,s} \quad \forall i, s \quad (22)$$

$$\underline{P}_{\ell} \leq P_{\ell} \leq \bar{P}_{\ell} \quad \forall \ell \quad (23)$$

$$\underline{F}_k \leq F_k \leq \bar{F}_k \quad \forall k \quad (24)$$

Moreover, the dispatch of generators and links may not only be constrained by their rated capacity but also by the weather-dependent availability of variable renewable energy or must-run conditions. This can be expressed as a time- and location-dependent availability factor $\bar{g}_{i,r,t}/\bar{f}_{k,t}$ and must-run factor $\underline{g}_{i,r,t}/\underline{f}_{k,t}$, given per unit of the nominal capacity:

$$\underline{g}_{i,r,t} G_{i,r} \leq g_{i,r,t} \leq \bar{g}_{i,r,t} G_{i,r} \quad \forall i, r, t \quad (25)$$

$$\underline{f}_{k,t} F_k \leq f_{k,t} \leq \bar{f}_{k,t} F_k \quad \forall k, t \quad (26)$$

The parameter $f_{\underline{k},t}$ can also be used to define whether a link is bidirectional or unidirectional. For instance, for HVDC links $f_{\underline{k},t} = -1$ allows power flows in either direction. On the other hand, a heat resistor has $f_{\underline{k},t} = 0$ since it can only convert electricity to heat.

The energy levels $e_{i,s,t}$ of all stores are constrained by their energy capacity

$$0 \leq e_{i,s,t} \leq E_{i,s} \quad \forall i, s, t, \quad (27)$$

and have to be consistent with the dispatch variable $h_{i,s,t} \in \mathbb{R}$ in all hours

$$e_{i,s,t} = \eta_{i,s,0}^{w_t} \cdot e_{i,s,t-1} + w_t \cdot h_{i,s,t}, \quad (28)$$

where $\eta_{i,s,0}$ denotes the standing loss. Furthermore, the storage energy levels are either assumed to be cyclic or given an initial state of charge,

$$e_{i,s,0} = e_{i,s,|\mathcal{T}|} \quad \forall i, s, \text{ or} \quad (29)$$

$$e_{i,s,0} = e_{i,s,\text{initial}} \quad \forall i, s. \quad (30)$$

The modelling of hydroelectricity storage deviates from regular storage to additionally account for natural inflow and spillage of water. We also assume fixed power ratings $H_{i,s}$ for hydroelectricity storage. The dispatch of hydroelectricity storage units is split into two positive variables; one each for charging $h_{i,s,t}^+$ and discharging $h_{i,s,t}^-$, and limited by $H_{i,s}$.

$$0 \leq h_{i,s,t}^+ \leq H_{i,s} \quad \forall i, s, t \quad (31)$$

$$0 \leq h_{i,s,t}^- \leq H_{i,s} \quad \forall i, s, t \quad (32)$$

The energy levels $e_{i,s,t}$ of all hydroelectric storage also have to match the dispatch across all hours

$$\begin{aligned} e_{i,s,t} = & \eta_{i,s,0}^{w_t} \cdot e_{i,s,t-1} + w_t \cdot h_{i,s,t}^{\text{inflow}} - w_t \cdot h_{i,s,t}^{\text{spillage}} \\ & + \eta_{i,s,+} \cdot w_t \cdot h_{i,s,t}^+ - \eta_{i,s,-}^{-1} \cdot w_t \cdot h_{i,s,t}^-, \end{aligned} \quad \forall i, s, t \quad (33)$$

whereby hydropower storage units can additionally have a charging efficiency $\eta_{i,s,+}$, a discharging efficiency $\eta_{i,s,-}$, natural inflow $h_{i,s,t}^{\text{inflow}}$ and spillage $h_{i,s,t}^{\text{spillage}}$, besides the standing loss $\eta_{i,s,0}$.

The nodal balance constraint for supply and demand (Kirchoff's current law for electricity buses) requires local generators and storage units as well as incoming or outgoing

energy flows $f_{\ell,t}$ of incident transmission lines ℓ to balance the perfectly inelastic electricity demand $d_{i,t}$ at each location i and snapshot t

$$\sum_r g_{i,r,t} + \sum_s (h_{i,s,t}^- - h_{i,s,t}^+) + \sum_s h_{i,s,t} + \sum_\ell K_{i\ell} f_{\ell,t} + \sum_k L_{ikt} f_{k,t} = d_{i,t} \quad \leftrightarrow \quad \lambda_{i,t} \quad \forall i, t, \quad (34)$$

where $K_{i\ell}$ is the incidence matrix of the electricity network with non-zero values -1 if line ℓ starts at node i and 1 if it ends at node i . L_{ikt} is the lossy incidence matrix of the network with non-zero values -1 if link k starts at node i and $\eta_{i,k,t}$ if one of its terminal buses is node i . For a link with more than two outputs (e.g. CHP converts gas to heat and electricity in a fixed ratio), the respective column of the lossy incidence matrix has more than two non-zero entries (hypergraph). The efficiency may be time-dependent and greater than one for certain technologies (e.g. for heat pumps converting electricity and ambient heat to hot water).

The Lagrange multiplier (KKT multiplier) $\lambda_{i,t}$ associated with the nodal balance constraint indicates the marginal price of the respective energy carrier and location of bus i at time t , e.g. the local marginal price (LMP) of electricity at the electricity bus.

The power flows $p_{\ell,t}$ are limited by their nominal capacities P_ℓ

$$|p_{\ell,t}| \leq \bar{p}_\ell P_\ell \quad \forall \ell, t, \quad (35)$$

where \bar{p}_ℓ acts as an additional per-unit security margin on the line capacity to allow a buffer for the failure of single circuits ($N - 1$ criterion) and reactive power flows.

Kirchoff's voltage law (KVL) imposes further constraints on the flow of AC transmission lines and there are several ways to formulate KVL with large impacts on performance. Here, we use linearised load flow assumptions, where the voltage angle difference around every closed cycle in the electricity transmission network must add up to zero. Using a cycle basis $C_{\ell c}$ of the network graph where the independent cycles c are expressed as directed linear combinations of lines ℓ ,^{S36} we can write KVL as

$$\sum_\ell C_{\ell c} \cdot x_\ell \cdot p_{\ell,t} = 0 \quad \forall c, t \quad (36)$$

where x_ℓ is the series inductive reactance of line ℓ .

We may further regard a constraint on the total annual CO₂ emissions Γ_{CO_2} to achieve sustainability goals. The emissions are determined from the time-weighted generator

dispatch $w_t \cdot g_{i,r,t}$ using the specific emissions ρ_r of technology r and the generator efficiencies $\eta_{i,r}$

$$\sum_{i,r,t} \rho_r \cdot \eta_{i,r}^{-1} \cdot w_t \cdot g_{i,r,t} + \sum_{i,s} \rho_s (e_{i,s,t=0} - e_{i,s,t=|\mathcal{T}|}) \leq \Gamma_{CO_2} \leftrightarrow \mu_{CO_2}. \quad (37)$$

In this case, the Lagrange multiplier (KKT multiplier) μ_{CO_2} denotes the shadow price of emitting an additional tonne of CO₂, i.e. the CO₂ price necessary to achieve the respective CO₂ emission reduction target.

Additionally, another global constraint may be set on the volume of electricity transmission network expansion

$$\sum_{\ell} l_{\ell} \cdot P_{\ell} \leq \Gamma_{LV} \leftrightarrow \mu_{LV}, \quad (38)$$

where the sum of transmission capacities P_{ℓ} multiplied by their lengths l_{ℓ} is bounded by a transmission volume cap Γ_{LV} . In this case, the Lagrange multiplier (KKT multiplier) μ_{LV} denotes the shadow price of a marginal increase in transmission volume.

This formulation does not include pathway optimisation (i.e. no sequences of investments), but searches for a cost-optimal layout corresponding to a given CO₂ emission reduction level and assumes perfect foresight for the reference year based on which capacities are optimised. This optimisation problem is implemented in the open-source Python-based modelling framework PyPSA.^{S30}

S13. Grid Reinforcement and Onshore Wind Potential Restrictions

S13.1. Cost of Electricity Grid Reinforcement Restrictions

In the following sensitivity runs, the model is allowed to build new electricity transmission infrastructure wherever is cost-optimal, but the total volume of new transmission capacity (sum of line length times capacity, TWkm) is successively limited. The volume limit is given in fractions of today's grid volume: a line volume limit of 100% means no new capacity is allowed beyond today's grid (since the model cannot remove existing lines); a limit of 125% means the total grid capacity can grow by 25% (25% is similar to the planned extra capacity in the European network operators' Ten Year Network Development Plan (TYNDP)^{S9}). For this investigation, a hydrogen network could be built.

Figure S21a shows the composition of total yearly system costs (including all investment and operational costs) as we vary the allowed grid expansion, from no expansion (only today's grid) to a doubling of today's grid capacities (the model optimises where new capacity is placed). As the grid is expanded, total costs decrease only slightly, despite the

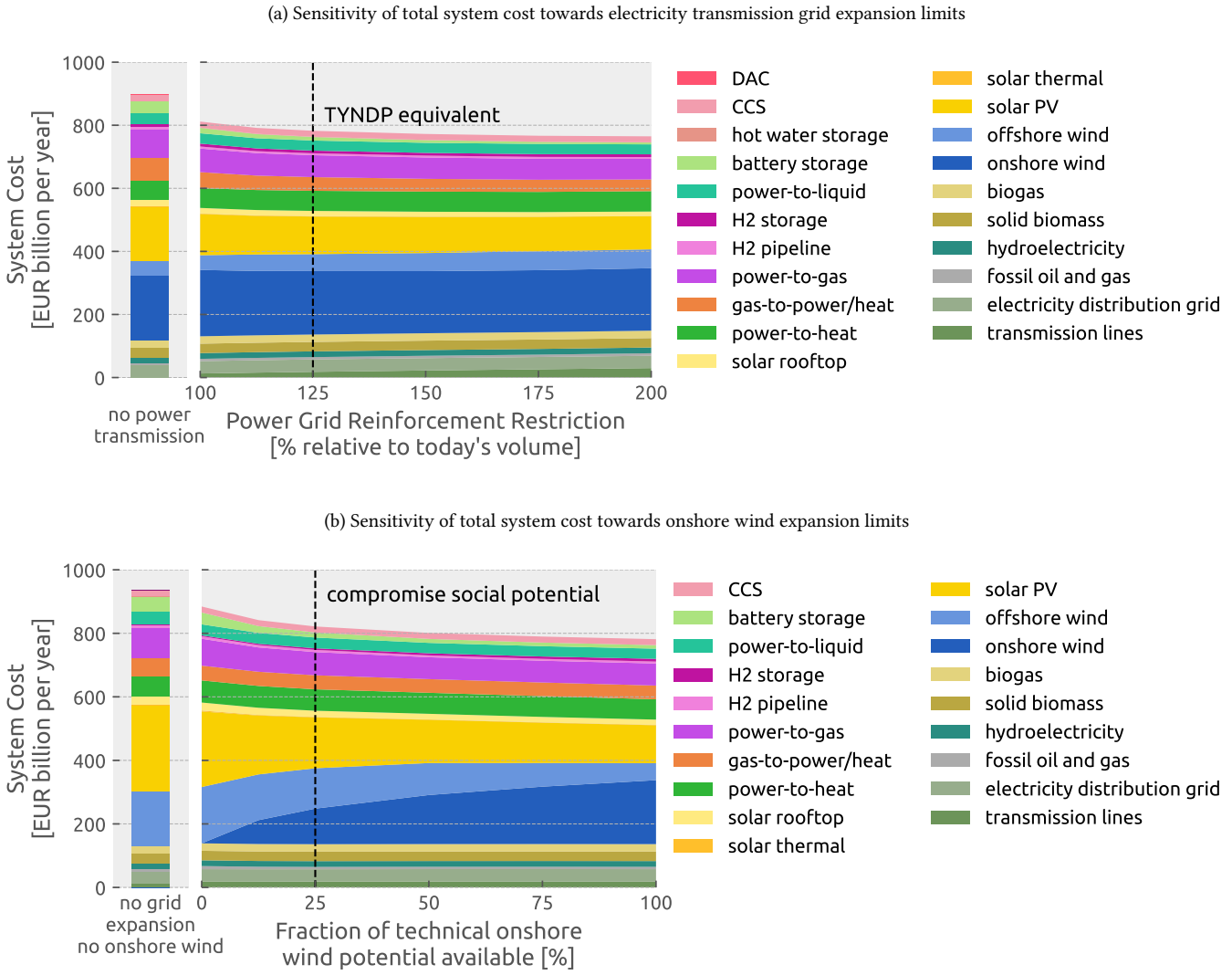


Figure S21: Sensitivity of total system cost towards electricity transmission grid expansion limits and onshore wind restrictions. The sweep for grid expansion restrictions allows full onshore wind potentials. The extreme case (a, left) removes all existing power transmission lines as well. The sweep for onshore wind potential restrictions allows power grid reinforcements by up to 25% of today's transmission capacities. The extreme case (b, left) combines no grid expansion with no onshore wind potentials.

increasing costs of the grid. The total cost benefit of a doubling of grid capacity is around 47 bn€/a corresponding to an expansion of 644 TWkm. However, over half of the benefit (29 bn€/a) is available already at a 25% expansion corresponding to an expansion of 403 TWkm.

[Figure S21a](#) also includes a scenario where today's electricity transmission infrastructure is completely removed from the model, similar to an electricity system study on geographic trade-offs by Tröndle et al.^{[S86](#)} While doubling the transmission grid yields a benefit of 47 bn€/a, removing what exists incurs a cost of 86 bn€/a. The lack of electricity grid is mostly compensated by more solar PV generation, battery storage and re-electrified hydrogen.

S13.2. Cost of Onshore Wind Potential Elimination

Like building new power transmission lines, the deployment of onshore wind may not always be socially accepted, such that it may not be possible to leverage its full potential.^{[S87-S89](#)} In the following additional sensitivity analysis, we explore the hypothetical impact of restricting the installable potentials of onshore wind down to zero ([Figure S22](#)).

We find that as onshore wind is eliminated, costs rise by € 104 bn/a (12%) when the electricity grid is fixed to today's capacities, but a hydrogen network can still be developed. In comparison to the least-cost solution with full network expansion, this solution is 23% more expensive. A solution in which neither a hydrogen network could be developed would be 30% more expensive. [Section S13.3](#) presents further intermediate results between full and no onshore wind expansion for scenarios with hydrogen network expansion and TYNDP-equivalent power grid reinforcements. The model substitutes onshore wind, particularly in the British Isles, for higher investment in offshore wind in the North Sea and solar generators in Southern Europe ([Figure S22c](#)). Because offshore capacities are concentrated near coastlines, and grid capacity is restricted, total spending on hydrogen electrolyzers and networks also increases to absorb the increased offshore generation. Without onshore wind, the potentials for rooftop solar PV and offshore wind in Europe are largely exhausted, such that in this self-sufficient scenario for Europe, the effect of installable potentials becomes critical.

Whereas with onshore wind, the British Isles and North Sea dominate hydrogen production, Southern Europe becomes a large exporter of solar-based hydrogen if the development of onshore wind capacities is restricted ([Figures S22a](#) and [S22b](#)). This shift in hydrogen infrastructure also impacts the share of gas pipelines being retrofitted for hydrogen transport. As the Iberian Peninsula becomes a preferred region for hydrogen production but has a more sparse gas transmission network today, the rate of retrofitted

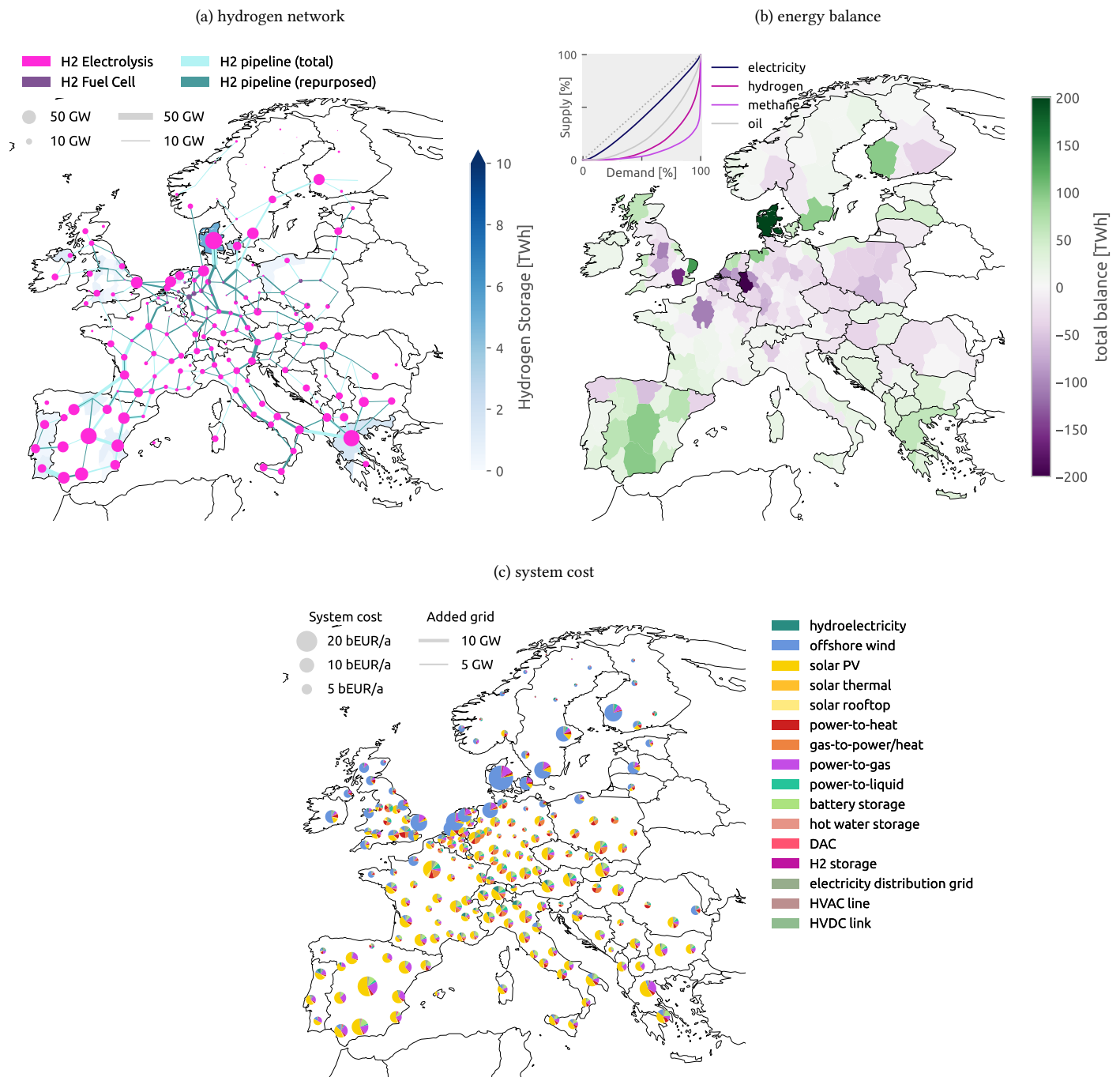


Figure S22: Maps of regional energy balance, hydrogen network and production sites, and spatial and technological distribution of system costs for a scenario without onshore wind and without power grid expansion.

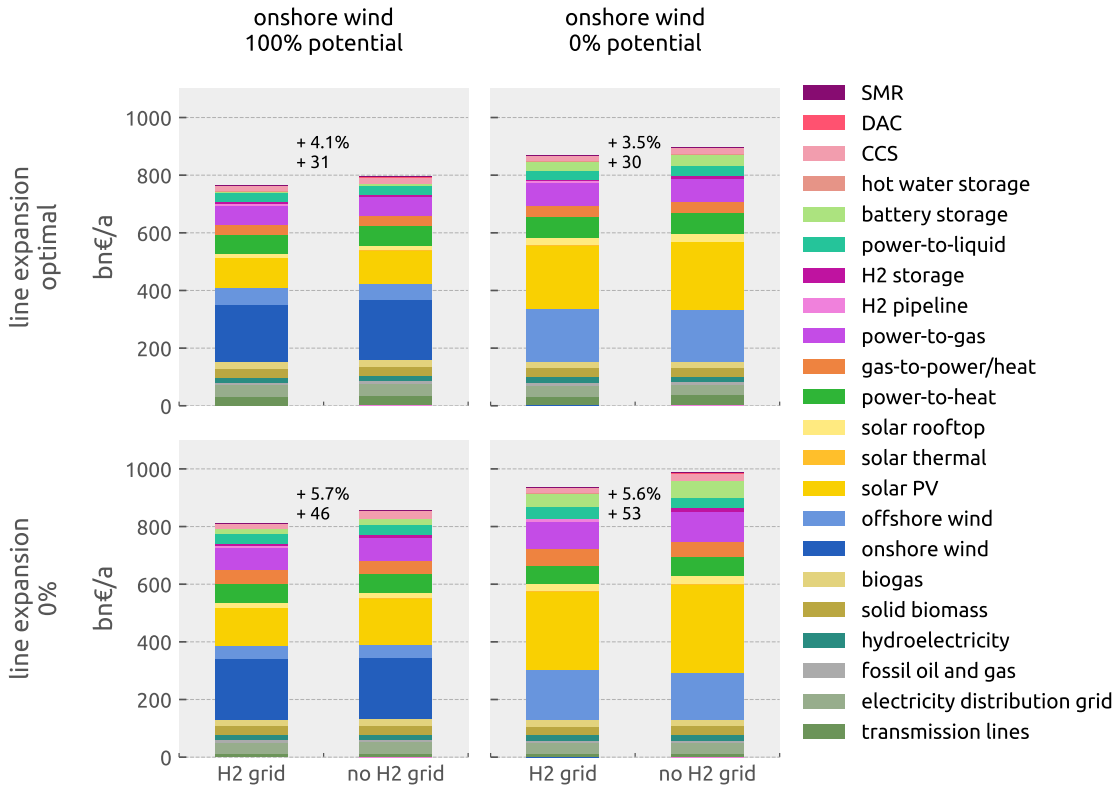


Figure S23: Varying benefits of hydrogen network infrastructure and changes in system composition as power grid and onshore wind expansion options are altered. The benefit of a hydrogen backbone is robust across all scenarios varying between 3.5% and 5.7%.

pipeline capacity reduces from 66% to 53%. Many new hydrogen pipelines are built to connect Spain with France, but also to connect increased hydrogen production from Danish offshore wind to Germany. Gas pipeline retrofitting is then concentrated in Germany, Austria and Italy.

The benefit of a hydrogen network is similar whether or not onshore wind capacities are built in Europe, even though the hydrogen network topology is then built around supply from offshore wind in the North Sea and solar PV from Southern Europe rather than from onshore wind in North-West Europe. As Figure S23 illustrates, the net benefit is again strongest when power grid expansion is restricted. If both onshore wind and power grid expansion are excluded, costs for a system without a hydrogen network option were by 53 bn€/a (5.6%) higher. With cost-optimal electricity grid reinforcement, the net benefit of a hydrogen network is still as high as 30 bn€/a (3.5%).

S13.3. Cost of Compromises on Onshore Wind Potential Restrictions

In the following sensitivity runs, the maximum installable capacity of onshore wind is successively restricted down to zero at each node. The upper limit is derived from land use restriction and yields a maximum technical potential corresponding to about 481 GW for Germany. For this investigation, a compromise electricity grid expansion by 25% compared to today and no limits on hydrogen network infrastructure are assumed.

As previously discussed in [Section S13.2](#), costs rise by 103 bn€/a (13%) by restricting the installable potentials of onshore down to zero. Just as in the case of restricted line volumes, [Figure S21b](#) reveals a nonlinear rise in system costs: if we constrain the model to 25% of the onshore potential (around 120 GW for Germany), costs rise by only 64 bn€/a (5%). Thereby, 25% of the onshore wind potential may represent a social compromise between total system cost, and social concerns about onshore wind development.

In comparison, Schlachterger et al.^{[S90](#)} found a smaller change between 9% and 12% in system costs in an electricity-only model when onshore wind potentials were restricted across various grid expansion limitations. The biggest change was observed when the power grid could not be reinforced. Onshore wind was largely replaced with offshore wind in that model. Unlike that model, here we have a higher grid resolution (181 versus 30 regions) which allows us to better assess the grid integration costs of offshore wind. Our results show that moderate power grid expansion is particularly important when onshore wind development is severely limited. For the extreme case where no onshore wind capacities would be built, reducing power grid expansion from 25% to none incurs another rise in system cost of an additional 50 bn€/a (6%).

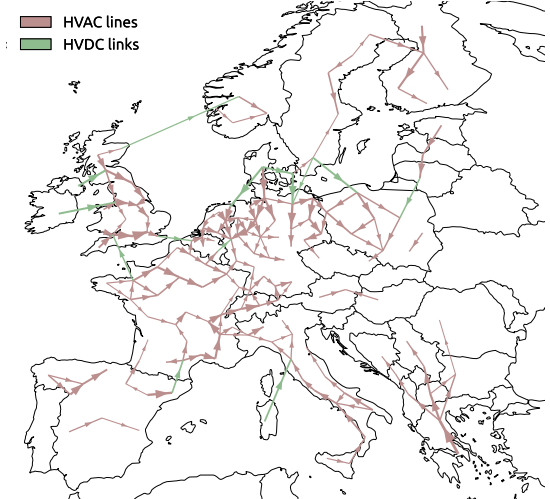
S14. Supplementary Results for Network Expansion Scenarios

In this section, supplementary results for the different network expansion scenarios are presented. [Figures S24](#) and [S25](#) display net electricity and hydrogen flows in their respective transmission networks. Further figures show the variation of average nodal prices of electricity and hydrogen in space ([Figures S26](#) and [S27](#)), in time ([Figures S28](#) and [S29](#)), and as duration curves ([Figure S30](#)). Sankey diagrams in [Figure S31](#) illustrate energy flows in the system. Across the scenarios, we infer that a carbon price between 435 €/t_{CO₂} with transmission infrastructure expansion and 513 €/t_{CO₂} without would be required to achieve both climate neutrality and self-sufficiency in Europe.

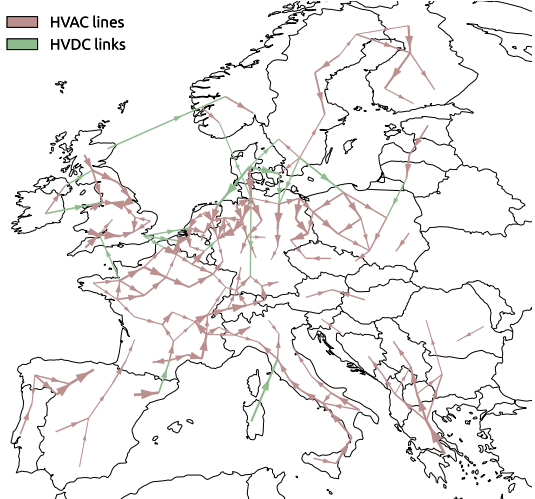
S15. Detailed Results of Least-Cost Solution with Full Grid Expansion

In the following section we present more detailed results from the scenario where both the hydrogen and electricity grid could be expanded. Among the scenarios we inves-

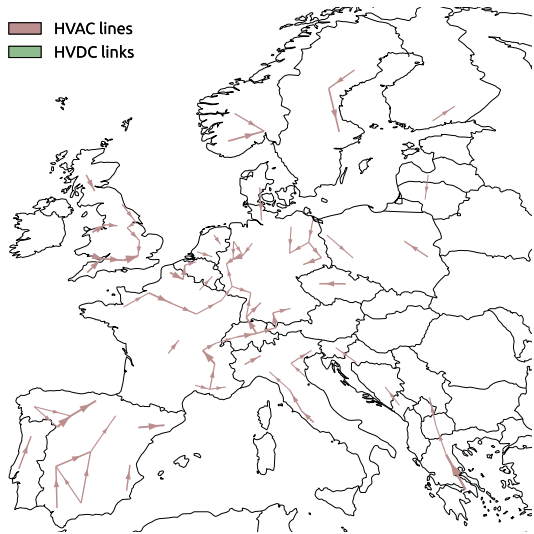
(a) With power grid expansion, with hydrogen network



(b) With power grid expansion, without hydrogen network



(c) Without power grid expansion, with hydrogen network



(d) Without power grid expansion, without hydrogen network

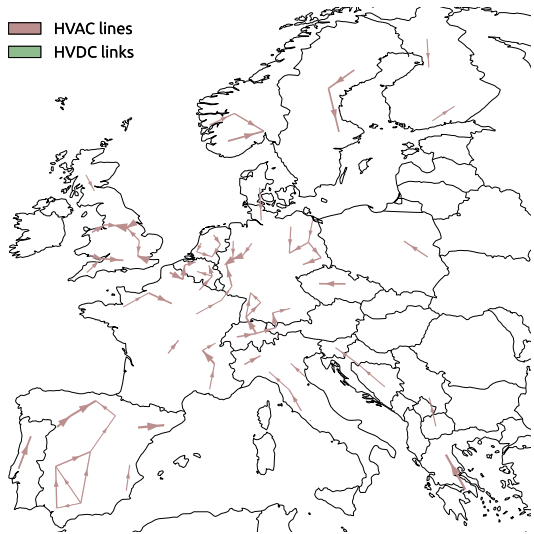


Figure S24: Net flow of electricity in the network. The maps show net flows larger than 10 TWh with arrow sizes proportional to net flow volume. Only power grid expansion enables bulk energy transport in form of electricity. With the existing transmission network, net flows are limited and the transmission infrastructure is rather used for synoptic balancing as weather systems pass the continent.

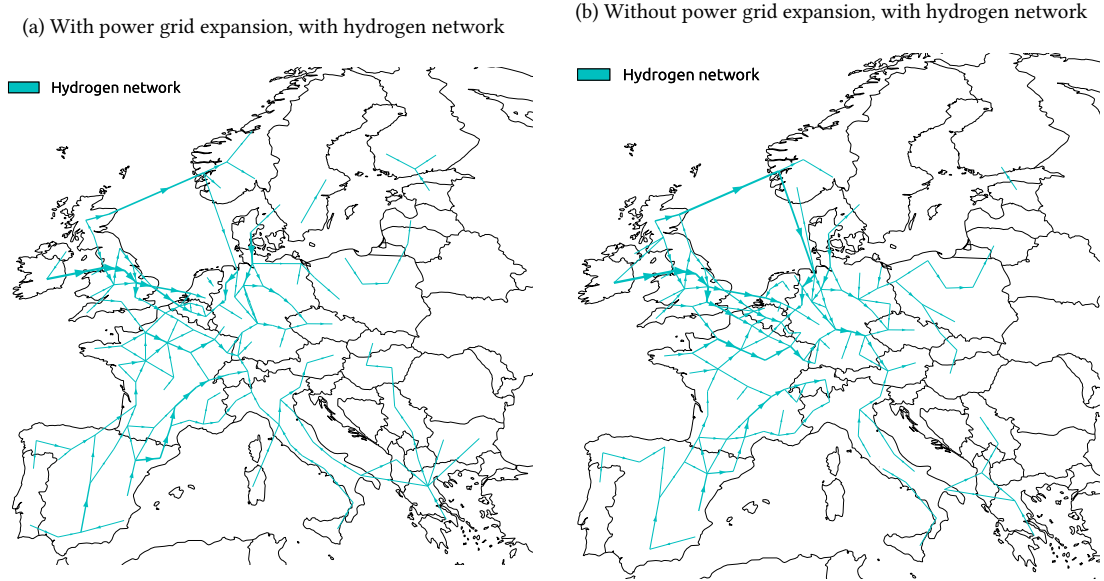


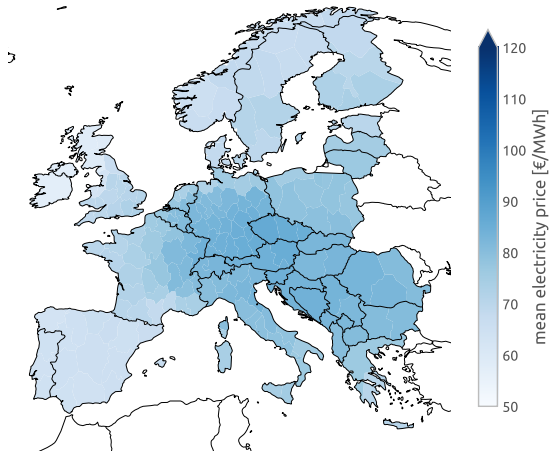
Figure S25: Net flow of hydrogen in the network. The maps shows net flows larger than 10 TWh with arrow sizes proportional to net flow volume. The flows indicate the integration of cheap production sites in Spain and the British Isles and high demands in Central Europe.

tigated, this represents the least-cost solution. [Figures S33 to S36](#) show temporally resolved energy balances for different carriers: electricity, hydrogen, heat, methane, oil-based products, and carbon dioxide. These are daily sampled time series for a year and 3-hourly sampled time series for the month February, and indicate how different technologies are operated both seasonally and daily. [Figure S37](#) displays the regional distribution of levelised cost of electricity for wind and solar generation. [Figure S38](#) indicates how synthetic fuel production facilities are operated regionally. How selected energy system components are operated throughout the year is shown in [Figure S40](#). The utilisation of electricity and hydrogen network assets are presented in [Figure S41](#), alongside information about where energy is curtailed and what congestion rents are incurred.

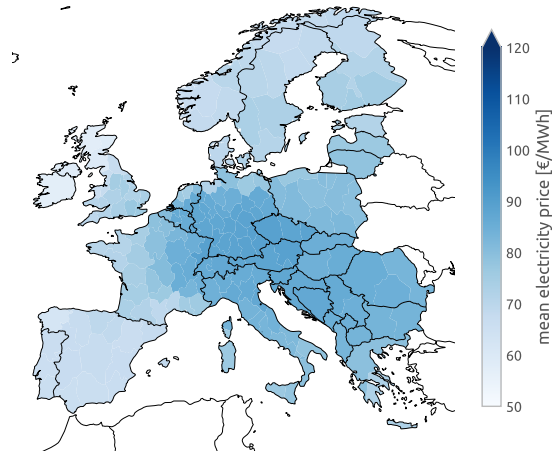
S16. Techno-Economic Assumptions

For the technological assumptions, we take estimates for the year 2030 ([Table S3](#)). Many of those come from a database published by the Danish Energy Agency (DEA).^{[S21](#)} We take 2030 technology assumptions to account for expected technology cost reductions and because the pathway to climate neutrality implies that much of the infrastructure must be built well in advance of 2050. Assumptions are maintained at github.com/pypsa/technology-data and were taken from version 0.3.0.

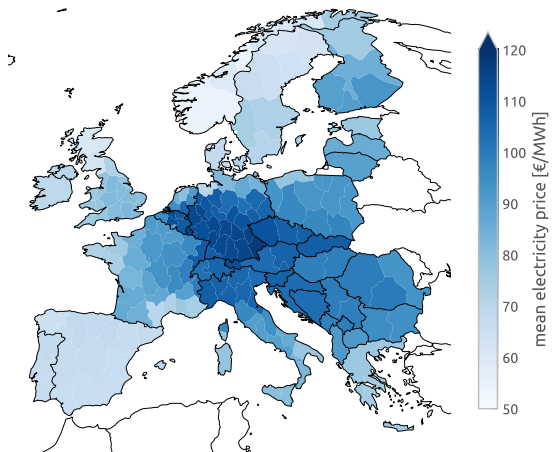
(a) With power grid expansion, with hydrogen network



(b) With power grid expansion, without hydrogen network



(c) Without power grid expansion, with hydrogen network



(d) Without power grid expansion, without hydrogen network

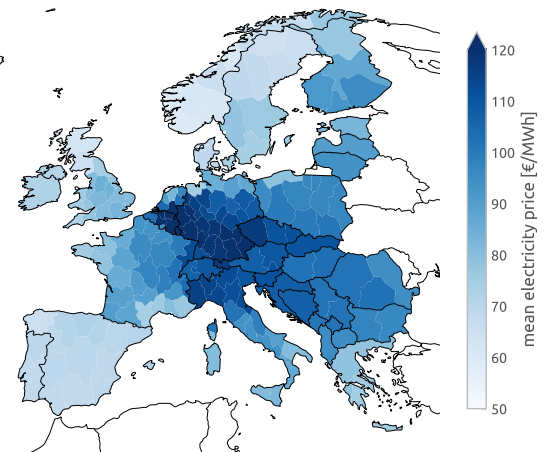
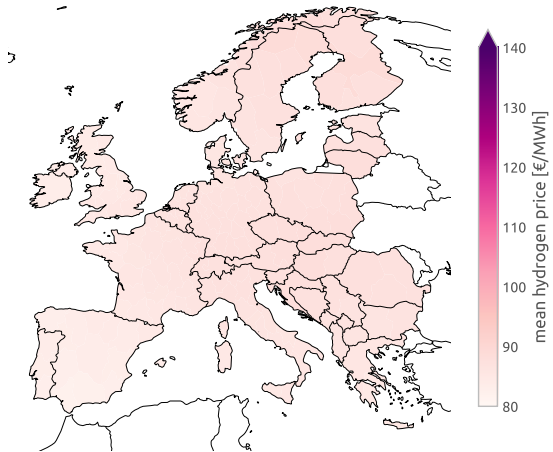
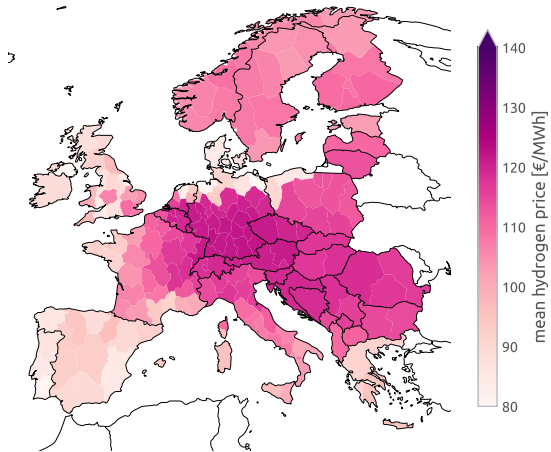


Figure S26: Regional distribution of average nodal electricity prices. The reinforcement of the electricity grid mitigates regional price differences. Some price differences persist because of expansion constraints on individual lines.

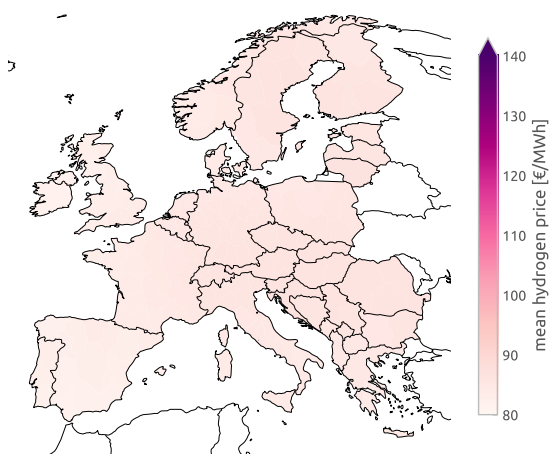
(a) With power grid expansion, with hydrogen network



(b) With power grid expansion, without hydrogen network



(c) Without power grid expansion, with hydrogen network



(d) Without power grid expansion, without hydrogen network

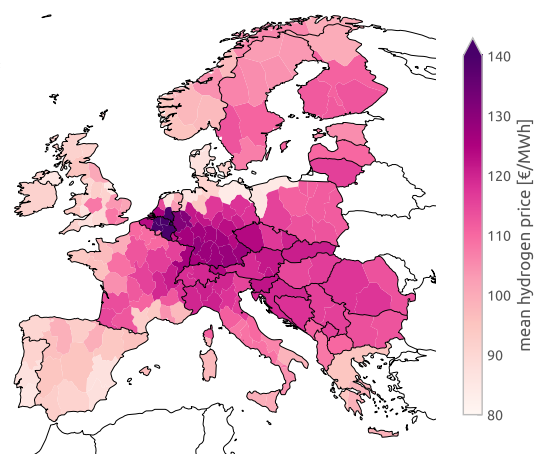


Figure S27: Regional distribution of average nodal hydrogen prices. The development of a hydrogen network evens out regional price differences. With limited H₂ network expansion prices are almost twice as high in Europe's industrial clusters than the most cost-effective hydrogen production sites.

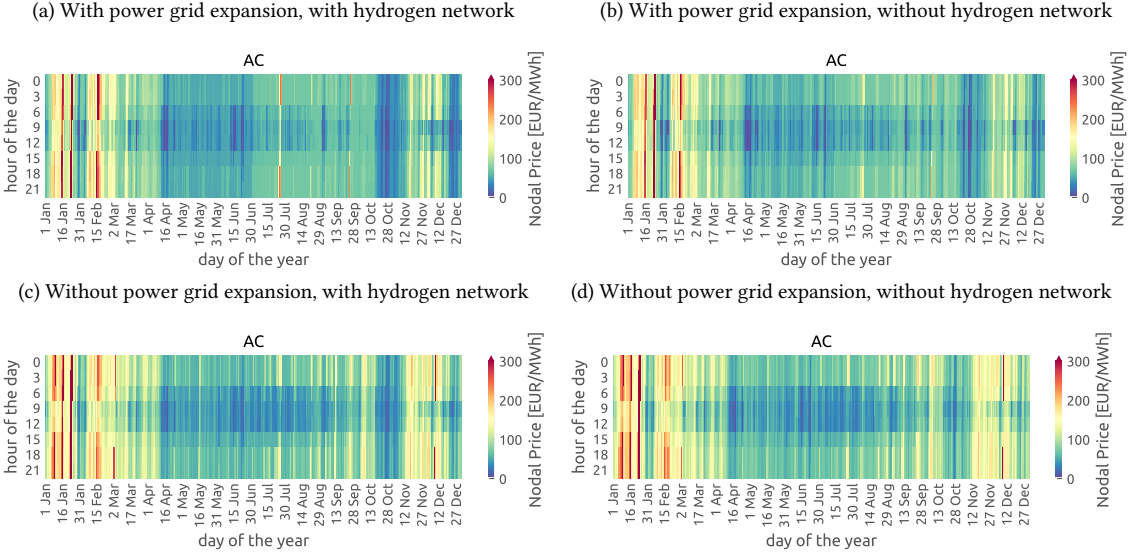


Figure S28: Temporal distribution of average nodal electricity prices. The graphs show daily patterns with price troughs during the day, especially in summer, as well as seasonal patterns with higher prices in winter than in the summer. A few periods in January and February are particularly challenging to the system, resulting in very high electricity prices.

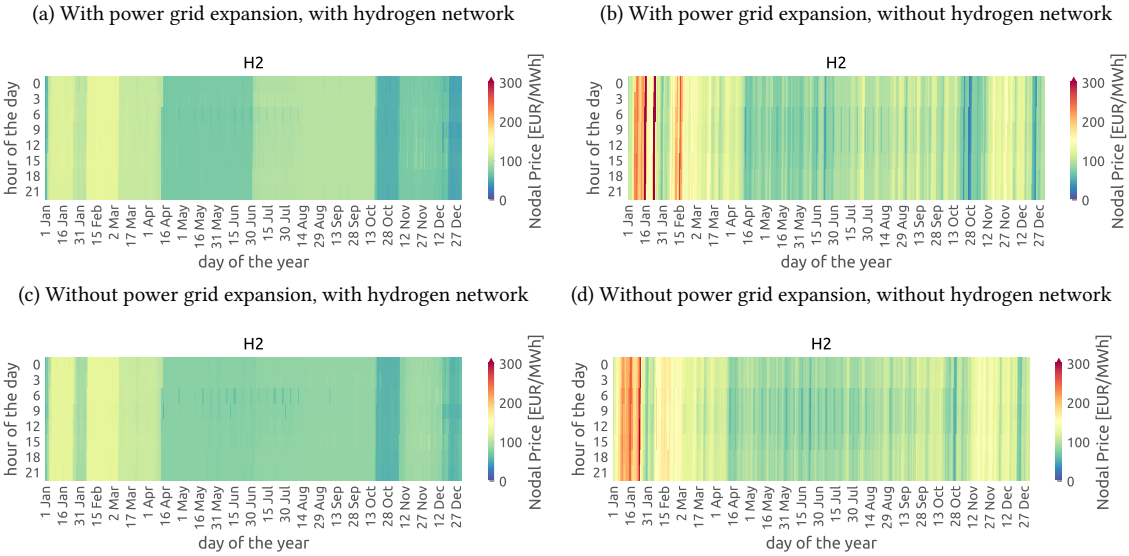
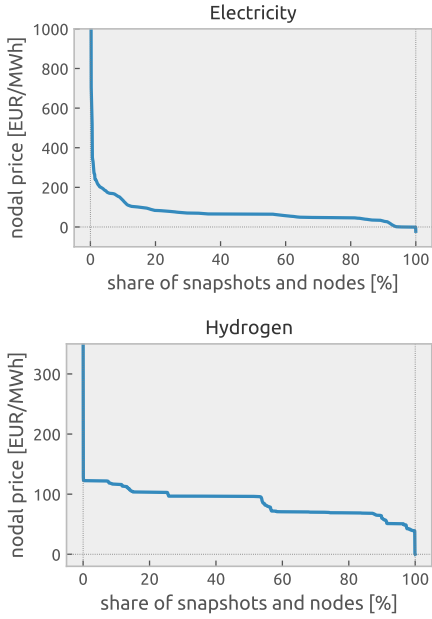
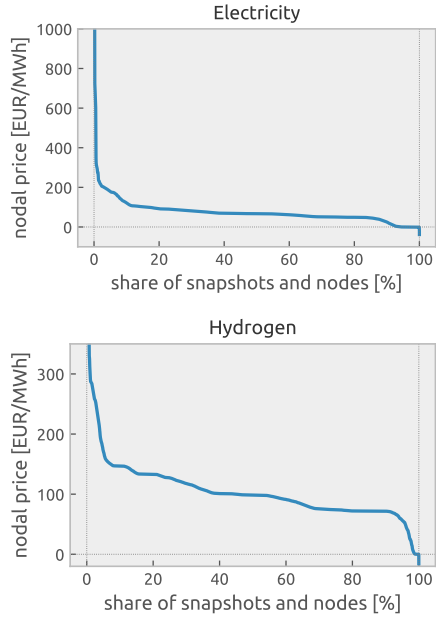


Figure S29: Temporal distribution of average nodal hydrogen prices. Compared to electricity prices, the seasonal component dominates daily patterns. Price spikes occur with limited H₂ network expansion in winter periods that are challenging to the system.

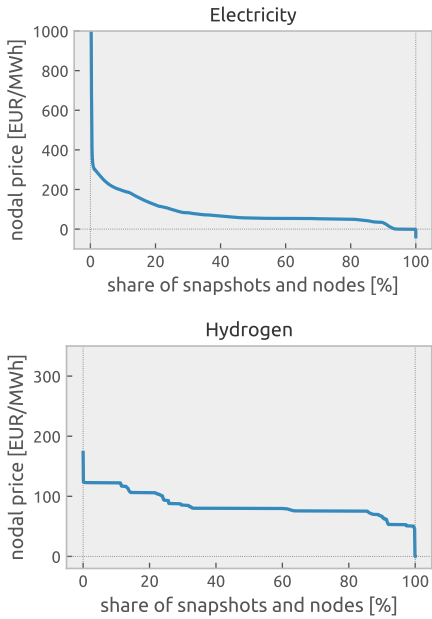
(a) With power grid expansion, with hydrogen network



(b) With power grid expansion, without hydrogen network



(c) Without power grid expansion, with hydrogen network



(d) Without power grid expansion, without hydrogen network

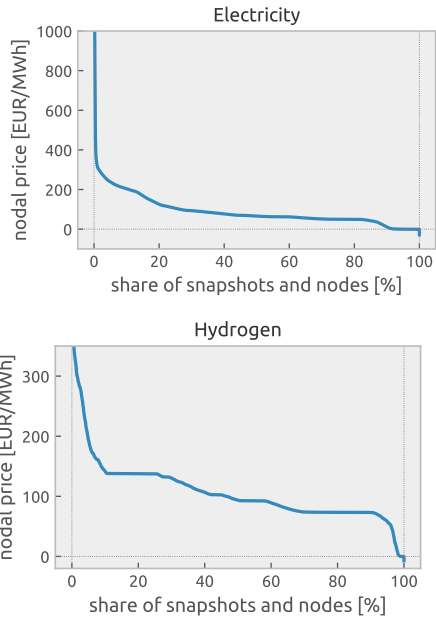
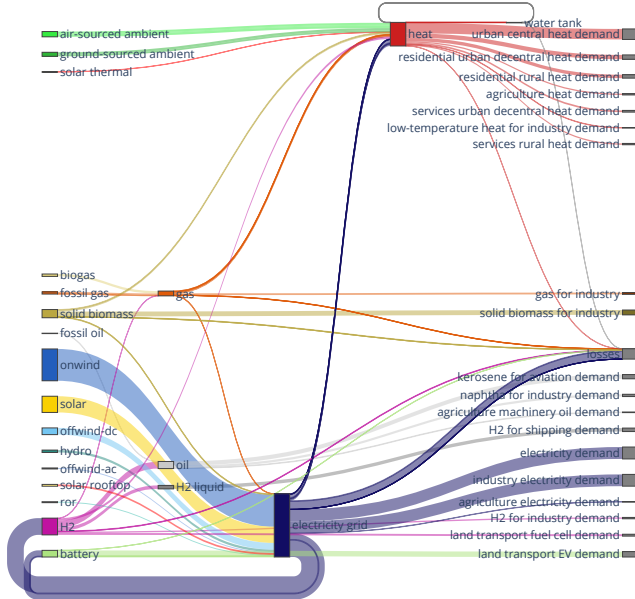
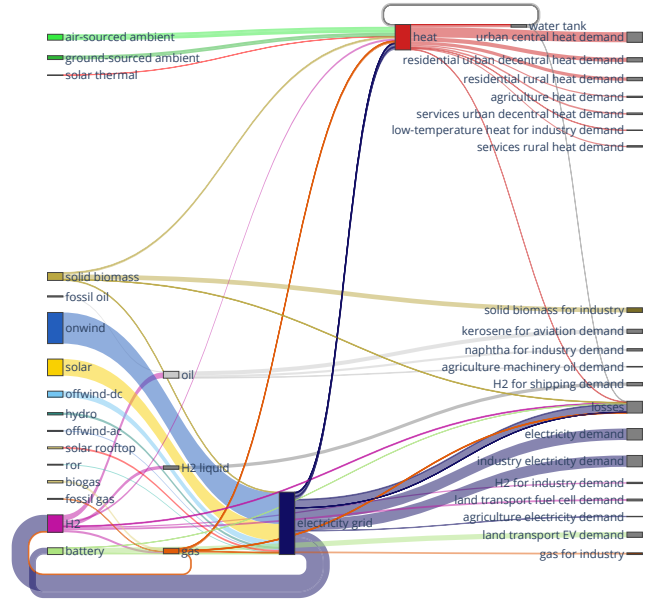


Figure S30: Duration curve of nodal electricity and hydrogen prices.

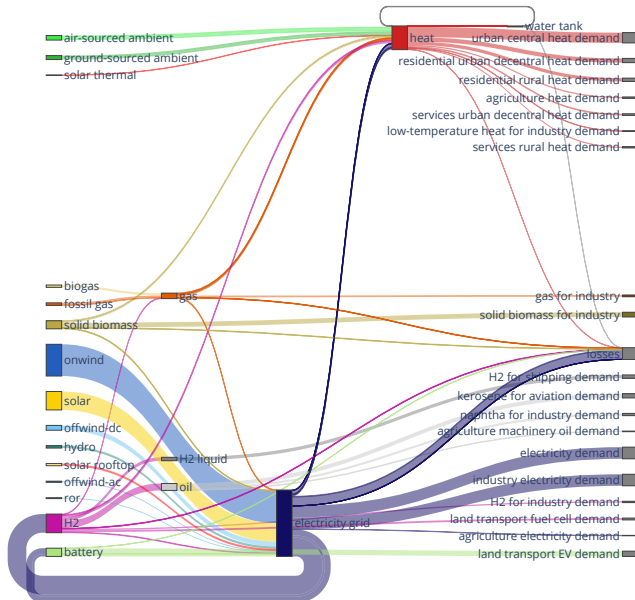
(a) With power grid expansion, with hydrogen network



(b) With power grid expansion, without hydrogen network



(c) Without power grid expansion, with hydrogen network



(d) Without power grid expansion, without hydrogen network

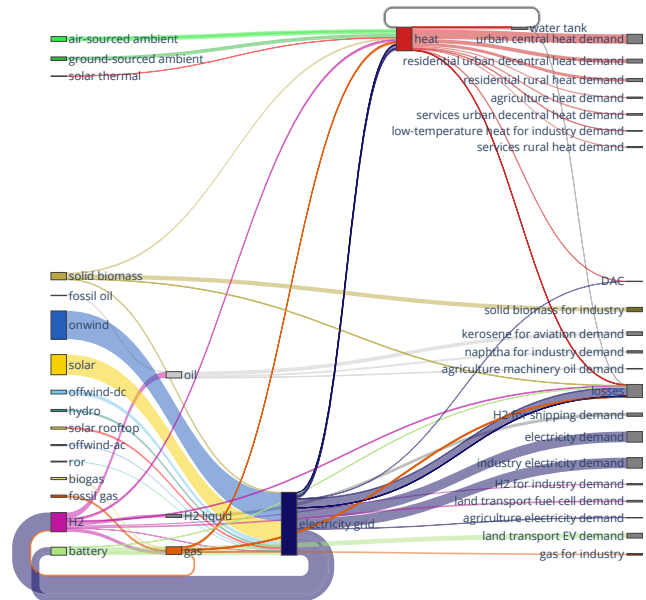
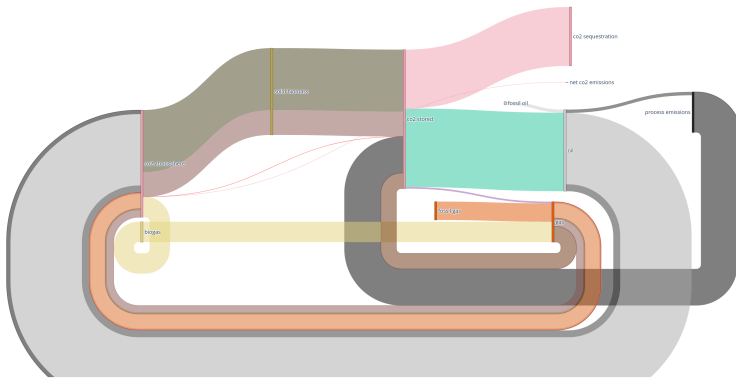
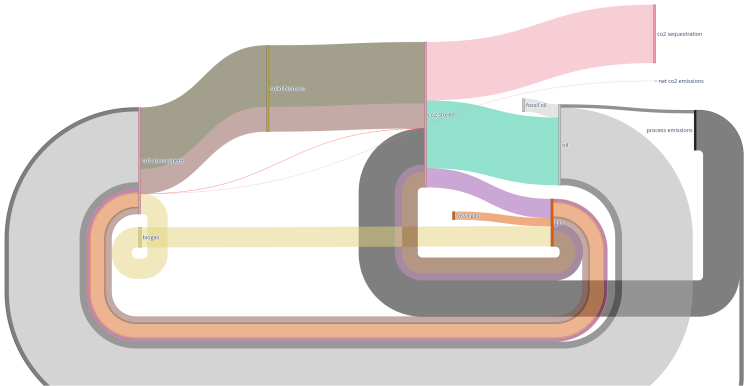


Figure S31: Sankey diagrams of energy flows in the European system. An interactive version of these plots can be explored at share.streamlit.io/fneum/spatial-sector-dashboard.

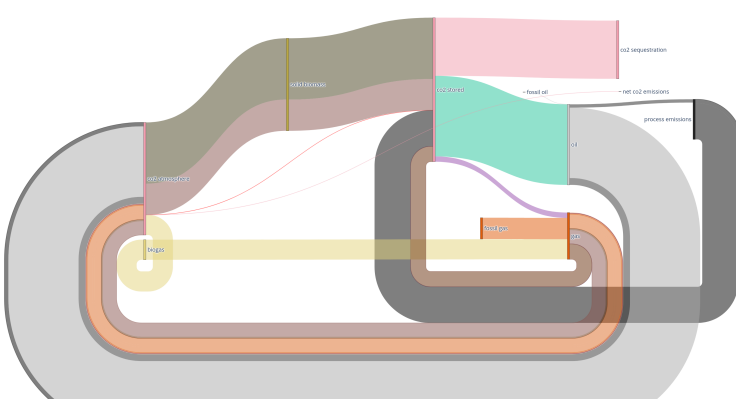
(a) With power grid expansion, with hydrogen network



(b) With power grid expansion, without hydrogen network



(c) Without power grid expansion, with hydrogen network



(d) Without power grid expansion, without hydrogen network

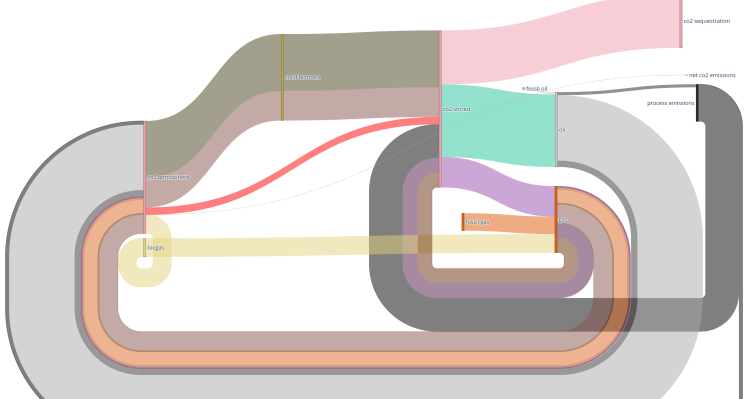
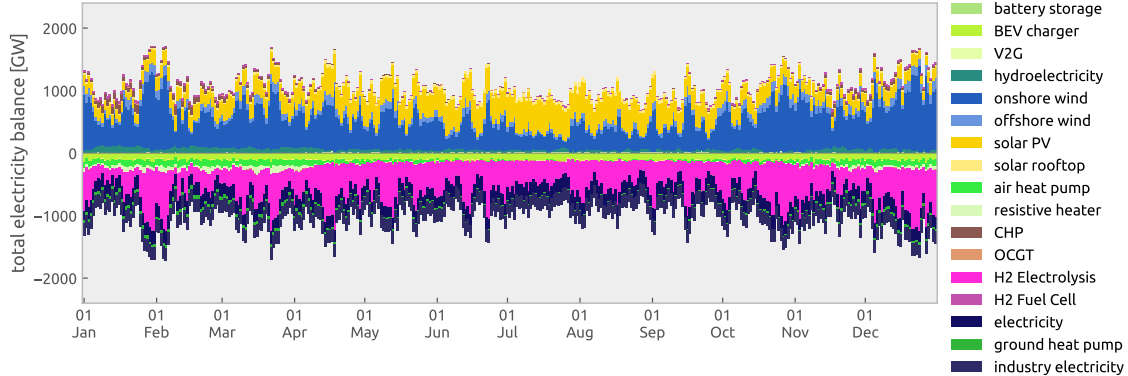
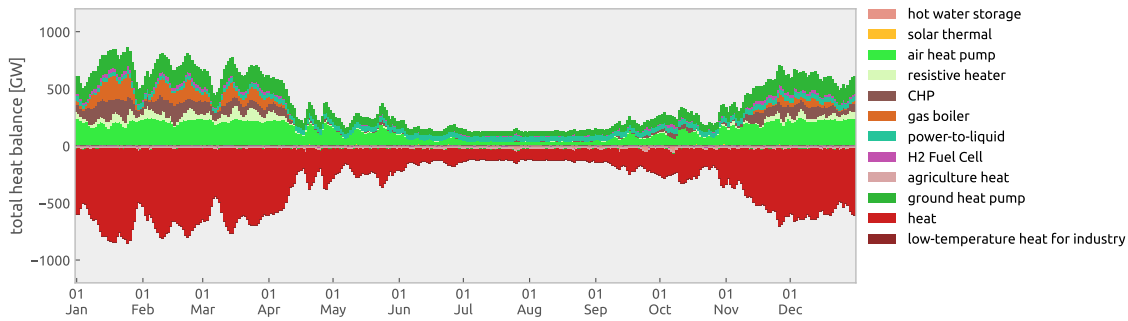


Figure S32: Sankey diagrams of carbon flows in the European system. An interactive version of these plots can be explored at share.streamlit.io/fneum/spatial-sector-dashboard.

(a) electricity



(b) space and water heating



(c) hydrogen

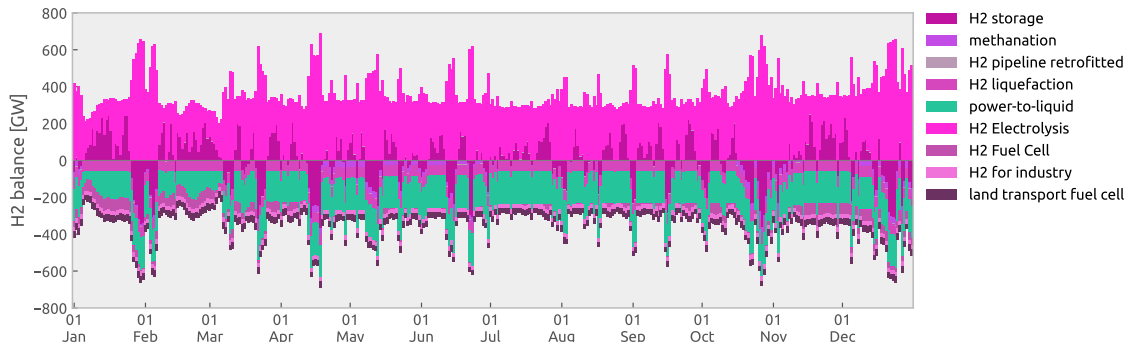
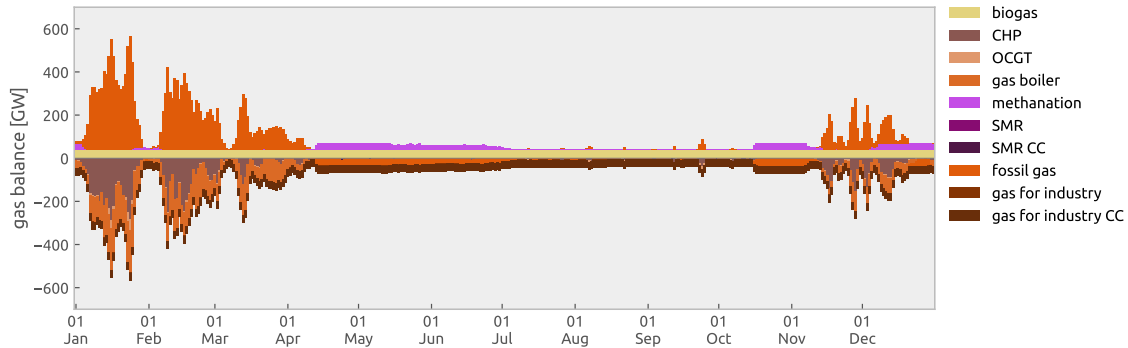
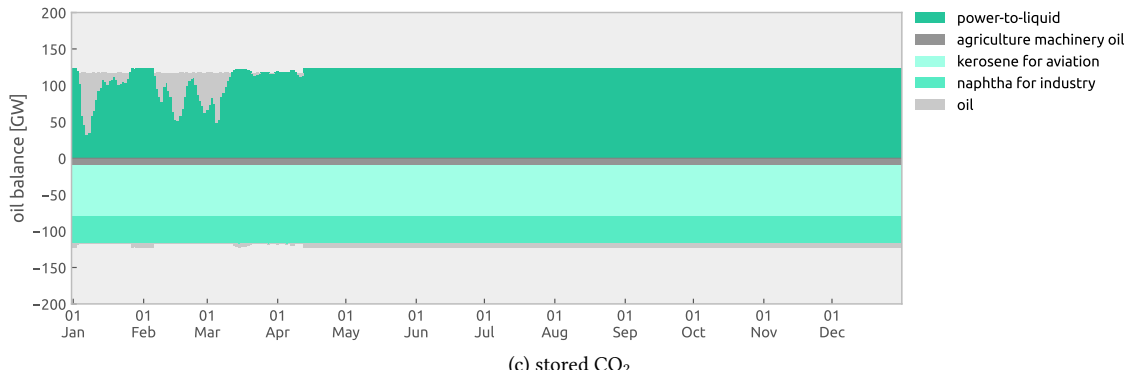


Figure S33: Daily sampled time series for (a) electricity, (b) heat, and (c) hydrogen supply (above zero) and consumption (below zero) composition. Supply and consumption balance for each bar by definition.

(a) methane



(b) oil-based products



(c) stored CO₂

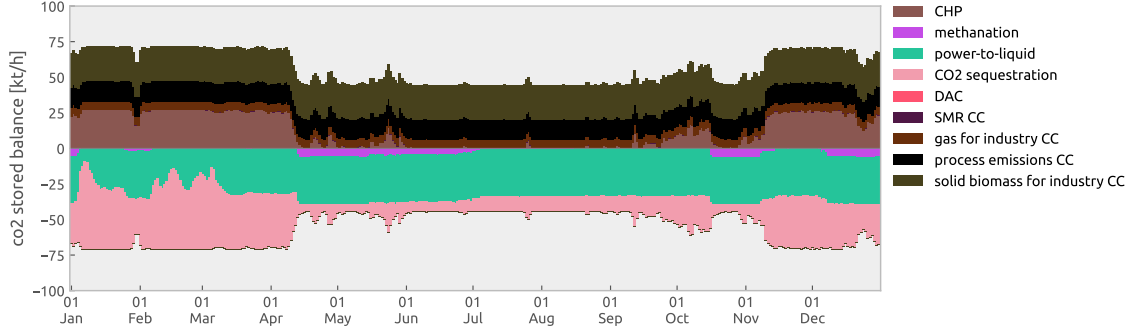
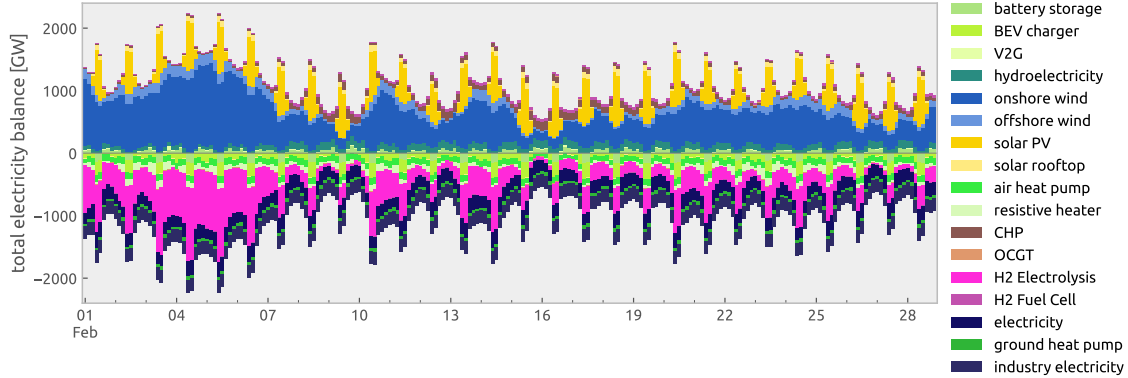
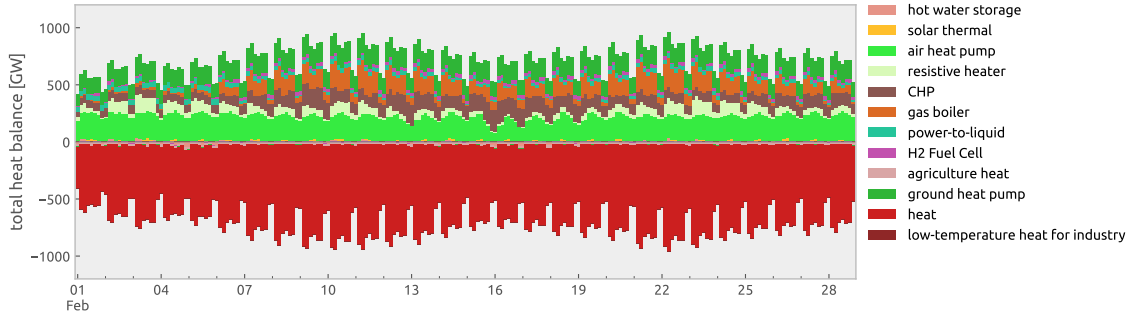


Figure S34: Daily sampled time series for (a) methane, (b) oil-based products, and (c) carbon dioxide supply (above zero) and consumption (below zero) composition. Supply and consumption balance for each bar.

(a) electricity



(b) space and water heating



(c) hydrogen

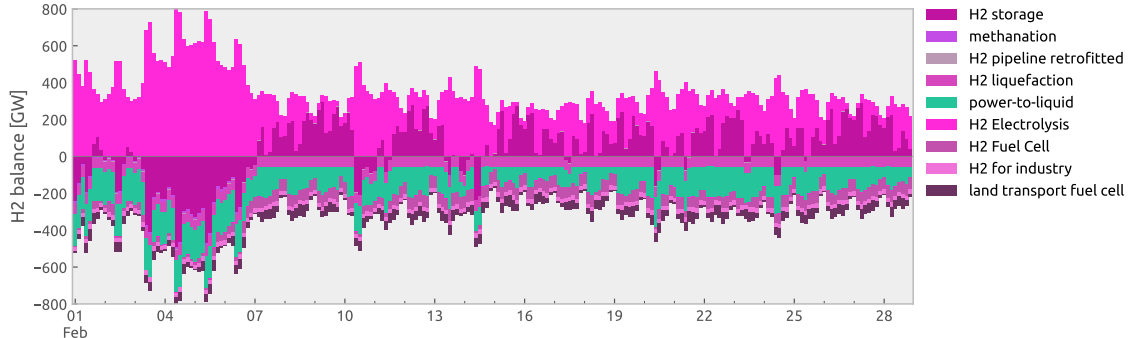


Figure S35: Hourly sampled time series of February for (a) electricity, (b) heat, and (c) hydrogen supply (above zero) and consumption (below zero) composition. Supply and consumption balance for each bar.

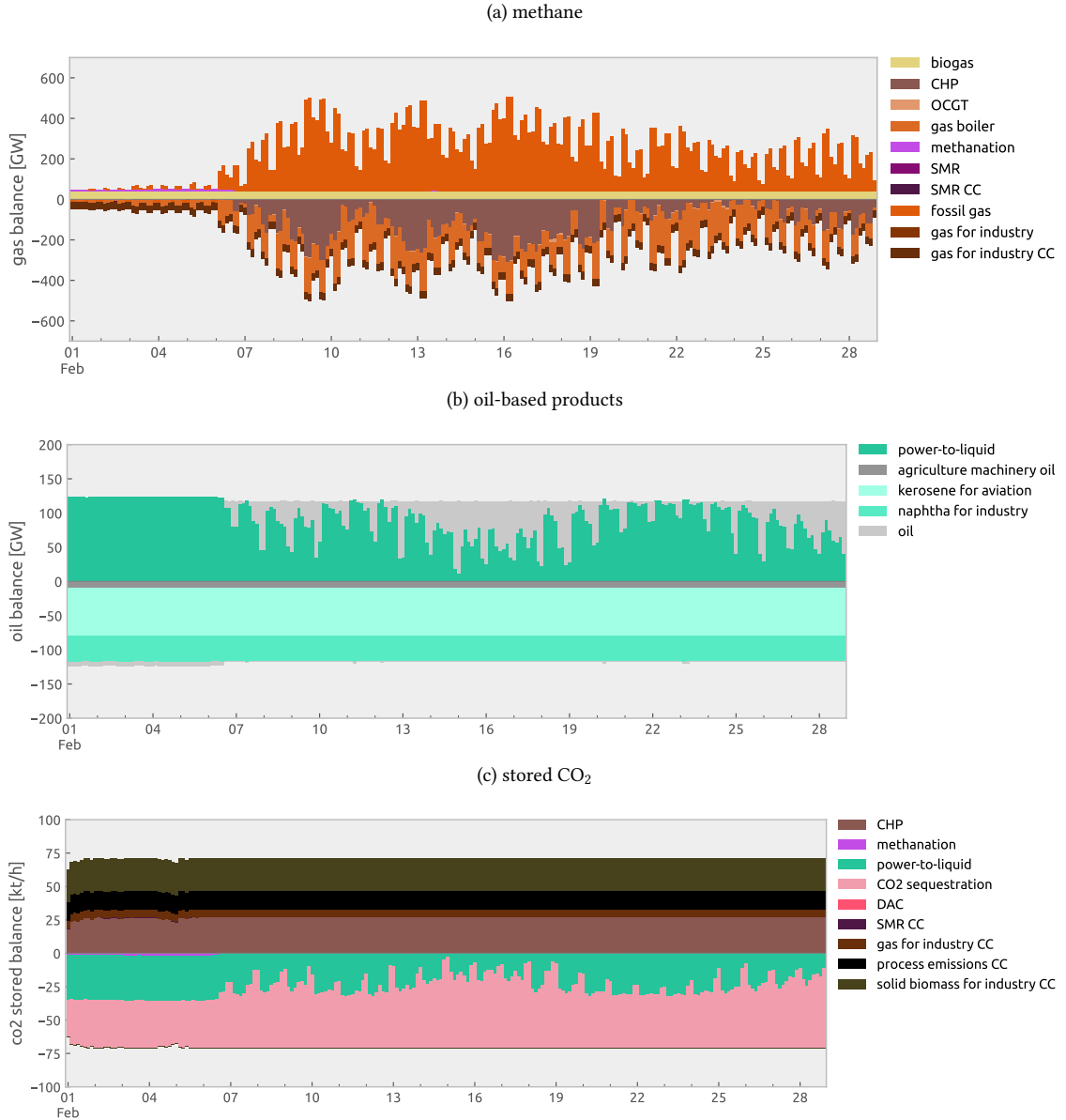


Figure S36: Hourly sampled time series of February for (a) methane, (b) oil-based products, and (c) carbon dioxide supply (above zero) and consumption (below zero) composition. Supply and consumption balance for each bar.

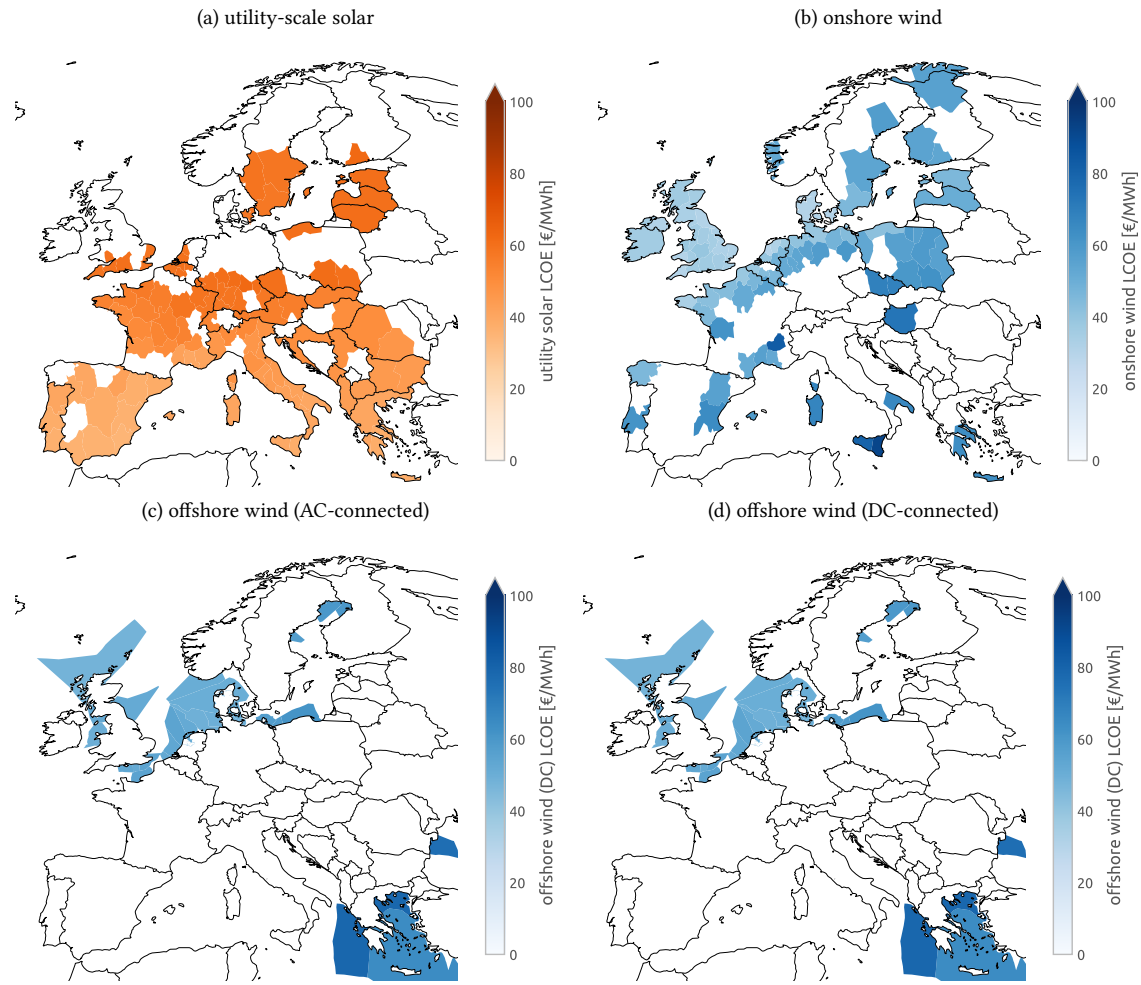


Figure S37: Levelised cost of electricity of wind and solar generation. Only shows locations where more than 1 GW of the respective technology were built.

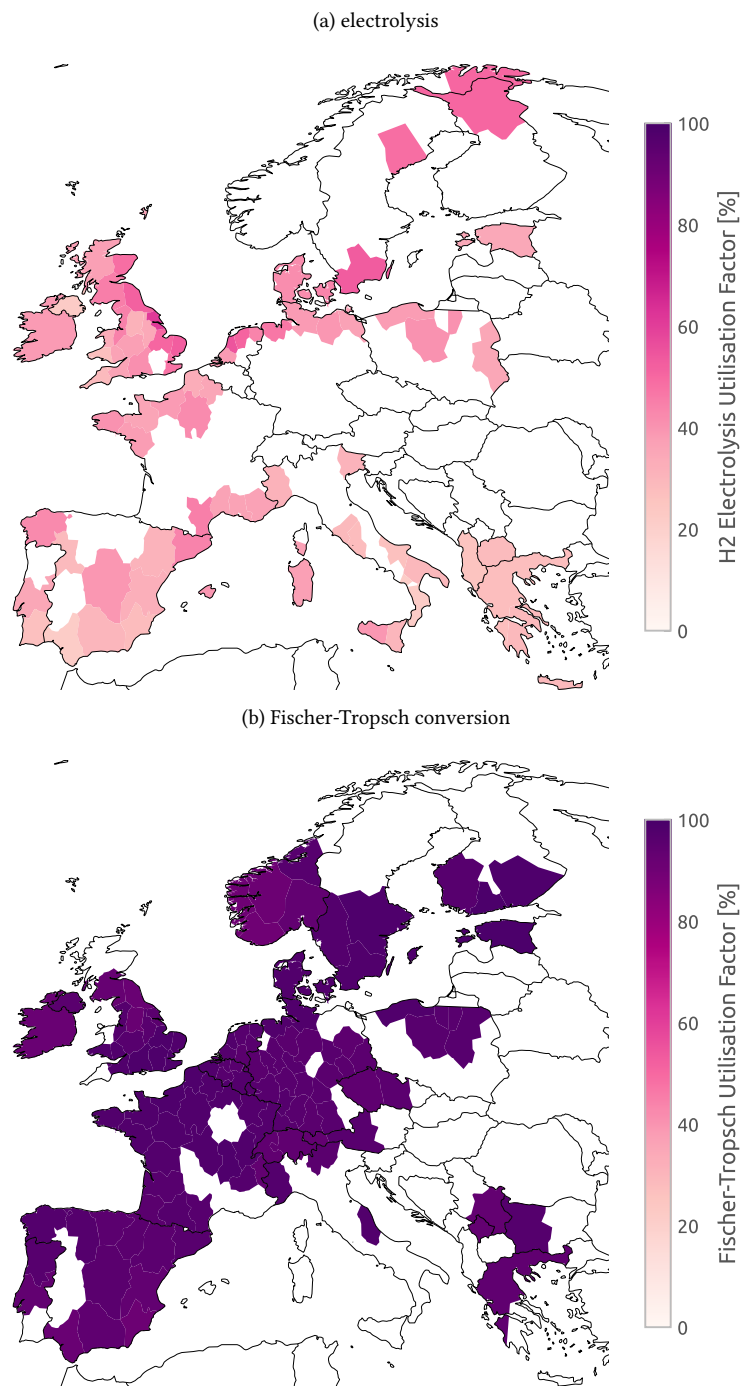
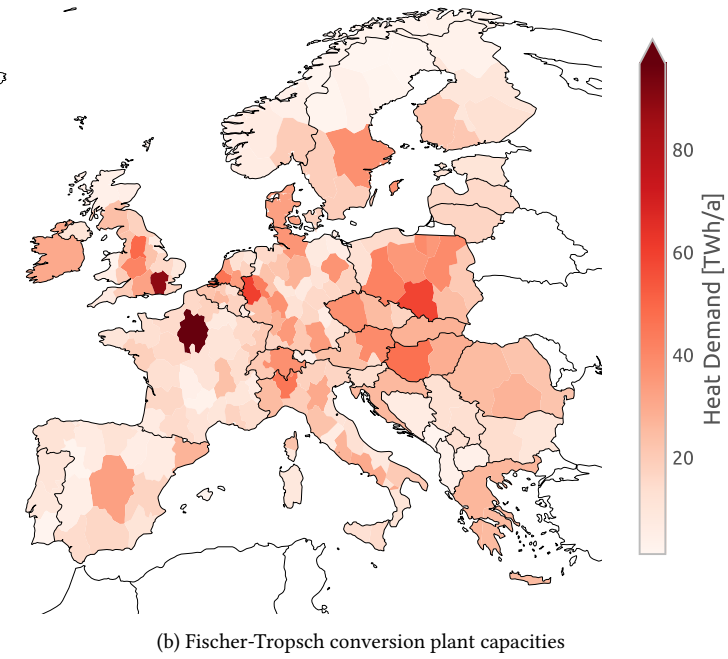


Figure S38: Utilisation rate of synthetic fuel production capacities. Only shows locations where more than 1 GW of the respective technology were built.

(a) annual space and water heat demand



(b) Fischer-Tropsch conversion plant capacities

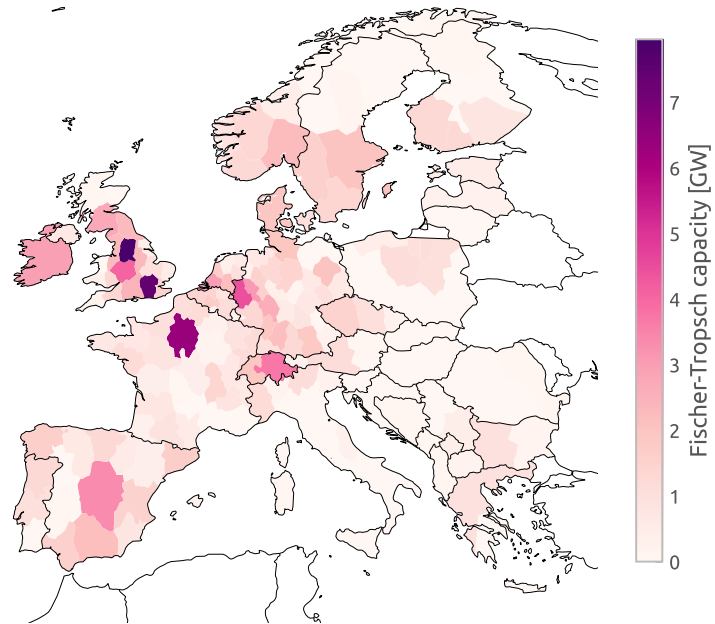


Figure S39: Pairing of Fischer-Tropsch fuel production sites and heat demand. Waste heat from synthetic fuel production can be used in the district heating networks of urban areas and supply a large share of hot water demand throughout the summer.

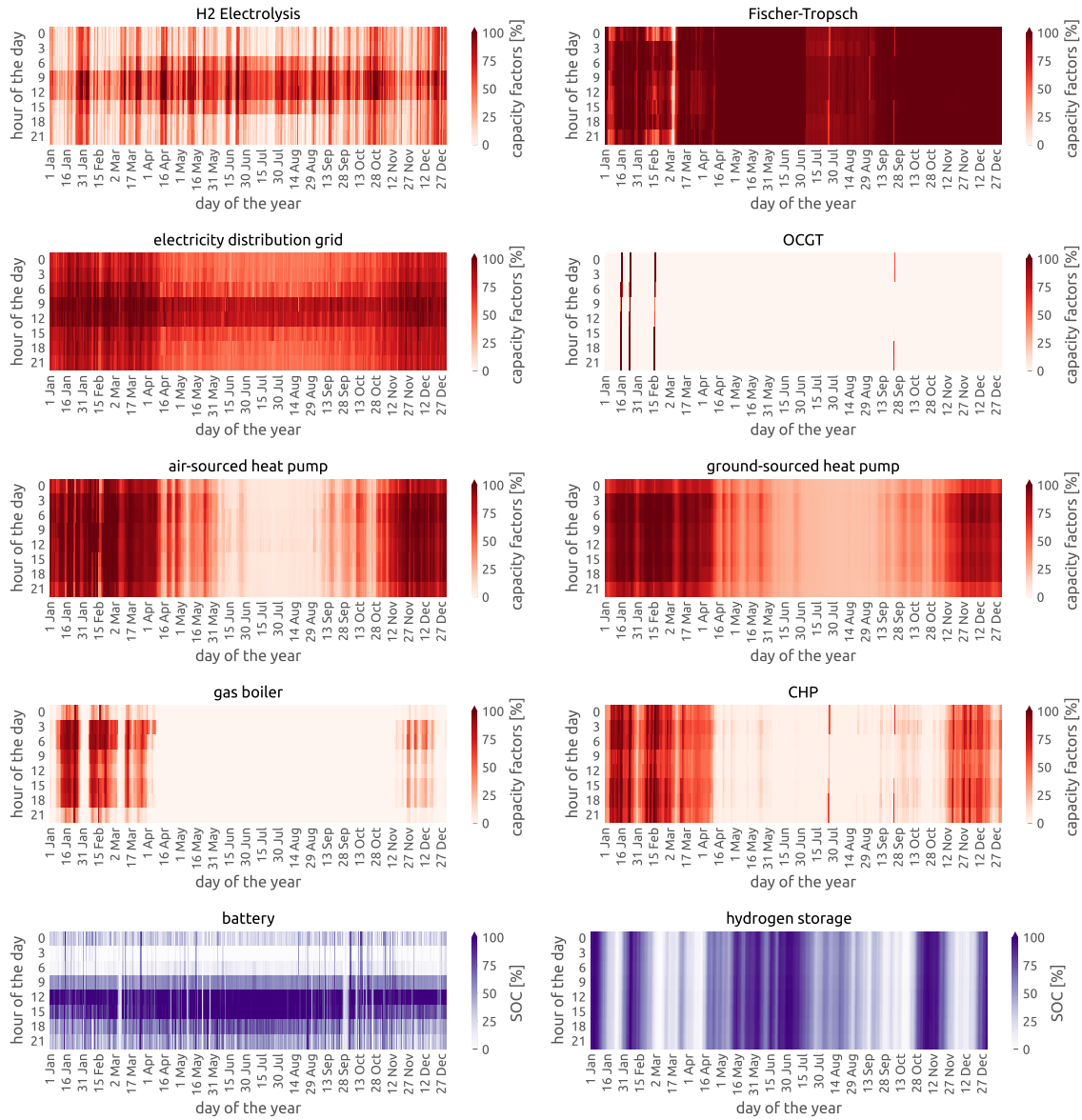


Figure S40: Operations and storage filling levels of selected energy system components. The figure outlines the flexible operation of electrolysers (both seasonally and daily) the near-constant operation of synthetic fuel production the backup role of gas power plants (OCGT), the seasonal operation of heat pumps, gas boilers, CHP, and hydrogen storage, the daily pattern of battery storage filling levels, and periods of peak loading of the power distribution grid.

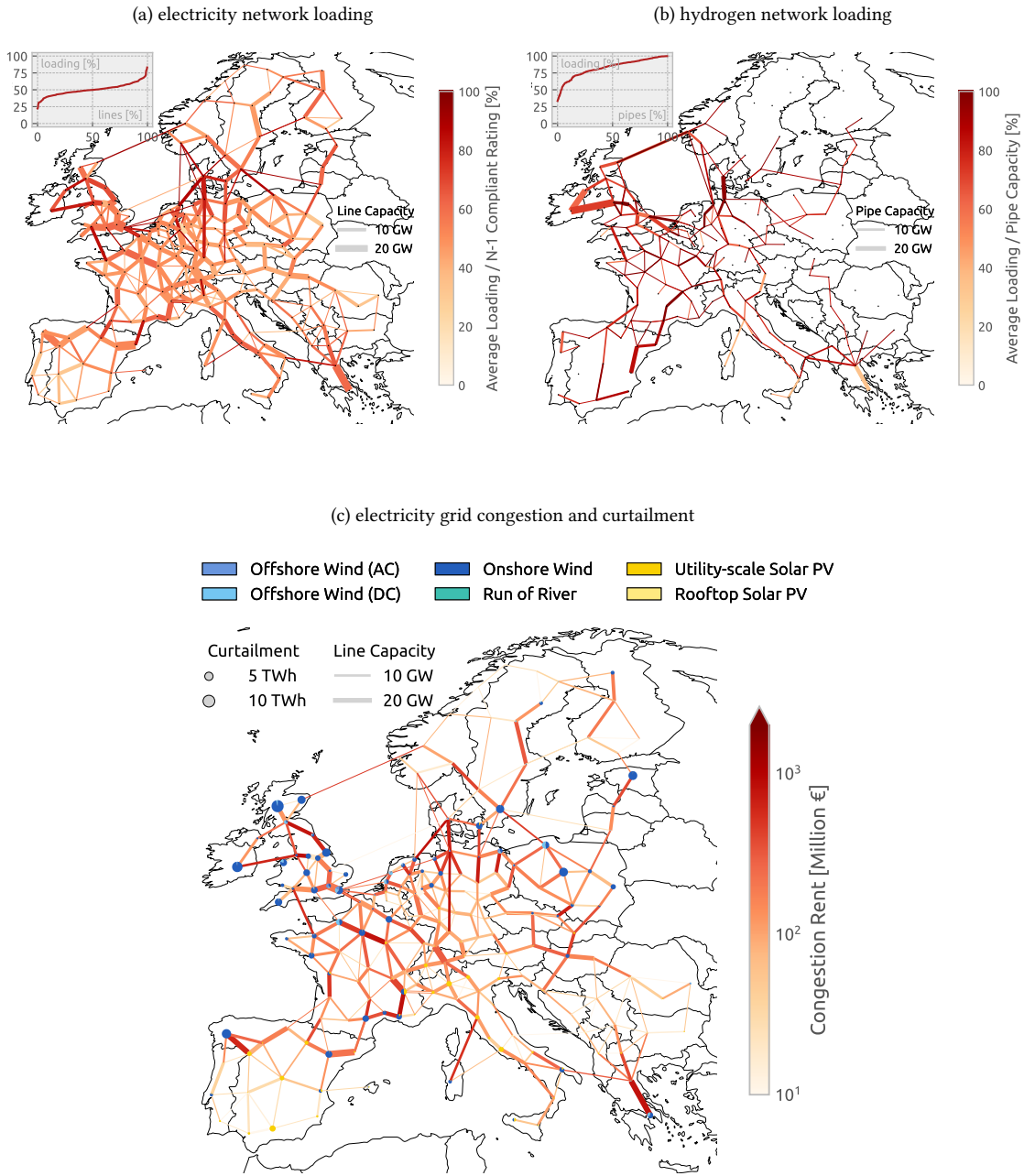


Figure S41: Utilisation rate of electricity and hydrogen network, curtailment and congestion. Subplot (a) shows average electricity network loading relative to $N - 1$ compliant line rating (70% of nominal rating) and the corresponding duration curve of line loadings. Subplot (b) shows the average hydrogen pipeline loading relative to the nominal pipeline capacity and also the corresponding duration curve of pipeline loadings. Subplot (c) shows the regional and technological distribution of curtailment in the system as well as realised congestion rents in the electricity network.

Table S3: Overview of technology assumptions.

technology	parameter	value	unit	source
AC grid connection (station)	overnight investment	250.00	€/kW _{el}	DEA S21
AC grid connection (submarine)	overnight investment	2,685.00	€/MW/km	DEA S21
AC grid connection (underground)	overnight investment	1,342.00	€/MW/km	DEA S21
CCGT	Cb coefficient	2.00	50°C/100°C	DEA S91
	Cv coefficient	0.15	50°C/100°C	DEA S91
	FOM	3.35	%/year	DEA S91
	VOM	4.20	€/MWh	DEA S91
	efficiency	0.58	per unit	DEA S91
	lifetime	25.00	years	DEA S91
	overnight investment	830.00	€/kW	DEA S91
CHP (biomass with carbon capture)	FOM	3.00	%/year	DEA S92
	carbon capture rate	0.90	per unit	DEA S92
	electricity input	0.08	MWh/tCO ₂	DEA S92
	electricity input	0.02	MWh/tCO ₂	DEA S92
	heat input	0.72	MWh/tCO ₂	DEA S92
	heat output	0.14	MWh/tCO ₂	DEA S92
	heat output	0.72	MWh/tCO ₂	DEA S92
	lifetime	25.00	years	DEA S92
	overnight investment	2,700,000.00	€/(tCO ₂ /h)	DEA S92
CHP (biomass)	Cb coefficient	0.46	40°C/80°C	DEA S91
	Cv coefficient	1.00	40°C/80°C	DEA S91
	FOM	3.58	%/year	DEA S91
	VOM	2.10	€/MWh _{el}	DEA S91
	efficiency	0.30	per unit	DEA S91
	efficiency (heat)	0.71	per unit	DEA S91
	lifetime	25.00	years	DEA S91
	overnight investment	3,210.28	€/kW _{el}	DEA S91
CHP (decentral)	FOM	3.00	%/year	Henning et al. S14
	discount rate	0.04	per unit	Palzer S94
	lifetime	25.00	years	Henning et al. S14
	overnight investment	1,400.00	€/kW _{el}	Henning et al. S14
CHP (gas, central)	Cb coefficient	1.00	50°C/100°C	DEA S91
	Cv coefficient	0.17	per unit	DEA S21

Continued on next page

Table S3: Overview of technology assumptions.

technology	parameter	value	unit	source
CHP (solid biomass, central)	FOM	3.32	%/year	DEA ^{S91}
	VOM	4.20	€/MWh	DEA ^{S91}
	efficiency	0.41	per unit	DEA ^{S91}
	lifetime	25.00	years	DEA ^{S91}
	overnight investment	560.00	€/kW	DEA ^{S91}
	Cb coefficient	0.46	40°C/80°C	DEA ^{S91}
	Cv coefficient	1.00	40°C/80°C	DEA ^{S91}
	FOM	4.10	%/year	DEA ^{S91}
	VOM	1.85	€/MWh _{el}	DEA ^{S91}
	efficiency	0.29	per unit	DEA ^{S91}
DC grid connection (station)	efficiency (heat)	0.69	per unit	DEA ^{S91}
	lifetime	25.00	years	DEA ^{S91}
	overnight investment	2,851.41	€/kW _{el}	DEA ^{S91}
	overnight investment	400.00	€/kW _{el}	Härtel et al. ^{S95}
	overnight investment	2,000.00	€/MW/km	Cole et al. ^{S96}
	overnight investment	1,000.00	€/MW/km	Härtel et al. ^{S95}
	FOM	3.00	%/year	Fasihi et al. ^{S97}
	VOM	4.20	€/MWh _{FT}	DEA ^{S98}
	efficiency	0.70	per unit	DEA ^{S98}
	lifetime	25.00	years	DEA ^{S98}
HELMETH (direct power-to-methane)	overnight investment	1,600.00	€/kW _{FT} /year	DEA ^{S98}
	FOM	3.00	%/year	no source
	efficiency	0.80	per unit	HELMETH press release
	lifetime	25.00	years	no source
	overnight investment	2,000.00	€/kW	no source
	FOM	2.00	%/year	Hagspiel et al. ^{S99}
	lifetime	40.00	years	Hagspiel et al. ^{S99}
	overnight investment	400.00	€/MW/km	Hagspiel et al. ^{S99}
	FOM	2.00	%/year	Hagspiel et al. ^{S99}
	lifetime	40.00	years	Hagspiel et al. ^{S99}
HVDC inverter pair	overnight investment	150,000.00	€/MW	Hagspiel et al. ^{S99}
	FOM	2.00	%/year	Hagspiel et al. ^{S99}
	lifetime	40.00	years	Hagspiel et al. ^{S99}
	overnight investment	400.00	€/MW/km	Hagspiel et al. ^{S99}
HVDC transmission line (overhead)	FOM	2.00	%/year	Hagspiel et al. ^{S99}
	lifetime	40.00	years	Hagspiel et al. ^{S99}
	overnight investment	400.00	€/MW/km	Hagspiel et al. ^{S99}
	FOM	2.00	%/year	Hagspiel et al. ^{S99}

Continued on next page

Table S3: Overview of technology assumptions.

technology	parameter	value	unit	source
HVDC transmission line (submarine)	FOM	0.35	%/year	Purvins et al. S100
	lifetime	40.00	years	Purvins et al. S100
	overnight investment	471.16	€/MW/km	Purvins et al. S100
OCGT	FOM	1.78	%/year	DEA S91
	VOM	4.50	€/MWh	DEA S91
	efficiency	0.41	per unit	DEA S91
	lifetime	25.00	years	DEA S91
	overnight investment	435.24	€/kW	DEA S91
battery inverter	FOM	0.34	%/year	DEA S101
	efficiency	0.96	per unit	DEA S101
	lifetime	10.00	years	DEA S101
	overnight investment	160.00	€/kW	DEA S101
battery storage	lifetime	25.00	years	DEA S101
	overnight investment	142.00	€/kWh	DEA S101
biogas	fuel	59.00	€/MWh _{th}	Zappa et al. S102
biogas upgrading	FOM	2.49	%/year	DEA S98
	VOM	3.18	€/MWh input	DEA S98
	lifetime	15.00	years	DEA S98
	overnight investment	381.00	€/kW input	DEA S98
biomass	FOM	4.53	%/year	Schröder et al. S103
	efficiency	0.47	per unit	Schröder et al. S103
	fuel	7.00	€/MWh _{th}	IEA S104
	lifetime	30.00	years	Schroeder et al. S103
	overnight investment	2,209.00	€/kW _{el}	Schröder et al. S103
cement capture	FOM	3.00	%/year	DEA S92
	carbon capture rate	0.90	per unit	DEA S92
	electricity input	0.08	MWh/tCO ₂	DEA S92
	electricity input	0.02	MWh/tCO ₂	DEA S92
	heat input	0.72	MWh/tCO ₂	DEA S92
	heat output	0.14	MWh/tCO ₂	DEA S92
	heat output	1.54	MWh/tCO ₂	DEA S92
	lifetime	25.00	years	DEA S92
	overnight investment	2,600,000.00	€/(tCO ₂ /h)	DEA S92
coal	FOM	1.60	%/year	Lazard 13.0 S105

Continued on next page

Table S3: Overview of technology assumptions.

technology	parameter	value	unit	source
decentral oil boiler	VOM	3.50	€/MWh _{el}	Lazard 13.0 ^{S105}
	carbon intensity	0.34	tCO ₂ /MWh _{th}	UBA ^{S106}
	efficiency	0.33	per unit	Lazard 13.0 ^{S105}
	fuel	8.15	€/MWh _{th}	BP ^{S107}
	lifetime	40.00	years	Lazard 13.0 ^{S105}
	overnight investment	3,845.51	€/kW _{el}	Lazard 13.0 ^{S105}
	FOM	2.00	%/year	Erlach et al. ^{S108}
	efficiency	0.90	per unit	Erlach et al. ^{S108}
	lifetime	20.00	years	Erlach et al. ^{S108}
	overnight investment	156.01	€/kW _{th}	Erlach et al. ^{S108}
direct air capture (DAC)	FOM	4.95	%/year	DEA ^{S92}
	electricity input	0.15	MWh/tCO ₂	DEA ^{S92}
	electricity input	0.32	MWh/tCO ₂	DEA ^{S92}
	heat input	2.00	MWh/tCO ₂	DEA ^{S92}
	heat output	0.20	MWh/tCO ₂	DEA ^{S92}
	heat output	1.00	MWh/tCO ₂	DEA ^{S92}
	lifetime	20.00	years	DEA ^{S92}
	overnight investment	6,000,000.00	€/(tCO ₂ /h)	DEA ^{S92}
	FOM	2.00	%/year	Element Energy ^{S109}
	lifetime	40.00	years	Element Energy ^{S109}
electricity distribution grid	overnight investment	500.00	€/kW	Element Energy ^{S109}
	FOM	2.00	%/year	Element Energy ^{S109}
	lifetime	40.00	years	Element Energy ^{S109}
	overnight investment	140.00	€/kW	DEA ^{S21}
electrolysis	FOM	2.00	%/year	DEA ^{S98}
	efficiency	0.68	per unit	DEA ^{S98}
	lifetime	30.00	years	DEA ^{S98}
	overnight investment	450.00	€/kW _{el}	DEA ^{S98}
fossil gas	carbon intensity	0.20	tCO ₂ /MWh _{th}	UBA ^{S106}
	fuel	20.10	€/MWh _{th}	BP ^{S107}
	FOM	2.46	%/year	DEA ^{S91}
fossil oil	VOM	6.00	€/MWh	DEA ^{S91}
	carbon intensity	0.27	tCO ₂ /MWh _{th}	UBA ^{S106}
	efficiency	0.35	per unit	DEA ^{S91}

Continued on next page

Table S3: Overview of technology assumptions.

technology	parameter	value	unit	source
fuel cell	fuel	50.00	€/MWh _{th}	IEA S104
	lifetime	25.00	years	DEA S91
	overnight investment	343.00	€/kW	DEA S91
	Cb coefficient	1.25	50°C/100°C	DEA S91
	FOM	5.00	%/year	DEA S91
	efficiency	0.50	per unit	DEA S91
	lifetime	10.00	years	DEA S91
gas boiler (central)	overnight investment	1,100.00	€/kW _{el}	DEA S91
	FOM	3.80	%/year	DEA S91
	VOM	1.00	€/MWh _{th}	DEA S91
	efficiency	1.04	per unit	DEA S91
gas boiler (decentral)	lifetime	25.00	years	DEA S91
	overnight investment	50.00	€/kW _{th}	DEA S91
	FOM	6.69	%/year	DEA S110
	discount rate	0.04	per unit	Palzer S94
	efficiency	0.98	per unit	DEA S110
heat pump (air-sourced, central)	lifetime	20.00	years	DEA S110
	overnight investment	296.82	€/kW _{th}	DEA S110
	FOM	0.23	%/year	DEA S91
	VOM	2.51	€/MWh _{th}	DEA S91
	efficiency	3.60	per unit	DEA S91
heat pump (air-sourced, decentral)	lifetime	25.00	years	DEA S91
	overnight investment	856.25	€/kW _{th}	DEA S91
	FOM	3.00	%/year	DEA S110
	discount rate	0.04	per unit	Palzer S94
	efficiency	3.60	per unit	DEA S110
heat pump (ground-sourced, central)	lifetime	18.00	years	DEA S110
	overnight investment	850.00	€/kW _{th}	DEA S110
	FOM	0.39	%/year	DEA S91
	VOM	1.25	€/MWh _{th}	DEA S91
	efficiency	1.73	per unit	DEA S91
heat pump (ground-sourced, decentral)	lifetime	25.00	years	DEA S91
	overnight investment	507.60	€/kW _{th}	DEA S91
	FOM	1.82	%/year	DEA S110

Continued on next page

Table S3: Overview of technology assumptions.

technology	parameter	value	unit	source
home battery inverter	discount rate	0.04	per unit	Palzer ^{S94}
	efficiency	3.90	per unit	DEA ^{S110}
	lifetime	20.00	years	DEA ^{S110}
	overnight investment	1,400.00	€/kW _{th}	DEA ^{S110}
	FOM		%/year	Ram et al. ^{S111} , DEA ^{S101}
	efficiency	0.96	per unit	Ram et al. ^{S111} , DEA ^{S101}
	lifetime	10.00	years	Ram et al. ^{S111} , DEA ^{S101}
	overnight investment	228.06	€/kW	Ram et al. ^{S111} , DEA ^{S101}
	lifetime	25.00	years	Ram et al. ^{S111} , DEA ^{S101}
	overnight investment	202.90	€/kWh	Ram et al. ^{S111} , DEA ^{S101}
hydrogen liquefaction	FOM	8.00	%/year	Reuß et al. ^{S112}
	lifetime	20.00	years	Reuß et al. ^{S112}
	overnight investment	1,497,967.32	€/MW _{H₂}	Reuß et al. ^{S112}
hydrogen pipeline	FOM	3.17	%/year	DEA ^{S113}
	lifetime	50.00	years	DEA ^{S113}
	overnight investment	226.47	€/MW/km	Gas for Climate ^{S2}
hydrogen pipeline (repurposed)	FOM	3.17	%/year	DEA ^{S113}
	lifetime	50.00	years	DEA ^{S113}
	overnight investment	105.88	€/MW/km	Gas for Climate ^{S2}
hydrogen pipeline (submarine)	FOM	3.00	%/year	Assume same as for CH4 (g) submarine pipeline.
	lifetime	30.00	years	Assume same as for CH4 (g) submarine pipeline.
	overnight investment	329.37	€/MW/km	Assume similar cost as for CH4 (g) submarine pipeline but with the same factor as between onland CH4 (g) pipeline and H ₂ (g) pipeline (2.86). This estimate is comparable to a 36in diameter pipeline calculated based on d'Amore-Domenech et al (2021): 10.1016/j.apenergy.2021.116625 , supplementary material (=251 EUR/MW/km).
	FOM	1.11	%/year	DEA ^{S101}
hydrogen storage (steel tank)	lifetime	30.00	years	DEA ^{S101}

Continued on next page

Table S3: Overview of technology assumptions.

technology	parameter	value	unit	source
hydrogen storage (underground)	overnight investment	44.91	€/kWh	DEA S101
	FOM	0.00	%/year	DEA S101
	VOM	0.00	€/MWh	DEA S101
	lifetime	100.00	years	DEA S101
lignite	overnight investment	2.00	€/kWh	DEA S101
	FOM	1.60	%/year	Lazard 13.0 S105
	VOM	3.50	€/MWh _{el}	Lazard 13.0 S105
	carbon intensity	0.41	tCO ₂ /MWh _{th}	UBA S106
	efficiency	0.33	per unit	Lazard 13.0 S105
	fuel	2.90	€/MWh _{th}	Schröder et al. S103
	lifetime	40.00	years	Lazard 13.0 S105
methanation	overnight investment	3,845.51	€/kW _{el}	Lazard 13.0 S105
	FOM	4.00	%/year	Fasihi et al. S97
	efficiency	0.80	per unit	Schaber S114 , Palzer S94
	lifetime	30.00	years	Fasihi et al. S97
natural gas pipeline	overnight investment	278.00	€/kW _{CH4}	Fasihi et al. S97
	FOM	1.50	%/year	Assume same as for H2 (g) pipeline in 2050 (CH4 pipeline as mature technology).
	lifetime	50.00	years	Assume same as for H2 (g) pipeline in 2050 (CH4 pipeline as mature technology).
natural gas pipeline (submarine)	overnight investment	79.00	€/MW/km	Guesstimate.
	FOM	3.00	%/year	d'Amore-Domenech et al. S115
	lifetime	30.00	years	d'Amore-Domenech et al. S115
offshore wind	overnight investment	114.89	€/MW/km	Kaiser S116
	FOM	2.32	%/year	DEA S91
	VOM	3.89	€/MWh _{el} , 2020	DEA S91
	lifetime	30.00	years	DEA S91
onshore wind	overnight investment	1,523.55	€/kW _{el} , 2020	DEA S91
	FOM	1.22	%/year	DEA S91
	VOM	1.35	€/MWh	DEA S91
	lifetime	30.00	years	DEA S91
pumped hydro storage	overnight investment	1,035.56	€/kW	DEA S91
	FOM	1.00	%/year	Schröder et al. S103
	efficiency	0.75	per unit	Schröder et al. S103

Continued on next page

Table S3: Overview of technology assumptions.

technology	parameter	value	unit	source
reservoir hydro	lifetime	80.00	years	IEA S104
	overnight investment	2,208.16	€/kW _{el}	Schröder et al. S103
	FOM	1.00	%/year	Schröder et al. S103
	efficiency	0.90	per unit	Schröder et al. S103
resistive heater (central)	lifetime	80.00	years	IEA S104
	overnight investment	2,208.16	€/kW _{el}	Schröder et al. S103
	FOM	1.70	%/year	DEA S91
	VOM	1.00	€/MWh _{th}	DEA S91
resistive heater (decentral)	efficiency	0.99	per unit	DEA S91
	lifetime	20.00	years	DEA S91
	overnight investment	60.00	€/kW _{th}	DEA S91
	FOM	2.00	%/year	Schaber S114
run of river	discount rate	0.04	per unit	Palzer S94
	efficiency	0.90	per unit	Schaber S114
	lifetime	20.00	years	Schaber S114
	overnight investment	100.00	€/kWh _{th}	Schaber S114
solar PV	FOM	2.00	%/year	Schröder et al. S103
	efficiency	0.90	per unit	Schröder et al. S103
	lifetime	80.00	years	IEA S104
	overnight investment	3,312.24	€/kW _{el}	Schröder et al. S103
solar PV (rooftop)	FOM	1.95	%/year	DEA S91
	VOM	0.01	€/MWh _{el}	RES costs made up to fix curtailment order
	lifetime	40.00	years	DEA S91
	overnight investment	492.11	€/kW _{el}	DEA S91
solar PV (utility-scale)	FOM	1.42	%/year	DEA S91
	discount rate	0.04	per unit	standard for decentral
	lifetime	40.00	years	DEA S91
	overnight investment	636.66	€/kW _{el}	DEA S91
solar thermal (central)	FOM	2.48	%/year	DEA S91
	lifetime	40.00	years	DEA S91
	overnight investment	347.56	€/kW _{el}	DEA S91
	FOM	1.40	%/year	Henning et al. S14
	lifetime	20.00	years	Henning et al. S14
	overnight investment	140,000.00	€/1000m ²	Henning et al. S14

Continued on next page

Table S3: Overview of technology assumptions.

technology	parameter	value	unit	source
solar thermal (decentral)	FOM	1.30	%/year	Henning et al. ^{S14}
	discount rate	0.04	per unit	Palzer ^{S94}
	lifetime	20.00	years	Henning et al. ^{S14}
	overnight investment	270,000.00	€/1000m ²	Henning et al. ^{S14}
solid biomass	carbon intensity	0.30	tCO ₂ /MWh _{th}	Element Energy ^{S109}
	fuel	25.20	€/MWh _{th}	Zappa et al. ^{S102}
steam methane reforming	FOM	5.00	%/year	DEA ^{S21}
	efficiency	0.76	per unit (in LHV)	IEA ^{S117}
	lifetime	30.00	years	IEA ^{S117}
	overnight investment	493,470.40	€/MW _{CH₄}	DEA ^{S21}
steam methane reforming with carbon capture	FOM	5.00	%/year	DEA ^{S21}
	carbon capture rate	0.90	€/MW _{CH₄}	IEA ^{S117}
	efficiency	0.69	per unit (in LHV)	IEA ^{S117}
	lifetime	30.00	years	IEA ^{S117}
	overnight investment	572,425.66	€/MW _{CH₄}	DEA ^{S21}
	FOM	0.55	%/year	DEA ^{S101}
thermal storage (water tank, central)	lifetime	25.00	years	DEA ^{S101}
	overnight investment	0.54	€/kWh	DEA ^{S101}
	FOM	1.00	%/year	Henning et al. ^{S14}
thermal storage (water tank, decentral)	discount rate	0.04	per unit	Palzer ^{S94}
	lifetime	20.00	years	Henning et al. ^{S14}
	overnight investment	18.38	€/kWh	Gerhardt et al. ^{S118}
	efficiency	0.84	per unit	DEA ^{S101}
water tank charger	efficiency	0.84	per unit	DEA ^{S101}
water tank discharger				

Supplementary References

- [S1] J. Köster, S. Rahmann, Snakemake – a scalable bioinformatics workflow engine, *Bioinformatics* (Oxford, England) 28 (19) (2012) 2520–2522. [doi:10/gd2xzq](https://doi.org/10/gd2xzq).
- [S2] Gurobi optimization.
URL <https://www.gurobi.com/>
- [S3] J. Hörsch, F. Hofmann, D. Schlachtberger, T. Brown, PyPSA-Eur: An open optimisation model of the European transmission system, *Energy Strategy Reviews* 22 (2018) 207–215. [arXiv:1806.01613](https://arxiv.org/abs/1806.01613), [doi:10.1016/j.esr.2018.08.012](https://doi.org/10.1016/j.esr.2018.08.012).
- [S4] J. Muehlenpfordt, Time series (Oct. 2020). [doi:10.25832/TIME_SERIES/2020-10-06](https://doi.org/10.25832/TIME_SERIES/2020-10-06).
- [S5] P. Manz, T. Fleiter, Georeferenced industrial sites with fuel demand and excess heat potential (Mar. 2018). [doi:10.5281/zenodo.4687147](https://doi.org/10.5281/zenodo.4687147).
- [S6] F. Gotzens, H. Heinrichs, J. Hörsch, F. Hofmann, Performing energy modelling exercises in a transparent way - The issue of data quality in power plant databases, *Energy Strategy Reviews* 23 (2019) 1–12. [doi:10.1016/j.esr.2018.11.004](https://doi.org/10.1016/j.esr.2018.11.004).
- [S7] ENTSO-E, ENTSO-E transmission system map.
URL <https://www.entsoe.eu/data/map/>
- [S8] B. Wiegmans, GridKit, Zenodo (Mar. 2016). [doi:10.5281/zenodo.47263](https://doi.org/10.5281/zenodo.47263).
- [S9] ENTSO-E, TYNDP: Ten-Year Network Development Plan (2018).
URL <https://tyndp.entsoe.eu/tyndp2018/>
- [S10] D. Oeding, B. R. Oswald, Elektrische Kraftwerke und Netze, Springer Berlin Heidelberg, Berlin, Heidelberg, 2011. [doi:10.1007/978-3-642-19246-3](https://doi.org/10.1007/978-3-642-19246-3).
- [S11] T. Ackermann, E. Tröster, P.-P. Schierhorn, T. Brown, Optimising the European transmission system for 77% renewable electricity by 2030, *IET Renewable Power Generation* 10 (1) (2016) 3–9. [doi:10/f75tr3](https://doi.org/10/f75tr3).
- [S12] J. Hörsch, H. Ronellenfitsch, D. Witthaut, T. Brown, Linear optimal power flow using cycle flows, *Electric Power Systems Research* 158 (2018) 126–135. [arXiv:1704.01881](https://arxiv.org/abs/1704.01881), [doi:10/gdb8kx](https://doi.org/10/gdb8kx).
- [S13] M. M. Frysztacki, J. Hörsch, V. Hagenmeyer, T. Brown, The strong effect of network resolution on electricity system models with high shares of wind and solar, *Applied Energy* 291 (2021) 116726. [arXiv:2101.10859](https://arxiv.org/abs/2101.10859), [doi:10/gmdkqc](https://doi.org/10/gmdkqc).

- [S14] J. Hörsch, T. Brown, The role of spatial scale in joint optimisations of generation and transmission for European highly renewable scenarios, in: Proceedings of 14th International Conference on the European Energy Market (EEM 2017), Dresden, 2017. [doi:10.1109/eem.2017.7982024](https://doi.org/10.1109/eem.2017.7982024).
- [S15] European Commission. Joint Research Centre., [JRC-IDEES: Integrated Database of the European Energy Sector : Methodological Note.](#), Publications Office, LU, 2017. URL <https://data.europa.eu/doi/10.2760/182725>
- [S16] Bundesanstalt für Straßenwesen, [Automatische Zählstellen auf Autobahnen und Bundesstraßen](#) (2021).
URL https://www.bast.de/DE/Verkehrstechnik/Fachthemen/v2-verkehrszaehlung/zaehl_node.html
- [S17] T. Brown, T. Bischof-Niemz, K. Blok, C. Breyer, H. Lund, B. V. Mathiesen, Response to ‘Burden of proof: A comprehensive review of the feasibility of 100% renewable-electricity systems’, *Renewable and Sustainable Energy Reviews* 92 (2018) 834–847. [arXiv:1709.05716](https://arxiv.org/abs/1709.05716), [doi:10.1016/j.rser.2018.04.113](https://doi.org/10.1016/j.rser.2018.04.113).
- [S18] eurostat, [Energy balances](#) (2021).
URL <https://ec.europa.eu/eurostat/web/energy/data/energy-balances>
- [S19] United States Geological Survey, [Ammonia production by country 2017](#) (2021).
URL <https://www.usgs.gov/media/files/nitrogen-2017-xlsx>
- [S20] A. M. Bazzanella, F. Ausfelder, DECHEMA Gesellschaft für Chemische Technik und Biotechnologie e.V., Tech. rep., DECHEMA (Jun. 2017). [\[link\]](#).
URL https://dechema.de/dechema_media/Downloads/Positionspapiere/Technology_study_Low_carbon_energy_and_feedstock_for_the_European_chemical_industry.pdf
- [S21] Bundesamt für Energie, [Energieverbrauch in der Industrie und im Dienstleistungssektor](#) (2021).
URL http://www.bfe.admin.ch/themen/00526/00541/00543/index.html?lang=de&dossier_id=00775
- [S22] T. Naegler, S. Simon, M. Klein, H. C. Gils, Quantification of the European industrial heat demand by branch and temperature level: Quantification of European industrial heat demand, *International Journal of Energy Research* 39 (15) (2015) 2019–2030. [doi:10.1002/er.3436](https://doi.org/10.1002/er.3436).

- [S23] M. Rehfeldt, T. Fleiter, F. Toro, A bottom-up estimation of the heating and cooling demand in European industry, *Energy Efficiency* 11 (5) (2018) 1057–1082. [doi:10.1007/s12053-017-9571-y](https://doi.org/10.1007/s12053-017-9571-y).
- [S24] M. Neuwirth, T. Fleiter, P. Manz, R. Hofmann, The future potential hydrogen demand in energy-intensive industries - a site-specific approach applied to Germany, *Energy Conversion and Management* 252 (2022) 115052. [doi:10.1016/j.enconman.2021.115052](https://doi.org/10.1016/j.enconman.2021.115052).
- [S25] A. Toktarova, V. Walter, L. Göransson, F. Johnsson, Interaction between electrified steel production and the north European electricity system, *Applied Energy* 310 (2022) 118584. [doi:10.1016/j.apenergy.2022.118584](https://doi.org/10.1016/j.apenergy.2022.118584).
- [S26] S. Lechtenböhmer, L. J. Nilsson, M. Åhman, C. Schneider, Decarbonising the energy intensive basic materials industry through electrification – Implications for future EU electricity demand, *Energy* 115 (2016) 1623–1631. [doi:10.1016/j.energy.2016.09.083](https://doi.org/10.1016/j.energy.2016.09.083).
- [S27] V. Vogl, O. Olsson, B. Nykvist, Phasing out the blast furnace to meet global climate targets, *Joule* 5 (10) (2021) 2646–2662. [doi:10.1016/j.joule.2021.09.007](https://doi.org/10.1016/j.joule.2021.09.007).
- [S28] N. Friedrichsen, G. Erdogmus, V. Duscha, Comparative analysis of options and potential for emission abatement in industry – summary of study comparison and study factsheets, Tech. rep., Fraunhofer ISI (Jul. 2018).
URL <http://www.umweltbundesamt.de/en/publikationen/comparative-analysis-of-options-potential-for>
- [S29] V. Vogl, M. Åhman, L. J. Nilsson, Assessment of hydrogen direct reduction for fossil-free steelmaking, *Journal of Cleaner Production* 203 (2018) 736–745. [doi:10.1016/j.jclepro.2018.08.279](https://doi.org/10.1016/j.jclepro.2018.08.279).
- [S30] HYBRIT, Summary of findings from HYBRIT Pre-Feasibility Study 2016–2017 (2021).
URL <https://dh5k8ug1gwbyz.cloudfront.net/uploads/2021/02/Hybrit-broschure-engelska.pdf>
- [S31] Material Economics, The circular economy – A powerful force for climate mitigation, Tech. rep.
URL <https://www.sitra.fi/app/uploads/2018/06/the-circular-economy-a-powerful-force-for-climate-mitigation.pdf>

- [S32] H. Mandova, S. Leduc, C. Wang, E. Wetterlund, P. Patrizio, W. Gale, F. Kraxner, Possibilities for CO₂ emission reduction using biomass in European integrated steel plants, *Biomass and Bioenergy* 115 (2018) 231–243. [doi:10.1016/j.biombioe.2018.04.021](https://doi.org/10.1016/j.biombioe.2018.04.021).
- [S33] H. Suopajarvi, K. Umeki, E. Mousa, A. Hedayati, H. Romar, A. Kemppainen, C. Wang, A. Phounglamcheik, S. Tuomikoski, N. Norberg, A. Andefors, M. Öhman, U. Lassi, T. Fabritius, Use of biomass in integrated steelmaking – Status quo, future needs and comparison to other low-CO₂ steel production technologies, *Applied Energy* 213 (2018) 384–407. [doi:10.1016/j.apenergy.2018.01.060](https://doi.org/10.1016/j.apenergy.2018.01.060).
- [S34] P. G. Levi, J. M. Cullen, Mapping Global Flows of Chemicals: From Fossil Fuel Feedstocks to Chemical Products, *Environmental Science & Technology* 52 (4) (2018) 1725–1734. [doi:10.1021/acs.est.7b04573](https://doi.org/10.1021/acs.est.7b04573).
- [S35] L. Wang, M. Xia, H. Wang, K. Huang, C. Qian, C. T. Maravelias, G. A. Ozin, Greening Ammonia toward the Solar Ammonia Refinery, *Joule* 2 (6) (2018) 1055–1074. [doi:10.1016/j.joule.2018.04.017](https://doi.org/10.1016/j.joule.2018.04.017).
- [S36] F. Kullmann, P. Markewitz, L. Kotzur, D. Stolten, The value of recycling for low-carbon energy systems - A case study of Germany's energy transition, *Energy* (2022) 124660 [doi:10.1016/j.energy.2022.124660](https://doi.org/10.1016/j.energy.2022.124660).
- [S37] R. Meys, A. Kätelhön, M. Bachmann, B. Winter, C. Zibunas, S. Suh, A. Bardow, Achieving net-zero greenhouse gas emission plastics by a circular carbon economy, *Science* 374 (6563) (2021) 71–76. [doi:10.1126/science.abg9853](https://doi.org/10.1126/science.abg9853).
- [S38] R. Meys, F. Frick, S. Westhues, A. Sternberg, J. Klankermayer, A. Bardow, Towards a circular economy for plastic packaging wastes – the environmental potential of chemical recycling, *Resources, Conservation and Recycling* 162 (2020) 105010. [doi:10/gmxv6z](https://doi.org/10/gmxv6z).
- [S39] F. Gu, J. Guo, W. Zhang, P. A. Summers, P. Hall, From waste plastics to industrial raw materials: A life cycle assessment of mechanical plastic recycling practice based on a real-world case study, *Science of The Total Environment* 601–602 (2017) 1192–1207. [doi:10/gf8n9w](https://doi.org/10/gf8n9w).
- [S40] S. R. Nicholson, N. A. Rorrer, A. C. Carpenter, G. T. Beckham, Manufacturing energy and greenhouse gas emissions associated with plastics consumption, *Joule* 5 (3) (2021) 673–686. [doi:10.1016/j.joule.2020.12.027](https://doi.org/10.1016/j.joule.2020.12.027).

- [S41] Material Economics, [Industrial Transformation 2050 - Pathways to Net-Zero Emissions from EU Heavy Industry](#) (2019).
URL <https://materialeconomics.com/publications/industrial-transformation-2050>
- [S42] P. S. Fennell, S. J. Davis, A. Mohammed, Decarbonizing cement production, Joule 5 (6) (2021) 1305–1311. [doi:10/gmsxpj](#).
- [S43] Danish Energy Agency, [Technology data](#) (2020).
URL <https://ens.dk/en/our-services/projections-and-models/technology-data>
- [S44] S. S. Akhtar, E. Ervin, S. Raza, T. Abbas, From coal to natural gas: Its impact on kiln production, Clinker quality and emissions, in: 2013 IEEE-IAS/PCA Cement Industry Technical Conference, IEEE, Orlando, FL, 2013, pp. 1–24. [doi:10.1109/CITCON.2013.6525276](#).
- [S45] T. Kuramochi, A. Ramírez, W. Turkenburg, A. Faaij, Comparative assessment of CO₂ capture technologies for carbon-intensive industrial processes, Progress in Energy and Combustion Science 38 (1) (2012) 87–112. [doi:10.1016/j.pecs.2011.05.001](#).
- [S46] D. D. Furszyfer Del Rio, B. K. Sovacool, A. M. Foley, S. Griffiths, M. Bazilian, J. Kim, D. Rooney, Decarbonizing the ceramics industry: A systematic and critical review of policy options, developments and sociotechnical systems, Renewable and Sustainable Energy Reviews 157 (2022) 112081. [doi:10.1016/j.rser.2022.112081](#).
- [S47] D. D. Furszyfer Del Rio, B. K. Sovacool, A. M. Foley, S. Griffiths, M. Bazilian, J. Kim, D. Rooney, Decarbonizing the glass industry: A critical and systematic review of developments, sociotechnical systems and policy options, Renewable and Sustainable Energy Reviews 155 (2022) 111885. [doi:10.1016/j.rser.2021.111885](#).
- [S48] B. K. Sovacool, M. Bazilian, S. Griffiths, J. Kim, A. Foley, D. Rooney, Decarbonizing the food and beverages industry: A critical and systematic review of developments, sociotechnical systems and policy options, Renewable and Sustainable Energy Reviews 143 (2021) 110856. [doi:10.1016/j.rser.2021.110856](#).
- [S49] E. Zeyen, V. Hagenmeyer, T. Brown, Mitigating heat demand peaks in buildings in a highly renewable European energy system, Energy 231 (2021) 120784. [arXiv: 2012.01831](#), [doi:10.1016/j.energy.2021.120784](#).
- [S50] F. Hofmann, J. Hampp, F. Neumann, T. Brown, J. Hörsch, Atlite: A Lightweight Python Package for Calculating Renewable Power Potentials and Time Series, Journal of Open Source Software 6 (62) (2021) 3294. [doi:10.21105/joss.03294](#).

- [S51] H. Hersbach, B. Bell, P. Berrisford, S. Hirahara, A. Horányi, J. Muñoz-Sabater, J. Nicolas, C. Peubey, R. Radu, D. Schepers, A. Simmons, C. Soci, S. Abdalla, X. Abel-lan, G. Balsamo, P. Bechtold, G. Biavati, J. Bidlot, M. Bonavita, G. De Chiara, P. Dahlgren, D. Dee, M. Diamantakis, R. Dragani, J. Flemming, R. Forbes, M. Fuentes, A. Geer, L. Haimberger, S. Healy, R. J. Hogan, E. Hólm, M. Janisková, S. Keeley, P. Laloyaux, P. Lopez, C. Lupu, G. Radnoti, P. de Rosnay, I. Rozum, F. Vamborg, S. Villaume, J.-N. Thépaut, The ERA5 global reanalysis, *Quarterly Journal of the Royal Meteorological Society* 146 (730) (2020) 1999–2049. [doi:10/gg9wx7](https://doi.org/10.1002/qj.377).
- [S52] BDEW, [BDEW heat demand profiles](https://github.com/oemof/demandlib) (2021).
URL <https://github.com/oemof/demandlib>
- [S53] I. Staffell, D. Brett, N. Brandon, A. Hawkes, A review of domestic heat pumps, *Energy & Environmental Science* 5 (11) (2012) 9291. [doi:10.1039/c2ee22653g](https://doi.org/10.1039/c2ee22653g).
- [S54] European Environment Agency (EEA), [Corine Land Cover \(CLC\) 2012](https://land.copernicus.eu/pan-european/corine-land-cover/clc-2012).
URL <https://land.copernicus.eu/pan-european/corine-land-cover/clc-2012>
- [S55] European Environment Agency (EEA), [Natura 2000 data - the European network of protected sites](https://www.eea.europa.eu/data-and-maps/data/natura-13).
URL <https://www.eea.europa.eu/data-and-maps/data/natura-13>
- [S56] K. Bódis, I. Koulias, A. Jäger-Waldau, N. Taylor, S. Szabó, A high-resolution geospatial assessment of the rooftop solar photovoltaic potential in the European Union, *Renewable and Sustainable Energy Reviews* 114 (2019) 109309. [doi:10.1016/j.rser.2019.109309](https://doi.org/10.1016/j.rser.2019.109309).
- [S57] GEBCO, [GEBCO 2014 Grid](https://www.gebco.net/data_and_products/historical_data_sets/#gebco_2014).
URL https://www.gebco.net/data_and_products/historical_data_sets/#gebco_2014
- [S58] M. Lerch, M. De-Prada-Gil, C. Molins, G. Benveniste, Sensitivity analysis on the levelized cost of energy for floating offshore wind farms, *Sustainable Energy Technologies and Assessments* 30 (2018) 77–90. [doi:10.1016/j.seta.2018.09.005](https://doi.org/10.1016/j.seta.2018.09.005).
- [S59] C.-S. Laura, D.-C. Vicente, Life-cycle cost analysis of floating offshore wind farms, *Renewable Energy* 66 (2014) 41–48. [doi:10.1016/j.renene.2013.12.002](https://doi.org/10.1016/j.renene.2013.12.002).
- [S60] A. Myhr, C. Bjerkseter, A. Ågotnes, T. A. Nygaard, Levelised cost of energy for offshore floating wind turbines in a life cycle perspective, *Renewable Energy* 66 (2014) 714–728. [doi:10.1016/j.renene.2014.01.017](https://doi.org/10.1016/j.renene.2014.01.017).

- [S61] M. Kausche, F. Adam, F. Dahlhaus, J. Großmann, Floating offshore wind - Economic and ecological challenges of a TLP solution, *Renewable Energy* 126 (2018) 270–280. [doi:10.1016/j.renene.2018.03.058](https://doi.org/10.1016/j.renene.2018.03.058).
- [S62] L. Castro-Santos, A. Filgueira-Vizoso, L. Carral-Couce, J. A. F. Formoso, Economic feasibility of floating offshore wind farms, *Energy* 112 (2016) 868–882. [doi:10.1016/j.energy.2016.06.135](https://doi.org/10.1016/j.energy.2016.06.135).
- [S63] R. McKenna, S. Pfenninger, H. Heinrichs, J. Schmidt, I. Staffell, C. Bauer, K. Gruber, A. N. Hahmann, M. Jansen, M. Klingler, N. Landwehr, X. G. Larsén, J. Lilliestam, B. Pickering, M. Robinius, T. Tröndle, O. Turkovska, S. Wehrle, J. M. Weinand, J. Wohland, High-resolution large-scale onshore wind energy assessments: A review of potential definitions, methodologies and future research needs, *Renewable Energy* 182 (2022) 659–684. [doi:10.1016/j.renene.2021.10.027](https://doi.org/10.1016/j.renene.2021.10.027).
- [S64] D. S. Ryberg, D. G. Caglayan, S. Schmitt, J. Linßen, D. Stolten, M. Robinius, The future of European onshore wind energy potential: Detailed distribution and simulation of advanced turbine designs, *Energy* 182 (2019) 1222–1238. [doi:10.1016/j.energy.2019.06.052](https://doi.org/10.1016/j.energy.2019.06.052).
- [S65] U. Pfeifroth, S. Kothe, R. Müller, J. Trentmann, R. Hollmann, P. Fuchs, M. Werscheck, Surface radiation data set - heliosat (SARAH) - edition 2 (2017). [doi:10/f77h](https://doi.org/10/f77h).
- [S66] P. J. Coker, H. C. Bloomfield, D. R. Drew, D. J. Brayshaw, Interannual weather variability and the challenges for Great Britain's electricity market design, *Renewable Energy* 150 (2020) 509–522. [doi:10/ghfgtv](https://doi.org/10/ghfgtv).
- [S67] J. Bosch, I. Staffell, A. D. Hawkes, Temporally explicit and spatially resolved global offshore wind energy potentials, *Energy* 163 (2018) 766–781. [doi:10/gfmhvm](https://doi.org/10/gfmhvm).
- [S68] H.-M. Henning, A. Palzer, A comprehensive model for the German electricity and heat sector in a future energy system with a dominant contribution from renewable energy technologies—Part I: Methodology, *Renewable and Sustainable Energy Reviews* 30 (2014) 1003–1018. [doi:10.1016/j.rser.2013.09.012](https://doi.org/10.1016/j.rser.2013.09.012).
- [S69] R. Nouvel, M. Cotrado Sehgelmeble, D. Pietruschka, European mapping of seasonal performances of air-source and geothermal heat pumps for residential applications (2015). [doi:10.5075/EPFL-CISBAT2015-543-548](https://doi.org/10.5075/EPFL-CISBAT2015-543-548).
- [S70] U.S. Energy Information Administration, [Hydroelectricity net generation](#) (Apr. 2022).

- URL <https://www.eia.gov/international/data/world/electricity/electricity-generation?pd=2&p=000000000000000000000000000000g&u=1&f=A&v=mapbubble&a=-&i=none&vo=value&t=R&g=0000000000000002&l=73-1028i008017kg6368g80a4k000e0ag00gg0004g8g0ho00g000400008&s=315532800000&e=1577836800000&ev=false&>
- [S71] I. Staffell, D. Scamman, A. Velazquez Abad, P. Balcombe, P. E. Dodds, P. Ekins, N. Shah, K. R. Ward, The role of hydrogen and fuel cells in the global energy system, *Energy & Environmental Science* 12 (2) (2019) 463–491. doi:[10.1039/C8EE01157E](https://doi.org/10.1039/C8EE01157E).
- [S72] Gas for Climate, European Hydrogen Backbone - How a dedicated hydrogen infrastructure can be created, Tech. rep. (Jun. 2020).
- URL https://gasforclimate2050.eu/wp-content/uploads/2020/07/2020_European-Hydrogen-Backbone_Report.pdf
- [S73] D. G. Caglayan, N. Weber, H. U. Heinrichs, J. Linßen, M. Robinius, P. A. Kukla, D. Stolten, Technical potential of salt caverns for hydrogen storage in Europe, *International Journal of Hydrogen Energy* 45 (11) (2020) 6793–6805. doi:[10.1016/j.ijhydene.2019.12.161](https://doi.org/10.1016/j.ijhydene.2019.12.161).
- [S74] A. Pluta, W. Medjroubi, J. C. Dietrich, J. Dasenbrock, H.-P. Tetens, J. E. Sandoval, O. Lunsdorf, SciGRID_gas - Data Model of the European Gas Transport Network, in: 2022 Open Source Modelling and Simulation of Energy Systems (OSMSES), IEEE, Aachen, Germany, 2022, pp. 1–7. doi:[10.1109/OSMSES54027.2022.9769122](https://doi.org/10.1109/OSMSES54027.2022.9769122).
- [S75] GEM Wiki, LNG Terminals (2021).
- URL https://www.gem.wiki/LNG_Terminals
- [S76] M. Gruber, P. Weinbrecht, L. Biffar, S. Harth, D. Trimis, J. Brabandt, O. Posdziech, R. Blumentritt, Power-to-Gas through thermal integration of high-temperature steam electrolysis and carbon dioxide methanation - Experimental results, *Fuel Processing Technology* 181 (2018) 61–74. doi:[10.1016/j.fuproc.2018.09.003](https://doi.org/10.1016/j.fuproc.2018.09.003).
- [S77] ENTSOG, Transmission Capacity and System Development Maps (2021).
- URL <https://www.entsoe.eu/maps#>
- [S78] Gas for Climate, European Hydrogen Backbone - Analysing future demand, supply, and transport of hydrogen, Tech. rep. (Jun. 2021).
- URL https://gasforclimate2050.eu/wp-content/uploads/2021/06/EHB_Analysing-the-future-demand-supply-and-transport-of-hydrogen_June-2021.pdf

- [S79] P. Ruiz, W. Nijs, D. Tarvydas, A. Sgobbi, A. Zucker, R. Pilli, R. Jonsson, A. Camia, C. Thiel, C. Hoyer-Klick, F. Dalla Longa, T. Kober, J. Badger, P. Volker, B. Elbersen, A. Brosowski, D. Thrän, ENSPRESO - an open, EU-28 wide, transparent and coherent database of wind, solar and biomass energy potentials, *Energy Strategy Reviews* 26 (2019) 100379. [doi:10/ggbgnk](https://doi.org/10/ggbgnk).
- [S80] N. S. Bentsen, Carbon debt and payback time – Lost in the forest?, *Renewable and Sustainable Energy Reviews* 73 (2017) 1211–1217. [doi:10.1016/j.rser.2017.02.004](https://doi.org/10.1016/j.rser.2017.02.004).
- [S81] W. Zappa, M. Junginger, M. van den Broek, Is a 100% renewable European power system feasible by 2050?, *Applied Energy* 233–234 (2019) 1027–1050. [doi:10/gf8fz5](https://doi.org/10/gf8fz5).
- [S82] E. Martin-Roberts, V. Scott, S. Flude, G. Johnson, R. S. Haszeldine, S. Gilfillan, Carbon capture and storage at the end of a lost decade, *One Earth* (2021) S2590332221005418[doi:10.1016/j.oneear.2021.10.002](https://doi.org/10.1016/j.oneear.2021.10.002).
- [S83] C. Breyer, M. Fasihi, A. Aghahosseini, Carbon dioxide direct air capture for effective climate change mitigation based on renewable electricity: A new type of energy system sector coupling, *Mitigation and Adaptation Strategies for Global Change* 25 (1) (2020) 43–65. [doi:10.1007/s11027-019-9847-y](https://doi.org/10.1007/s11027-019-9847-y).
- [S84] IEA, *Is carbon capture too expensive? – Analysis*.
URL <https://www.iea.org/commentaries/is-carbon-capture-too-expensive>
- [S85] T. Brown, J. Hörsch, D. Schlachtberger, PyPSA: Python for Power System Analysis, *Journal of Open Research Software* 6 (2018) 4. [doi:10.5334/jors.188](https://doi.org/10.5334/jors.188).
- [S86] T. Tröndle, J. Lilliestam, S. Marelli, S. Pfenninger, Trade-Offs between Geographic Scale, Cost, and Infrastructure Requirements for Fully Renewable Electricity in Europe, *Joule* (2020) S2542435120303366[doi:10/gg8zk2](https://doi.org/10/gg8zk2).
- [S87] R. McKenna, J. M. Weinand, I. Mulalic, S. Petrović, K. Mainzer, T. Preis, H. S. Moat, Scenicness assessment of onshore wind sites with geotagged photographs and impacts on approval and cost-efficiency, *Nature Energy* 6 (6) (2021) 663–672. [doi:10.1038/s41560-021-00842-5](https://doi.org/10.1038/s41560-021-00842-5).
- [S88] J. M. Weinand, R. McKenna, M. Kleinebrahm, F. Scheller, W. Fichtner, The impact of public acceptance on cost efficiency and environmental sustainability in decentralized energy systems, *Patterns* 2 (7) (2021) 100301. [doi:10/gmdkp8](https://doi.org/10/gmdkp8).

- [S89] J. M. Weinand, R. McKenna, H. Heinrichs, M. Roth, D. Stolten, W. Fichtner, Exploring the trilemma of cost-efficient, equitable and publicly acceptable onshore wind expansion planning (2021). [doi:10.48550/arXiv.2106.15198](https://doi.org/10.48550/arXiv.2106.15198).
- [S90] D. P. Schlachtberger, T. Brown, M. Schäfer, S. Schramm, M. Greiner, Cost optimal scenarios of a future highly renewable European electricity system: Exploring the influence of weather data, cost parameters and policy constraints, Energy 163 (2018) 100–114. [arXiv:1803.09711](https://doi.org/10.1016/j.energy.2018.02.071), [doi:10/gfk5cj](https://doi.org/10.1016/j.energy.2018.02.071).
- [S91] Danish Energy Agency, [Technology Data for Generation of Electricity and District Heating](https://ens.dk/en/our-services/projections-and-models/technology-data/technology-data-generation-electricity-and) (Mar. 2018).
URL <https://ens.dk/en/our-services/projections-and-models/technology-data/technology-data-generation-electricity-and>
- [S92] Danish Energy Agency, [Technology Data for Industrial Process Heat](https://ens.dk/en/our-services/projections-and-models/technology-data/technology-data-industrial-process-heat) (May 2020).
URL <https://ens.dk/en/our-services/projections-and-models/technology-data/technology-data-industrial-process-heat>
- [S93] H.-M. Henning, A. Palzer, A comprehensive model for the German electricity and heat sector in a future energy system with a dominant contribution from renewable energy technologies—Part I: Methodology, Renewable and Sustainable Energy Reviews 30 (2014) 1003–1018. [doi:10.1016/j.rser.2013.09.012](https://doi.org/10.1016/j.rser.2013.09.012).
- [S94] A. Palzer, [Sektorübergreifende Modellierung und Optimierung eines zukünftigen deutschen Energiesystems unter Berücksichtigung von Energieeffizienzmaßnahmen im Gebäudesektor](https://publica.fraunhofer.de/documents/N-408742.html), Ph.D. thesis, KIT (2016).
URL <http://publica.fraunhofer.de/documents/N-408742.html>
- [S95] P. Härtel, T. K. Vrana, T. Hennig, M. von Bonin, E. J. Wiggelinkhuizen, F. D. Nieuwenhout, Review of investment model cost parameters for VSC HVDC transmission infrastructure, Electric Power Systems Research 151 (2017) 419–431. [doi:10.1016/j.epsr.2017.06.008](https://doi.org/10.1016/j.epsr.2017.06.008).
- [S96] S. Cole, P. Martinot, S. Rapoport, G. Papaefthymiou, V. Gori, [Study of the Benefits of a Meshed Offshore Grid in Northern Seas Region](https://ec.europa.eu/energy/sites/ener/files/documents/2014_nsog_report.pdf), Tech. rep. (2014).
URL https://ec.europa.eu/energy/sites/ener/files/documents/2014_nsog_report.pdf
- [S97] M. Fasihi, D. Bogdanov, C. Breyer, Long-Term Hydrocarbon Trade Options for the Maghreb Region and Europe—Renewable Energy Based Synthetic Fuels for a Net Zero Emissions World, Sustainability 9 (2) (2017) 306. [doi:10.3390/su9020306](https://doi.org/10.3390/su9020306).

- [S98] Danish Energy Agency, [Technology Data for Renewable Fuels](#) (Mar. 2018).
URL <https://ens.dk/en/our-services/projections-and-models/technology-data/technology-data-renewable-fuels>
- [S99] S. Hagspiel, C. Jägemann, D. Lindenberger, T. Brown, S. Cherevatskiy, E. Tröster, Cost-optimal power system extension under flow-based market coupling, *Energy* 66 (2014) 654–666. doi:[10.1016/j.energy.2014.01.025](https://doi.org/10.1016/j.energy.2014.01.025).
- [S100] A. Purvins, L. Sereno, M. Ardelean, C.-F. Covrig, T. Efthimiadis, P. Minnebo, Submarine power cable between Europe and North America: A techno-economic analysis, *Journal of Cleaner Production* 186 (2018) 131–145. doi:[10/gmdkp9](https://doi.org/10/gmdkp9).
- [S101] Danish Energy Agency, [Technology Data for Energy Storage](#) (Oct. 2018).
URL <https://ens.dk/en/our-services/projections-and-models/technology-data/technology-data-energy-storage>
- [S102] W. Zappa, M. Junginger, M. van den Broek, Is a 100% renewable European power system feasible by 2050?, *Applied Energy* 233–234 (2019) 1027–1050. doi:[10.1016/j.apenergy.2018.08.109](https://doi.org/10.1016/j.apenergy.2018.08.109).
- [S103] A. Schröder, F. Kunz, F. Meiss, R. Mendelevitch, C. von Hirschhausen, [Current and prospective costs of electricity generation until 2050](#), Data Documentation, DIW 68. Berlin: Deutsches Institut.
URL <https://www.econstor.eu/handle/10419/80348>
- [S104] International Energy Agency, [World Energy Outlook 2017](#), Tech. rep. (2017).
URL <https://www.iea.org/reports/world-energy-outlook-2017>
- [S105] [Lazard's Levelized Cost of Energy Analysis, version 13.0](#) (2019).
URL <https://www.lazard.com/media/451086/lazards-levelized-cost-of-energy-version-130-vf.pdf>
- [S106] Development of the specific carbon dioxide emissions of the German electricity mix in the years 1990 - 2011 (2019).
URL https://www.umweltbundesamt.de/sites/default/files/medien/1410/publikationen/2019-04-10_cc_10-2019_strommix_2019.pdf
- [S107] BP Statistical Review of World Energy (2019).
URL <https://www.bp.com/content/dam/bp/business-sites/en/global/corporate/pdfs/energy-economics/statistical-review/bp-stats-review-2019-full-report.pdf>

- [S108] B. Erlach, H.-M. Henning, C. Kost, A. Palzer, C. Stephanos, Optimierungsmodell REMod-D Materialien zur Analyse Sektorkopplung – Untersuchungen und Überlegungen zur Entwicklung eines integrierten Energiesystems, Tech. rep. (Apr. 2018).
 URL https://energiesysteme-zukunft.de/fileadmin/user_upload/Publikationen/PDFs/ESYS_Materialien_Optimierungsmodell_REMod-D.pdf
- [S109] Hydrogen supply chain: Evidence base, Department for Business, Energy & Industrial Strategy, GovUK, Tech. rep. (2018).
 URL https://assets.publishing.service.gov.uk/government/uploads/system/uploads/attachment_data/file/760479/H2_supply_chain_evidence_-_publication_version.pdf
- [S110] Danish Energy Agency, Technology Data for Individual Heating Plants (Mar. 2018).
 URL <https://ens.dk/en/our-services/projections-and-models/technology-data/technology-data-individual-heating-plants>
- [S111] M. Ram, D. Bogdanov, A. Aghahosseini, A. Gulagi, A. S. Oyewo, M. Child, U. Caldera, K. Sadovskaia, J. Farfan, L. S. Barbosa, S. Khalili, C. Breyer, Global energy system based on 100% renewable energy – power, heat, transport and desalination sectors., Tech. rep. (2019).
 URL <http://energywatchgroup.org/new-study-global-energy-system-based-100-renewable-energy>
- [S112] M. Reuß, T. Grube, M. Robinius, P. Preuster, P. Wasserscheid, D. Stolten, Seasonal storage and alternative carriers: A flexible hydrogen supply chain model, Applied Energy 200 (2017) 290–302. doi:[10.1016/j.apenergy.2017.05.050](https://doi.org/10.1016/j.apenergy.2017.05.050).
- [S113] Danish Energy Agency, Technology Catalogue for Transport of Energy (Mar. 2018).
 URL <https://ens.dk/en/our-services/projections-and-models/technology-data/technology-catalogue-transport-energy>
- [S114] K. Schaber, Integration of Variable Renewable Energies in the European power system: A model-based analysis of transmission grid extensions and energy sector coupling, Ph.D. thesis, TU München (2013).
 URL <https://d-nb.info/1058680781/34>
- [S115] R. d'Amore-Domenech, T. J. Leo, B. G. Pollet, Bulk power transmission at sea: Life cycle cost comparison of electricity and hydrogen as energy vectors, Applied Energy 288 (2021) 116625. doi:[10.1016/j.apenergy.2021.116625](https://doi.org/10.1016/j.apenergy.2021.116625).

- [S116] M. J. Kaiser, Offshore pipeline construction cost in the U.S. Gulf of Mexico, *Marine Policy* 82 (2017) 147–166. doi:10.1016/j.marpol.2017.05.003.
- [S117] Global average levelised cost of hydrogen production by energy source and technology, 2019 and 2050 – Charts – Data & Statistics.
URL <https://www.iea.org/data-and-statistics/charts/global-average-levelised-cost-of-hydrogen-production-by-energy-source-and-technology-2019-and-2050>
- [S118] N. Gerhardt, A. Scholz, F. Sandau, Hahn H., *Interaktion EE-Strom, Wärme und Verkehr*. Fraunhofer IWES (2015).
URL http://www.energiesystemtechnik.iwes.fraunhofer.de/de/projekte/suche/2015/interaktion_strom_waerme_verkehr.html

Contents

Introduction	4
Hydrogen network benefit is robust, strongest without power grid expansion	6
Common features across four scenarios of European climate neutrality	8
Hydrogen backbone takes over role of bulk energy transport	11
New hydrogen backbone can leverage repurposed natural gas pipelines	15
Regional imbalance of supply and demand is reinforced by transmission	16
Discussion	18
Conclusion	22
Experimental Procedures	22
References	26
Supplementary Information	32
S1 Model Overview	35
S2 Electricity Sector	35
S2.1 Electricity Demand	35
S2.2 Electricity Supply	37
S2.3 Electricity Storage	37
S2.4 Electricity Transport	37
S3 Transport Sector	40
S3.1 Land Transport	40
S3.2 Aviation	41
S3.3 Shipping	42
S4 Industry Sector	42
S4.1 Overview	45
S4.2 Iron and Steel	46
S4.3 Chemicals Industry	47
S4.4 Non-metallic Mineral Products	49
S4.5 Non-ferrous Metals	50

S4.6	Other Industry Subsectors	51
S5	Heating Sector	51
S5.1	Heat Demand	51
S5.2	Heat Supply	52
S5.3	Heat Storage	53
S6	Renewables	53
S6.1	Potentials	53
S6.2	Time Series	55
S7	Hydrogen	59
S7.1	Hydrogen Demand	59
S7.2	Hydrogen Supply	59
S7.3	Hydrogen Transport	60
S7.4	Hydrogen Storage	60
S8	Methane	62
S8.1	Methane Demand	62
S8.2	Methane Supply	62
S8.3	Methane Transport	62
S9	Oil-based Products	64
S9.1	Oil-based Product Demand	64
S9.2	Oil-based Product Supply	64
S9.3	Oil-based Product Transport	64
S10	Biomass	64
S10.1	Biomass Supply and Potentials	64
S10.2	Biomass Demand	65
S10.3	Biomass Transport	66
S11	Carbon dioxide capture, usage and sequestration (CCU/S)	66
S11.1	Carbon Capture	66
S11.2	Carbon Usage	67
S11.3	Carbon Transport and Sequestration	67
S12	Mathematical Model Formulation	67
S13	Grid Reinforcement and Onshore Wind Potential Restrictions	71
S13.1	Cost of Electricity Grid Reinforcement Restrictions	71
S13.2	Cost of Onshore Wind Potential Elimination	73

S13.3 Cost of Compromises on Onshore Wind Potential Restrictions	76
S14 Supplementary Results for Network Expansion Scenarios	76
S15 Detailed Results of Least-Cost Solution with Full Grid Expansion	76
S16 Techno-Economic Assumptions	78
Supplementary References	103